Mechanical Design of a Sonar Mount for an Unmanned Surface Vehicle

Jackson Rand Pearson

Thesis submitted to the Faculty of the
Virginia Polytechnic Institute and State University
in partial fulfillment of the requirements for the degree of

Master of Science
In
Mechanical Engineering

Robert L. West, Chair
Daniel J. Stilwell
Pablo A. Tarazaga

September 22, 2015
Blacksburg, VA

Keywords: Mechanical Design, Sonar Mount,
Unmanned Surface Vehicle

Mechanical Design of a Sonar Mount
for an Unmanned Surface Vehicle

Jackson Rand Pearson

Abstract

Trends in USV research will continue on the path toward a fully autonomous USV capable of troop transport or enemy engagement. Imaging sonar will be an integral part of this development. However, due in part to sonar's inherent physical limitations, as well as its sensitivity to environmental factors, sonar technology represents a bottleneck to the development of situationally aware USVs capable of high-speed maneuvers. The work presented in this thesis is intended to provide a platform to bridge this gap, which is the design, analysis, and field testing of a mount for an imaging sonar intended as a retrofit for an existing vessel. The result of this work represents a step toward the ultimate goal of a fully autonomous USV, and will enable the advancement of research in the use of imaging sonar on surface vehicles.

This thesis examines the problem of mounting a sonar on a surface vehicle from a fundamental perspective. It describes the development of a list of customer needs, presents a prototype design, and presents the important analyses for the prototype. The prototype mount was built, and field testing for proof of concept was carried out on the Virginia Tech USV, which is a Rigid Hull Inflatable Boat (RHIB), and the Navy Special Operations Craft – Riverine (SOC-R) on the Pearl River at Stennis Space Center. Testing showed the mount to be highly effective at limiting risk to personnel and equipment while operating in difficult environments like swamps. However, it also exposed some limitations associated with the mount's breakaway device, and the mounting location at the side in 2012, and at the stern in 2013.

Based on experience gained from testing, a new mount design is presented for use at the bow. The bow location offers better impact protection to the sonar as long as the sonar can be positioned above the boat's draft. Field tests also exposed the need for an omnidirectional breakaway device which limits impact loads on the sonar during collisions. The Ball and Socket Breakaway (BSB) device was designed to satisfy this need. The BSB is acts as a "mechanical fuse," which holds the sonar rigidly under normal operating conditions, but will slip and rotate when the sonar strikes an object. It is designed to respond to impact loads on the sonar from the front, sides, or back, resulting in improved sonar protection during the varied maneuvers necessary for operation in shallow, narrow passageways. The expected moment holding capacity of the BSB as it is currently designed is 300 N-m (2650 lb-in), which should allow for speeds up to 3 m/s (6 kt) before drag-induced breakaway.

Acknowledgements

No research project is completed in a vacuum. Throughout this process there were many people that enabled its successful completion. I'd like to thank the members of my committee for their support. Thanks to Dr. Stilwell for the opportunity to work in the ASCL. He is an inspiration to me both professionally and personally. I'd also like to thank Dr. West for being extremely generous with his time, and for his positive and encouraging attitude throughout this process. I am indebted to Dr. Tarazaga for providing the facilities required for the sonar pole vibration testing, and for making himself available to answer questions during the testing process. I am grateful to the Office of Naval Research for their support via grants N00014-11-10532 and N00014-13-1-0411.

There were a few members of the ASCL that helped out with this project. Kevin Kline deserves special recognition. Kevin and I were teammates in the design of the prototype sonar mount. I'd like to thank him for doing the majority of the prototype mount CAD and helping with the design. Having someone to discuss ideas with is important for any design project, but having an engineer with the professionalism, creativity, and competence Kevin has is invaluable. Aditya Gadre is an extremely competent, positive, and easy to work with engineer, and was instrumental in giving my designs the electromechanical power to bring them to life. Thanks also to Tim Pratt, for his insight about manufacturing processes and his help checking over my detail drawings, and also for letting me bounce ideas off of him from time to time.

I'd like to thank Adam Shoemaker for his significant contributions to the vibration analysis and testing of the sonar mount pole.

I'd also like to thank Dr. Woolsey for allowing the use of his lab space for fiberglass work, and his students Artur Wolek for his insight into fiberglass layups, and Victor Zamora for his help using the CNC foam cutter.

Thanks to our three collaborators at the Naval Postgraduate School: Sean Kragelund, for providing dimensions and specs for sonars; Aurelio Monarrez; and Tad Masek, for his insight into the potential effects of mounting location on sonar data quality.

I'd also like to thank the gentlemen of SBT-22 at Stennis Space Center for their help with testing in 2012 and 2013. They were beyond accommodating. Our POC in 2012, whom I can't name for security reasons, was especially generous with his time. A stressed out grad student once called this POC asking for photos of SOC-R's structure as well as some measurements. "Sure!" the POC replied, "I'm on vacation, but I can have one of my guys take some photos and send them to you." The grad student had everything he needed within 48 hours.

Lastly, I want to thank my family. For my parents for bringing me into the world, and for their constant love and encouragement. If everyone had parents like you the world would be a far

better place. And for my sister, Kerry, for her strength and support, and her willingness to lend an ear when I needed it.

80/20® is a registered trademark of 80/20 Inc. of Columbia City, IN, U.S.A., Reg. No. 2699302.

ULTEM® is a registered trademark of General Electric Company of Schenectady, NY, U.S.A., Reg. No. 3083540

Torlon® is a registered trademark of Amoco Chemicals Corporation, of Chicago, IL, 60601, Reg. No. 1200074

Vespel® is a registered trademark of E. I. du Pont de Nemours and Company, Wilmington, DE, 19898, Reg. No. 1083519

Contents

List of Tables

List of Figures

Chapter 1

Introduction

1.1 Overview and Statement of Need

The United States military has demonstrated significant interest in unmanned surface vehicles (USVs) over the last couple decades. This is not surprising when the advantages of the technology are considered. By assuming decision making responsibility, either in part or in whole, USVs can reduce the cost of operator training, and allow for force multiplication with fewer personnel. USVs reduce communications and data exchange requirements when these activities can be automated [1]. There is also an undeniable element of intimidation, detrimental to enemy morale, which comes with the ability to engage an adversary without placing your own soldiers at risk. But ultimately the two most important benefits of USV technology, and the two primary elements driving their development, are their ability to limit costs and the number of people put at risk to achieve an objective.

Contrary to what most people would expect, the United States military has been using USV technology for decades. Immediately following the atomic blasts at Bikini Atoll in 1946 during Operation Crossroads, radio-controlled drone boats were used to collect water samples near the blast site [2]. During the Vietnam War, USVs were deployed off the waters of Saigon to conduct mine hunting operations [3]. This helped clear the waters without placing many people at risk. More recently, significant technological advancements have led to greater levels of USV autonomy. In 2003 the Spartan Scout, a semi-autonomous USV was used at the Advanced Capability Technology Demonstration (ACTD) to demonstrate its ability to conduct Intelligence, Surveillance, Reconnaissance (ISR) missions [4].

Until recently, despite these technological advancements, operating a semi-autonomous USV in a riverine or littoral environment remained a challenge. Boat travel in these areas has a unique set of hazards that make the use of USVs inadvisable, particularly if the USV is being used to transport soldiers. Conditions can shift from day to day due to heavy rains, flooding, tides, mudslides, dam releases, etc. Hidden obstacles such as submerged rocks, logs, shipwrecks, or old bridge/dam structures also pose a threat. In addition to these physical hazards, there are also inherent tactical hazards. On the water, soldiers will always be occupying the low ground, and have little to no cover, putting them at a significant disadvantage. Also, if a crew is attacked in a riverine environment, there are only two directions to go: up river or down river. These factors leave boat crews extremely vulnerable.

To mitigate the risks inherent to traveling in littoral and riverine environments, boat crews use several tactics. Large amounts of firepower and smoke grenades help, but by far the most important tactic is speed. Moving quickly through an area is simply the most effective way to reduce your exposure to a threat in that area. Unfortunately traveling fast is not always possible, especially in areas that have not been scouted before, or when subsurface conditions may have changed due to weather events. When speed is not an option crews use the "poke and prod" method, in which a member of the crew stands on the bow of the boat and prods the river bottom with a long pole. As he does this he directs the helmsman to the deep water. In some cases, he is forced to exit the boat and walk in front while giving directions. Another method used is the "nose in." This is where the helmsman uses the bow of the boat to "feel" his way forward. With this method he traverses forward slowly until he strikes something, and then backs off and tries another route until he finds a way to pass.

Clearly current methods of traversing an unfamiliar area are insufficient, especially if a situation is life threatening. One area of USV research in particular that could prove useful to the Navy in making river travel by boat safer is in the application of sonar, specifically imaging sonar. This would give the helmsman the ability to see subsurface obstacles in front of him in real time, eliminating the need to have a person at the front of the boat directing him. This could have several significant effects. Having a sonar in the water would free up personnel for other tasks, and would enable the helmsman to traverse an unfamiliar area much quicker. It would also allow waterways to be scouted and mapped so that future trips through the same area could be completed at a much higher speed. It would increase the helmsman's situational awareness, and also generate valuable feedback for autonomous systems engineers.

Trends in USV research have been, and will continue to be toward greater and greater levels of vehicle autonomy. This will not happen quickly, as there are numerous technical challenges to solve, and ethical questions to answer before a fully autonomous surface vehicle capable of troop delivery and even enemy engagement will be realistic. It will also take time for the technology to gain the trust of soldiers. However, as autonomous vehicle technology develops and is more widely adopted, even high-level tasks like driving could be offloaded to the vehicle's systems, greatly reducing the crew's exposure to the hazards described above.

This thesis presents a small but significant step towards the goal of a fully autonomous, situationally aware riverine vessel, which is the design and testing of a mechanical structure for mounting an imaging sonar to the boat. The intention is not to define *the design* of a mounting structure for a sonar, but rather to come up with one of many possible solutions that will enable the advancement of USV technology. The following sections of this chapter serve to clearly define the functions the sonar mount must fulfill, define the scope of the project, and give a brief overview of the content included in subsequent chapters.

1.2 Research Goals and Objectives

The goal of this research is to develop a method of mounting an imaging sonar on a boat. A successful design will be defined as one that does the following:

The sonar mount must…

1. Hold the sonar securely, and in an appropriate position to gather useful data.
2. Have minimal influence on the capabilities of the boat and its crew.
3. Limit damage to the sonar in the event of a collision.
4. Be capable of mounting to a wide variety of vessels.
5. Be designed such that it can be used with autonomous vessels with minimal modifications.

1.3 Scope of Thesis

This thesis will discuss the design and testing of a sonar mount. The mount will be designed with the understanding that more and more autonomy will be necessary in the future. Therefore the mount does not have to be actuated, but it should be designed such that it could be in the future.

1.4 Thesis Outline

Chapter 2 of this thesis discusses the customer needs, and the most important design challenges for this project. It touches on some potential solutions to these challenges and presents three initial concepts, along with a selection process for determining the best concept. Chapter 3 focuses on the design of the concept selected in Chapter 2. It gives a complete description of the prototype, and presents some of the more important computations for the mount. The remainder of the computations can be viewed in Appendix C. It then discusses modeling and testing conducted to characterize the vibration of the pole. Chapter 4 discusses the field tests conducted at Stennis Space Center in 2012 and 2013 and the major findings from these tests. Chapter 5 presents the Bow mount design, with particular focus on the Ball and Socket Breakaway device. Chapter 6 offers some concluding remarks, as well as some suggestions for future research. Lastly, the appendices include a list of design challenges associated with sonar mounts, a detailed cost sheet for the prototype mount, design computations, vibration response functions, a description of the manufacturing process for a fiberglass fairing, MATLAB code, and

permissions. All CAD files, simulations, photographs, and any other document associated with this work can be located in C:\Users\rpearson\My Documents\USV Sonar Mount on the ASCL computer with VT Property Tag VT000376316.

Chapter 2

Initial Concepts

2.1 Development of Customer Needs

As with any design project, one of the first priorities is developing a list of needs the end product must satisfy. Table 2.1 shows a list of customer needs and their respective metrics. These needs were generated based on information gathered in interviews with the USV project's PI, Naval Postgraduate School (NPS) collaborators with sonar and USV experience, and members of the US Navy Seals Special Boat Team 22. Some needs are more important than others, as shown by the rank column. For example, the ability to break away or absorb impacts in some way is important to protect the sonar and boat from damage, while the mount's cost is less important. Ease of retraction is also very important because of the dangerous nature of the situations boat crews may find themselves in. If a fast escape is necessary the sonar mount should not prohibit this action.

Table 2.1: Customer needs for first gen sonar mount

Customer Needs	Metric	Rank
1. Must be safe to use	Customer survey	1
2. Mount needs to be easy to remove from the water	Customer survey	2
3. Need to break away if collision with an obstacle occurs	Binary	3
4. Mount must be durable	Yield strength (N/mm^2)	
5. Mount needs to maintain its rigidity unless collision occurs	Deflection at head (mm)	4
6. Mount must not corrode or rust	Scale (1-3) 1=good, 3=not usable	5
7. Sonar head needs to be at an appropriate depth	Sonar head depth (m)	
8. Mount needs to be easy to service/maintain	Customer survey	6
9. Must be capable of pointing sonar	Binary	7
10. Mount must be lightweight	Mass (kg)	8
11. Mount needs to be easy to install	Customer survey	
12. Mount must be hydrodynamic	Drag force (N)	9
13. Must be inexpensive	USD, Customer survey	10
14. Mount can be used with different types of boats	Customer survey	
15. Mount must be compatible with BlueView P-450-45 Sonar	Binary	11
16. Aesthetic appeal	Customer survey	12

The ranks in Table 2.1 were acquired by comparing each need to the others in a prioritization matrix. This matrix can be viewed in Appendix A. Clearly safety is the top priority, followed by ease of retraction, which has implications for safety as mentioned above. Breakaway capability, durability, and rigidity are also important to protect the sonar and the boat, and to ensure good sonar performance. The less important needs are the mount's aesthetic appeal, its compatibility with the P-450 sonar, cost, its ability to mount to different boats, and its hydrodynamics.

One thing to note about customer need number 15 is that this is a hard requirement for the prototype, but not for the final sonar mount. The P-450 is the sonar used on the NPS USV, and as a result it is well understood. Thus it makes the most sense, both from a time and a financial standpoint, to use it during the prototype stage. An image of the BlueView P-450-45 sonar is shown in Fig. 2.1. It is a 2D multibeam imaging sonar with a 45° field of view, and a maximum range of 137 m (450 ft). It emits 256 individual beams, each with a frequency of 450 kHz and a width of 1°x15°. The update rate can be set as high as 10 Hz [5]. Its cylindrical portion is 10.16 cm (4 in) in diameter.

Fig. 2.1: BlueView P450-45 sonar [6] <"P450 Series 2D Imaging Sonar Data Sheet," BlueView Technologies, Retrieved from http://pdf.nauticexpo.com/pdf/blueview-technologies/p450-series/39788-54947.html.> (used under fair use, 2015)

Initial assumptions were that sonar heading would be manipulated with the use of a commercial waterproof pan-tilt unit, and that the sonar would be operated at a depth of 1 m. These assumptions were made based on current practices on the NPS USV. All initial concepts incorporate the pan-tilt unit, but due to its high cost and added drag it is not used beyond the concept stage. The 1 m depth constraint is used throughout the concept, prototype, and testing stages, but its importance is not well understood. It is well known that sonars perform better at greater distances from the surface due to reduced reflection and scatter of sound pulses from the water-air interface. It is also true that positioning the sonar deeper will increase its chances of hitting the river bottom or submerged objects. To the author's knowledge, the scattering phenomenon and its effect on sonar image quality has not been quantified in a way that allows for the development of design criteria. Ultimately the question of sonar depth becomes a tradeoff, although a poorly understood one, between image quality and sonar protection.

The mount is intended to be universal, but there are two boats that it will need to go on during the development and testing stage which are pictured in Fig. 2.2 below. The left figure is the boat

used for the Virginia Tech USV, which is a 4.9 m (16 ft) rigid hull inflatable boat (RHIB). The right figure is the 9.75 m (32 ft) Navy Special Operations Craft-Riverine (SOC-R).

Fig. 2.2: Ribcraft 4.8 (left) [7] <"Ribcraft 4.8," Ribcraft USA, Retrieved from http://www.ribcraftusa.com/rib48.html.> (used under fair use, 2015), and Navy SOC-R (right) [8] <Powerhouse Systems, Retrieved from http://www.powerhousesystems.net/u.s.-navy-special-warfare-command.html.> (used under fair use, 2015)

2.2 Breaking Down the Problem

Before generating concepts it is helpful to break the design problem into smaller challenges. This enables examination of the problem from a fundamental perspective, making it more manageable, and ensuring better understanding of the overall goal. For the sonar mount design, six design challenges are specified in the form of questions that must be answered. Each question will have a variety of different answers or solutions. While some of these solutions will be more plausible than others, it must be kept in mind that these design challenges are not necessarily independent of one another; how one design challenge is solved may affect how other challenges can be solved. The six design challenges are as follows:

1. Where on the boat should the mount be positioned?
2. How should it attach to the boat?
3. How should retraction be achieved?
4. Where should the motive power come from?
5. How should the sonar be protected from collisions?
6. Are depth adjustments necessary? If so, how should this be achieved?

A detailed description of the pros and cons to the various solutions investigated to answer these questions follows. For a tabular summary, see Table A.1 on page 64.

Location

The question of determining a mounting location is of critical importance. This is because the mounting location has implications for sonar data quality, sensor longevity, and due to potentially large forces on the mounting structure, the structural integrity of the boat. Also, because function dictates form in boat design, a sonar mounting location that is right for one boat may not be appropriate or possible on another. The following locations were considered:

1. Transom
2. Bow
3. Side
4. Hull

The transom is the surface that forms the stern of a vessel. By necessity it is very strong, so it is capable of withstanding large loads. Mounting here also means that the top portion of the pole will experience reduced drag, since it will be located in the low pressure region directly behind the boat. However, it also means that the sonar must be positioned at a depth that is greater than the boat's draft to ensure the FOV is not blocked by the hull. This increases drag and the risk of impact to the sonar. Also, on boats powered by outboard motors, the transom is usually occupied by the motor or motors, leaving little space for anything else. Lastly, mounting at the stern may cause diminished sonar performance due to turbulence and air bubbles from the hull and propulsion system.

The second potential mounting location is the bow. Mounting at the bow is beneficial in that it positions the sonar in front of the hull and propulsion system, thus mitigating their effect. This also removes the need to position the sonar deeper than the hull. Unfortunately the bow has a drawback in that it is often the tallest part of a vessel, which leads to a larger, heavier, and more expensive mount. Furthermore, on the VT RHIB used for testing, there is no structure at the front of the boat strong enough to mount to without heavy modifications to the fiberglass hull.

Mounting to the side of a vessel was the third location considered. This is the best option in terms of being able to mount to both the VT USV and Navy SOC-R. Like the bow position, mounting at the side places the sonar in front of the propulsion system, but it is lower to the water, and is more likely to have useful structures to mount to. Thus it is a compromise between sonar performance and ease of implementation. However, the sonar still needs to be positioned below the hull to have an unrestricted FOV.

The last location considered was mounting directly to the hull. In this case we are considering somehow fixing the sonar directly to the hull in a permanent or semi-permanent fashion. By necessity, this means that the device would need to be streamlined and as small as possible to minimize adverse effects on boat dynamics. The advantages of such a system are not insignificant. This option would be the smallest, and would probably have the least impact on the capabilities of the boat and crew. It would require minimal mechanical maintenance, use no deck

space, and would be very easy to use. Unfortunately a hull-mounted sonar is not feasible as an add-on to an existing vessel. It would be very difficult to protect the sonar from impacts, and hull proximity may negatively affect sonar images. It would also make troubleshooting the sonar very difficult as it would be inaccessible unless the boat were trailered. For these reasons the hull-mounted sonar was not considered for prototyping, but it is conceivable that many of the downsides associated with a hull-mounted sonar could be mitigated if the hull were designed from the beginning with the intention of integrating a sonar.

Attachment Method

How the mount is attached to the boat is another important challenge that will depend largely on the boat being used. Some vessels will have a wide variety of strong points available, while others, like the VT USV, have very few. Thus there will not be a single solution for the sonar mount, but rather a family of solutions that may be employed depending on the boat being used. The six attachment methods investigated were the following:

1. Rare earth magnets
2. Suction cups
3. Pipe clamps
4. U-bolts
5. C-clamps
6. Scissor clamps

Two neodymium magnets could be used to clamp down on the side of the boat to fix the mount in place. While these would be strong and easy to use, they require a thin wall for maximum clamping, and may not be strong enough to hold the mount during a breakaway. Suction cups were also considered and have similar strengths, and do not require a thin wall. They do however require a smooth clean surface in order to work properly. But even in the best case they may still lack the necessary strength to hold the mount securely during a breakaway event. Fig. 2.3 shows an example of the suction cups and magnets considered.

Fig. 2.3: High strength suction cups (left) [9] <"Hand-Held Suction-Cup Lifter: Aluminum Handle, 3 Cups, 220 Pound Lift Capacity," McMaster-Carr, Retrieved from http://www.mcmaster.com/#5608a91/=z2vc4g.> (used under fair use, 2015), neodymium magnet (right) [10] <"Cylinder Magnets: DZ0X8-N52," K&J Magnetics, Inc., Retrieved from https://www.kjmagnetics.com/proddetail.asp?prod=DZ0X8-N52.> (used under fair use, 2015)

Pipe clamps and clamping U-bolts are an alternative that would be very strong, but they require a strong rail to mount to, which not all vessels will have. Fig. 2.4 depicts an example of these two methods.

Fig. 2.4: Pipe clamps (left) [11] <"Shaft Mounting Collars 2-Piece Stackable," Stafford Manufacturing Corp., Retrieved from http://www.staffordmfg.com/Product-Categories/Shaft-Mounting-Collars-2-Piece-Stackable.> (used under fair use, 2015) and clamping U-bolts (right) [12] <"83mm / M8 U BOLT EXHAUST CLAMP WITH NUTS PIPE CLAMPS TUBE CLIPS CONNECTORS," eBay, User ID: armartradingltd, Retrieved from http://www.ebay.co.uk/itm/83mm-M8-U-BOLT-EXHAUST-CLAMP-WITH-NUTS-PIPE-CLAMPS-TUBE-CLIPS-CONNECTORS-/321332404796.> (used under fair use, 2015)

C-clamps and scissor clamps would also be very strong, easy to use, and easy to adjust, but could crack hulls made of more brittle materials like fiberglass. Bolts are also an option. They have major advantages in that they are the strongest and also the cheapest option, but they may require modifications to the boat, and would likely be difficult to adjust.

More permanent methods of fixing the mount, like welding, brazing, or epoxies, could also be utilized, but these were not considered for the prototype because they restrict our ability to remove it from a boat once it is attached. For the final recommendation these methods will not be ruled out, but it is understood that mounting in this way could have negative consequences for some customer needs, particularly with ease of installation and mounting to different vessels.

Retraction Method

The method of retraction is important because it will have significant safety and cost implications. The six retractions considered can be classified into three types: linear retraction; rotational retraction; and four-bar linkage.

In the linear retraction category a telescoping method, a linear slide, and a large ball screw were examined. All three categories share the ability to easily adjust the sonar depth, especially if they are actuated and can be controlled remotely. Ball screws will be much stronger than necessary, slow, and expensive, making them a poor choice. The linear slide and telescopic methods will be faster, but will not be as strong as a single pole. Linear slides and telescopic mechanisms can also be rendered useless if dented or bent, and will be difficult to make hydrodynamic.

In the rotational retraction category rotations about the roll axis and the pitch axis were considered. Rotation about the pitch axis is best because breakaway will most likely occur about this axis. If retraction instead occurs by rotation about the roll axis, a degree of freedom is added which must be constrained, needlessly complicating the mount.

The last retraction method considered is the four bar linkage. This is an attractive option because it is very strong, and also because the sonar and mount can be made to retract completely inboard. The sonar mount in use on the NPS USV is a four bar linkage. The major downsides to this type of retraction are that it is much heavier and more complex. It also requires much more cutting and welding, which will significantly increase costs.

Motive Power (Retraction)

Five types of motive power were considered for retraction. They are:

1. Motor and gearbox
2. Linear actuator
3. Pneumatics/hydraulics
4. Cable and winch
5. Manpower

A motor and gearbox combination should have plenty of torque to retract the sonar regardless of which retraction method is used. Such a combination can also be geared to work quickly. Motors and gearboxes are fairly expensive though, and need to be tolerant of splashing at a minimum. Therefore the Ingress Protection (IP) rating for any components on the mount must be at least IP65. Linear actuators are simple and cheap, and come with various IP ratings to withstand water. Their one drawback is that they are relatively slow. Pneumatic/hydraulic systems have the benefit of being fast, but require a compressor/pump, tanks, and high pressure lines, are difficult to setup, and expensive. A cable system with a winch is a promising solution as water resistant

winches are common. They can also be set up with a block and tackle to give a mechanical advantage. But again the setup may be difficult. There are also safety concerns with having highly tensioned cables that could break or become tangled. The last option considered is manpower. This is likely the most foolproof source of power. It is both simple and effective, but will almost certainly require some mechanical advantage, either in the form of a lever or crank. It must also be kept in mind that future trends will be toward greater and greater vehicle autonomy, so if a manual retraction is chosen, it should be done in a way that would allow for the motion to be actuated without major design changes.

Collision Protection

Protecting the sonar from collisions is a high-level priority. Five solutions were considered: two are nondestructive; and three incorporate a "mechanical fuse". The mechanical fuses considered were an acrylic block, shear dowel, or shear bolt. All shared the common trait of failing in shear. Mechanical fuses possess the advantage of being cheap and simple, but they require replacing the fuse after a breakaway. The shear bolts have the advantage of coming in a standard size with a nut to secure them in place.

The two nondestructive devices considered were a torque limiter and rare earth (neodymium) magnets. Both would be used to carry the moment induced by sonar drag. Torque limiters are devices typically used in machinery to protect a motor or other rotating equipment from torque overloads. Fig. 2.5 shows a cutaway rendering of a torque limiter. They act to limit the amount of torque a drive shaft will transmit with the use of spring-loaded ball bearings. The ball bearings fit into depressions which rotate with the driven shaft. When the torque from the drive shaft to the driven shaft exceeds the torque limiter's specification, the bearings are forced into the springs, compressing them. This causes the bearings to slip out of their depressions, allowing the two shafts to slip relative to one another until the torque is reduced.

Fig. 2.5: Cutaway rendering of a torque limiter [13] <"EAS®-smartic® Installation space-optimised torque limiting clutches," [Product guide] Mayr, Retrieved from http://www.industrialclutch.com/pdf/mayr-eas-smartic.pdf.> (used under fair use, 2015)

Neodymium magnets are beneficial in that they require no power, are available in a variety of sizes, and can exert upwards of 1530 N (344 lbs). Mounting one magnet to a rigid surface, and another to the sonar pole such that they would come in contact when the sonar were deployed, would act as an overload protection.

Both magnets and torque limiters have the advantage of not requiring the user to replace a part each time the sonar breaks away. Neodymium magnets could be very effective, but care would need to be taken to ensure they were safe, as clamping forces are very high. Torque limiters pose much lower risk, but they are very expensive and heavy for high torque applications.

Depth Adjustments

One important parameter for any sonar mount is sonar depth. It is well known that the closer a sonar is to the surface, the worse it performs. This is because the sound pulse reflects off of the water-air interface leading to scatter and inaccuracies in positioning and ranging. For this reason some method of depth adjustment is necessary. Based on current practices on the NPS USV, a depth of one meter must be achievable, but the importance of this constraint is poorly understood. Four possible solutions were considered:

1. Telescoping tube sections
2. Linear slide
3. Interchangeable sections of varying length
4. Single long tube fixed with pipe clamps

Telescoping tube sections would be extremely convenient in that they would allow users to make depth adjustments quickly and on the go. This convenience could be magnified with an actuated telescope. However, since a telescoping tube will be weaker than a single tube, it must be larger and therefore heavier and much more expensive. A linear slide would provide similar functionality, but it limits the shape of the post. It will also be expensive. Interchangeable sections could be useful in limiting the weight of the installed mount, but cannot be adjusted easily, and require storage for the unused tube sections. Lastly, a single tube section fixed with pipe clamps was considered as it has fewer moving parts, is simpler, and therefore more universal. However, it is also limited in that adjustments require tools, which makes them difficult to make while underway.

2.3 Concept Generation

Three concepts were designed with the customer needs in Table 2.1 in mind. There are two common features for all of the concepts. Each design incorporates a commercial pan-tilt unit to

allow the sonar to be manipulated independently. Also, to satisfy the need for the mount to be hydrodynamic, the sonar pole consists of three poles constrained by ribs. This structure is designed to have a metal or plastic skin around it to reduce drag. This feature will be discussed in more detail in Chapter 3.

Design 1, shown in Fig. 2.6, bolts to the transom and retracts with a cable and winch. The winch is mounted to a support structure that bolts to the transom. In the deployed position, the pole is held in place with a latch, the striker of which is made of a soft material that will break if the sonar strikes an object. When retracting, tension in the cable releases the latch, and then pulls the sonar out of the water. Not shown in the figure is the skin around the support poles which acts to reduce drag.

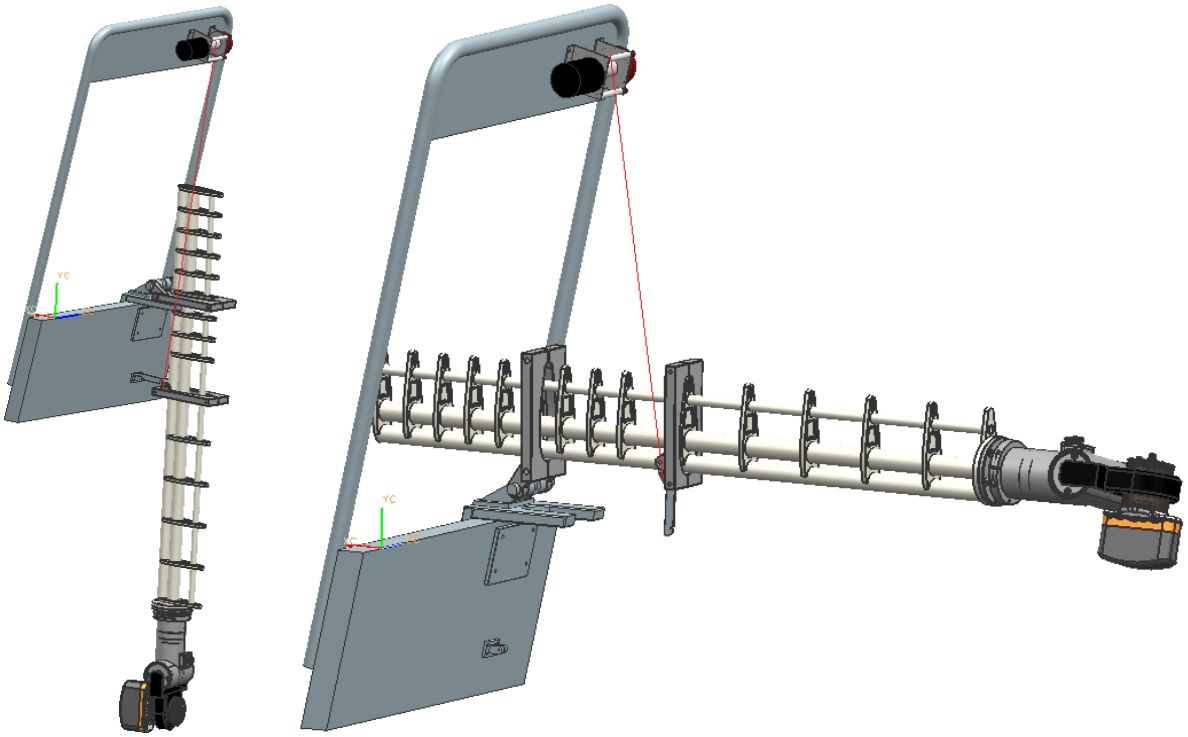

Fig. 2.6: Transom mount with winch retraction. Deployed on left, retracted on right

Design 2 is shown in Fig. 2.7. As its name implies, Design 2 mounts to the side of the boat along the gunnel. Retraction occurs about the pitch axis, and is achieved with a linear actuator acting on a lever. The sonar is protected via a shear bolt at the base of the lever. The breakaway mechanism is discussed in more detail in Section 3.4. Design 2 has the advantage of being positioned in front of the propulsion system, and of positive positioning during both deployment and retraction.

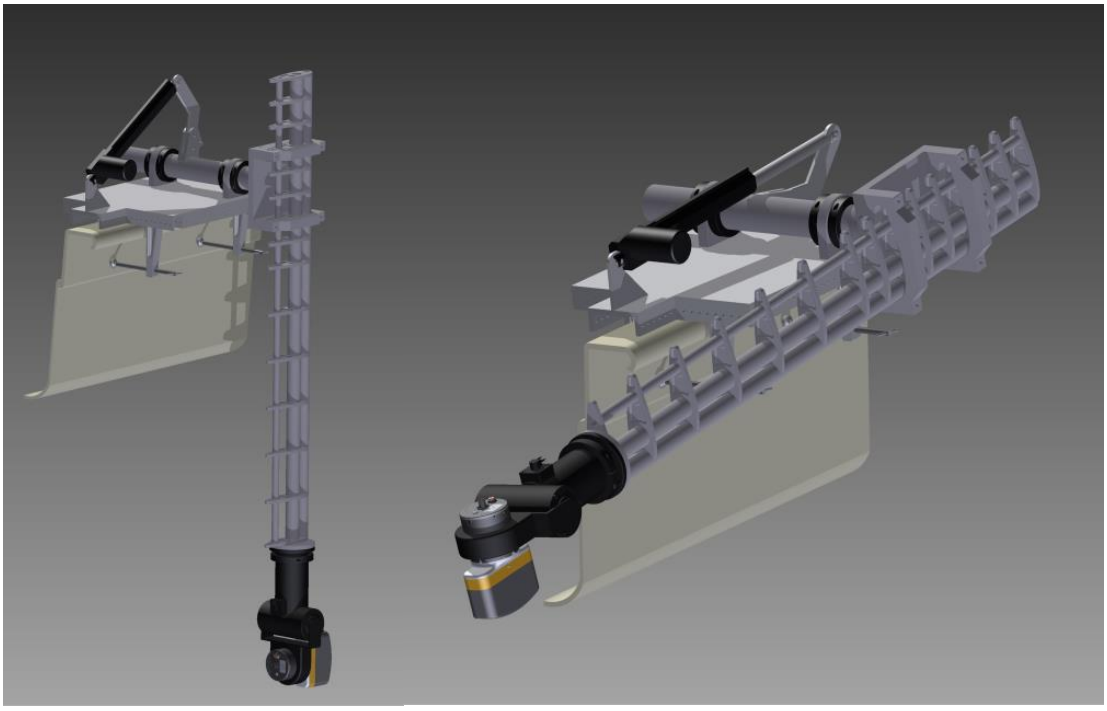

Fig. 2.7: Side mount with linear actuator for retraction (Image courtesy of Kevin Kline, 2015)

The third design concept is a four-bar linkage that retracts with a cable and winch. This design was based on the sonar mount used by the Naval Postgraduate School on their Sea Fox USV. The Sea Fox sonar mount is shown in Fig. 2.8 below. The top photo shows the mount in the retracted position and the bottom photo shows it in the deployed position. The vertical pole of the Sea Fox mount is capable of breaking away after an impact. This is accomplished with a shear pin which fits through a tab welded to the top of the pole.

Fig. 2.8: Naval Postgraduate School's Sea Fox USV with 4-bar linkage sonar mount (Image courtesy of Sean Kragelund, 2015)

Fig. 2.9 shows the four-bar linkage design for the VT USV. The structure attaches to the side of the boat using two large clamps. Retraction is accomplished with a winch and cable. As with the Sea Fox mount, breakaway occurs about the pitch axis.

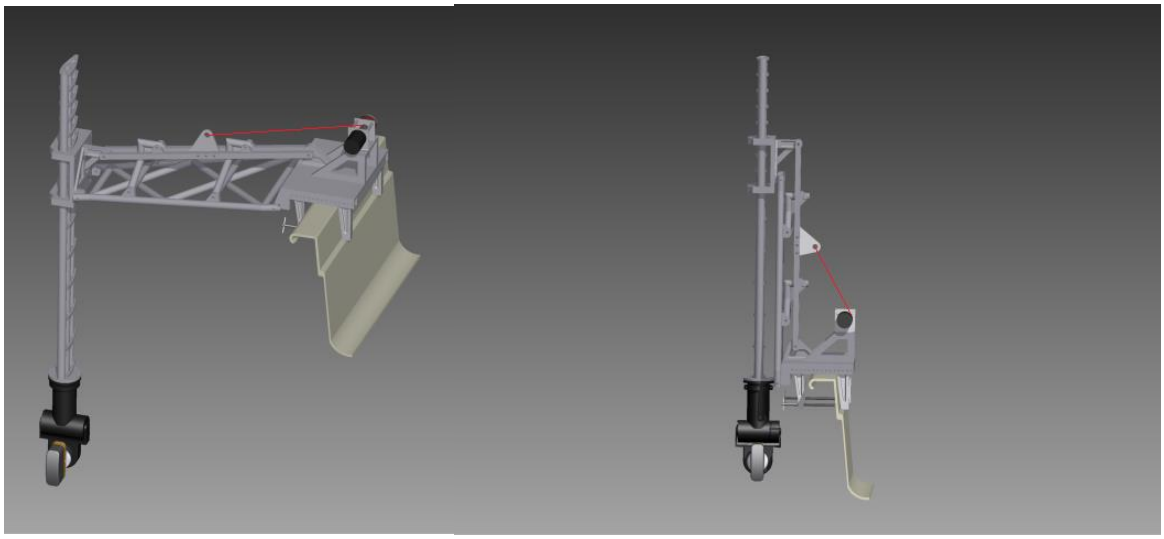

Fig. 2.9: Side mount with four-bar linkage (Image courtesy of Kevin Kline, 2015)

2.4 Concept Selection

With the concept designs completed, determining which concept best meets the customer needs is the next step. Table 2.2 shows a detailed concept selection matrix for the first generation sonar mount. Each design concept was given a score from 1 to 3 based on how well it satisfies the objectives listed on the left of the table relative to the other designs. Weights for each objective are taken from the prioritization matrix in Appendix A.

One notable difference between the designs is in their durability. Design 1 scores well in this category because it is the simplest design and has the fewest parts. This also means it will be easier to maintain and install. Because it mounts very close to the boat, it should induce the lowest yaw moments of any of the designs. Another important difference between the designs is in their ability to mount to different boats. Design 1 mounts to the transom, which is a very strong feature that almost all boats have in common. Designs 2 and 3 both mount to the side, but due to the longer moment arm of Design 3, its mounting structure must be stronger. This makes Design 3 more expensive and difficult to add to an existing vessel.

There is also a scoring difference in ease of retraction. Design 2 scores highest here because the other designs use cables to retract. Cables could become frayed or tangled, leaving the retraction system ineffective. Another limitation with cables is that deployment is achieved with the weight of the sonar and pole, which may make deploying while underway difficult. Safety is also an area where not all of the designs are created equal. The major problem with Design 1 is with its position. The transom is often a crowded area, especially on boats powered by outboard motors. For some vessels there may not be enough room to mount to the transom, and doing so could

result in damage to the propulsion system. Design 2 scores highest on this objective because it does not infringe on the limited transom space, and it experiences lower moments relative to Design 3.

The last objectives of note are the weight and expense. Design 1 is simplest and has few parts, which make it both lightweight and inexpensive. Design 3 requires more material and a large amount of welding, so it will be the most expensive.

Table 2.2: Concept selection matrix for first gen sonar mount

		Design					
		1		2		3	
Objectives	**Weight (%)**	**Score**	**Weighted Score**	**Score**	**Weighted Score**	**Score**	**Weighted Score**
Hydrodynamic	4.58	3	13.73	3	13.73	3	13.73
Breakaway	8.24	3	24.71	3	24.71	3	8.24
Durability	8.24	3	24.71	2	16.48	1	8.24
Depth	6.41	2	12.81	2	12.81	2	12.81
Mounts to different boats	3.89	3	11.67	3	11.67	2	7.78
Rigid	7.78	3	23.34	3	23.34	2	15.56
Ease of retraction	9.61	2	19.22	3	28.83	2	19.22
Easy to maintain	6.18	3	18.54	2	12.36	2	12.36
Easy to install	5.26	3	15.79	2	10.53	2	10.53
Corrosion	6.41	2	12.81	2	12.81	2	12.81
Safe	11.67	1	11.67	3	35.01	2	11.67
Aesthetic appeal	3.20	2	6.41	2	6.41	3	9.61
Lightweight	5.26	3	15.79	2	10.53	1	5.26
Compatible with P-450-45 sonar	3.43	2	6.86	2	6.86	2	6.86
Steerable sonar	5.95	2	11.90	2	11.90	2	11.90
Inexpensive	3.89	3	11.67	2	7.78	1	3.89
Total	**100.00**		**229.98**		**237.99**		**194.74**

We see from the table that Design 2 scores highest, Design 1 is just below, and Design 3 comes in a distant third. The score of Design 2 is driven mainly by its safety and ease of retraction relative to Design 1, which are the top two customer needs. Low scores of Design 3 are attributed to its high cost, complexity, weight, and large bending moments. Design 1 scores very well on many objectives due to its simplicity, but it may be unwise to assume the transom will have available space on most boats.

2.5 Conclusions

The preceding chapter discussed the generation of a detailed list of customer needs for a sonar mount. Each need was compared to the others in a prioritization matrix to quantify their relative importance. The design problem was broken into smaller sub-problems, and pros and cons of each potential solution to these sub-problems were examined. These sub-problems are important because they allow for a design independent formulation of the problem. These sub-problems will need to be either solved or bypassed for any sonar mounting solution. After clarifying the problem and a discussion of sub-problem solutions, three detailed concepts were presented. These concepts were compared based on how well they satisfy the customer needs. Final scoring revealed that Design 2 best meets the customer needs.

Chapter 3 discusses the design and lab testing conducted on the prototype sonar mount.

Chapter 3

Prototype

3.1 Prototype Overview

Fig. 3.1 depicts the prototype sonar mount. The design incorporates a universal base plate which is reinforced with 80/20® slotted aluminum for strength. Slotted aluminum was chosen because it allows for a wide variety of mounting configurations. This ensures the mount can be used on many different boats while keeping necessary modifications to a minimum. As mentioned earlier, the mount retracts and deploys the sonar with the use of a linear actuator which pushes on a lever attached to the horizontal tube in the figure. At the base of the lever is a breakaway mechanism which acts as a mechanical fuse. If the sonar is loaded too heavily, the fuse breaks and the vertical tube is allowed to rotate back (clockwise in the figure). This breakaway system is discussed in more detail in the following sections. The horizontal tube has a flange on each end, and is supported by two bushing blocks, with a split plastic bushing in each. The horizontal tube connects to the vertical tube via a plate with a bolt pattern matching that of the flanges; the vertical tube is then secured to this plate with two steel pipe clamps.

The vertical tube is actually made up of an outer structural tube which is visible, and a smaller inner tube which is capable of rotating on bearings which are press fit in the ends of the outer tube. The inner tube protrudes slightly from the top and bottom of the outer tube, and is secured with pipe clamps. The purpose of the inner tube is to give the user the capability to point the sonar independently of the boat. This is accomplished with a motor and gearbox attached to the top of the outer pole. The motor and gearbox solution was chosen over the pan-tilt solution because it is much cheaper. The orange object in the figure is a fiberglass and foam fairing which reduces drag on the tube. This fairing is free to rotate 360° around the outer pole, which allows it to maintain a low angle of attack at all times. Lastly, the sonar is clearly visible at the bottom of the figure. It is mounted in a Delrin® clamp attached to an aluminum bracket which attaches to the smaller inner tube. The sonar can be mounted in either a vertical (as shown) or horizontal configuration, depending on the operating environment and what is to be measured. The sonar is also capable of being manually tilted by adjusting the bolts connecting the aluminum bracket to the inner tube.

All components in the sonar mount are made of 6061-T6 aluminum to withstand both salt and fresh water environments. Alloy 6061-T6 was chosen for its high availability, strength, and good machinability. All hardware is either 316 stainless steel or galvanized steel. Due to lack of availability, the bearings are not stainless, but are double sealed to keep out contaminants. All

motors, actuators, and gearboxes have an ingress protection rating of IP65 or better. A bill of materials for the prototype mount can be viewed in Appendix B.

The following sections will discuss in greater detail the reasoning behind the design decisions introduced above. A few of the more important calculations are presented here. The remainder are included in Appendix C.

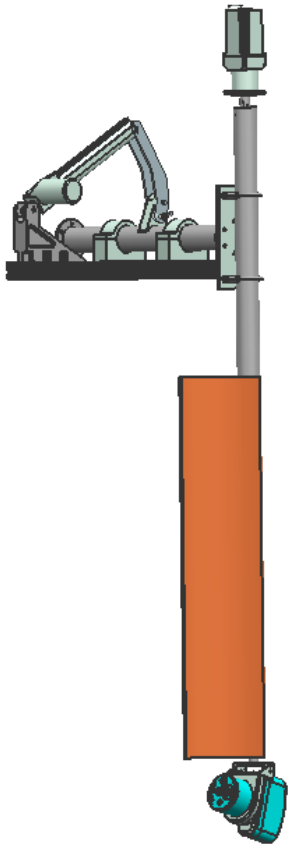

Fig. 3.1: Prototype sonar mount

3.2 Estimating Hydrodynamic Drag

Estimating the hydrodynamic drag on the sonar and sonar mount is one of the single most important considerations for the design of the mount. Hydrodynamic drag is responsible for the largest forces present other than those from an impact. This section presents an overview of the drag computations performed and their results. More detailed calculations can be found in Appendix C.

One important question with regards to computing drag is: what speed will the sonar and sonar pole be moving through the water? Answering this question depends largely on the performance of the sonar. Sonar performance diminishes with increased flow velocity as turbulence and cavitation begin to cause self-noise, resulting in noisy data. Also, because of the relatively slow speed of sound in water compared to the wave speeds of other sensors like RADAR or LIDAR, higher boat speeds mean that the sonar travels much farther between each transmit-receive cycle. Depending on the range setting of the sonar, these long transmit-receive cycle times can result in delayed display updates. Unfortunately the effect of flow speed on sonar imagery is sonar dependent, and not something that is typically quantified in sonar documentation. It is therefore up to the user to determine by experience how fast is too fast. For the purposes of design, an arbitrary speed of 5.14 m/s (10 kt) is assumed.

A simplified drawing showing the underwater components of the mount is shown in Fig. 3.2. The drawing shows the 63.5 mm (2.5 in) diameter pole, the sonar, modeled as a rectangular prism, and a bracket attaching the sonar to the end of the pole. Also present are the lengths and depths required for analysis.

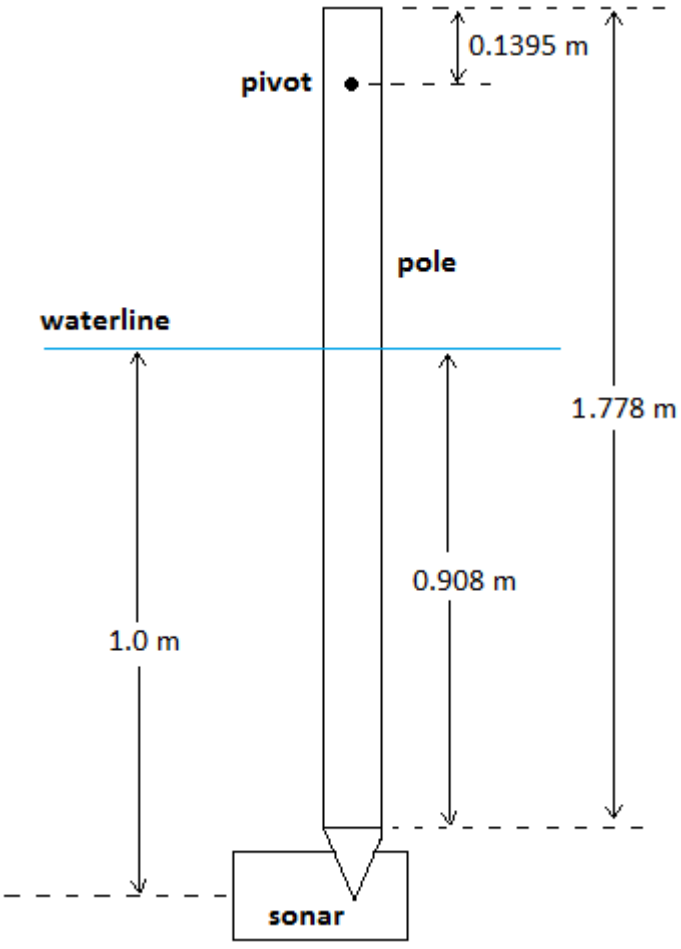

Fig. 3.2: Dimension drawing of a sonar and pole

To compute the drag on the sonar and pole of Fig. 3.2, the following simplifying assumptions of Table 3.1 are used.

Table 3.1: Assumptions used to simplify drag calculations

1. The drag on the sonar and pole can be computed independently of one another, with the total drag simply being the sum of the two forces.
2. The center of pressure for each body acts at the centroid of its submerged portion.
3. The front of the sonar will be modeled as a rectangular prism. The back will be modeled as a cylinder.
4. The brackets and clamps holding the sonar, and the sonar's cables will be accounted for with a correction factor applied to the computed sonar drag

These assumptions are approximations. The sonar and pole will not experience drag independent of one another. The flow around the sonar will affect the flow around the pole and vice versa, which will affect the location of the center of pressure for each body. Referring to Fig. 2.1, it is clear that the sonar is not a rectangular prism, so representing it in this way does not reflect reality. Despite these simplifications, the above assumptions are expected to result in numbers that are higher than the actual values. Because a failure of the mount would be far worse than the extra cost and weight of a larger mount, this tradeoff is deemed acceptable.

To compute the drag acting on the pole, we must first compute the Reynolds number using Eq. (3.1).

$$Re = \frac{\rho u D}{\mu} \tag{3.1}$$

Where ρ is the density of water, u is the velocity, D is the diameter of the pole, and μ is the dynamic viscosity. Using the design velocity of 5.14 m/s (10 kt) gives $Re = 3.25 \times 10^5$. For this Reynolds number the coefficient of drag for a smooth cylinder is taken from Figure 9.21 in [14] and has a value of 0.8. The drag force acting on the pole is computed from

$$F_{dB} = C_{dB} \frac{1}{2} \rho u^2 D l \tag{3.2}$$

Where C_{dB} is the coefficient of drag, and l is the submerged length of the pole. F_{dB} is found to be $F_{dB} = 609.2\ N\ (137\ lb)$.

Computing the drag acting on the forward facing sonar is not quite as straightforward and requires some simplifying assumptions. Due to its complex geometry, it is not feasible to analyze the sonar in its actual shape. The sonar is modeled as a rectangular prism with the dimensions shown in Fig. 3.3. These dimensions reflect the full frontal area of the sonar extended back for its entire length.

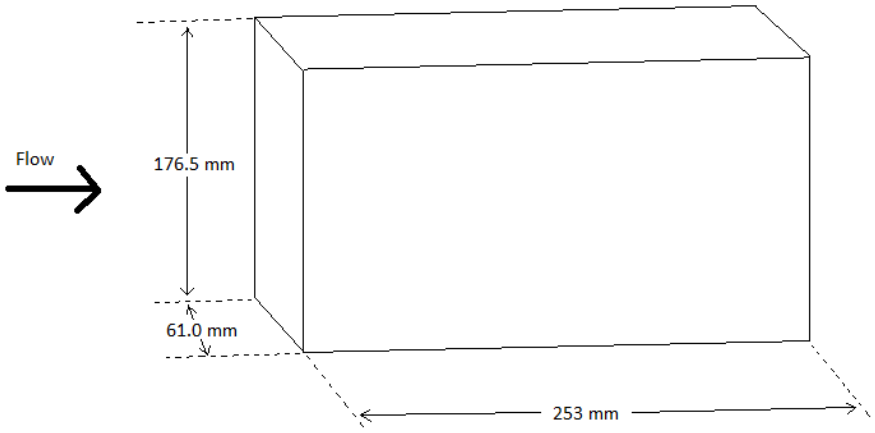

Fig. 3.3: Dimensions of rectangular prism used to represent sonar

To determine the drag force on the sonar, we must obtain the coefficient of drag. Studies conducted on 3D flow around rectangular prisms have found that for high Reynolds number flows ($Re > 10^5$), the coefficient of drag on a rectangular prism is highly dependent on the chord to depth ratio [15]. For a chord to depth ratio of $253/176.5 = 1.43$, we find the coefficient of drag to be 1.74 (see Appendix C, pg. 73 for details). The drag force is computed using the following equation.

$$F_{ds} = C_{ds}\frac{1}{2}\rho u^2 A f \tag{3.3}$$

where A is the frontal area of the sonar, and f is a correction factor accounting for the brackets and cables and is taken to be 1.2. Due to the small size of the brackets and cables relative to the sonar, it is not expected that they will increase drag by more than 20%. The drag force on the sonar is found to be 300 N (67 lb). So with the pole and sonar moving through the water at 5.14 m/s, the total drag is 910 N (205 lb).

The sonar will not always be facing forward due to the fact that it is steerable. For this reason the analysis above represents the most common case, but not the worst case. The worst case sonar drag will occur when it is facing 90˚ from the boat heading. Fig. 3.4 shows the sonar dimensions used in the analysis. The worst case flow is into the page. Due to the sonar's complex shape, assumptions 1, 2, and 4 in Table 3.1 are used to simplify the analysis. These assumptions allow the sonar's component shapes, a rectangular prism and a cylinder, to be analyzed independently. These two shapes have been tested extensively, making drag data much easier to find.

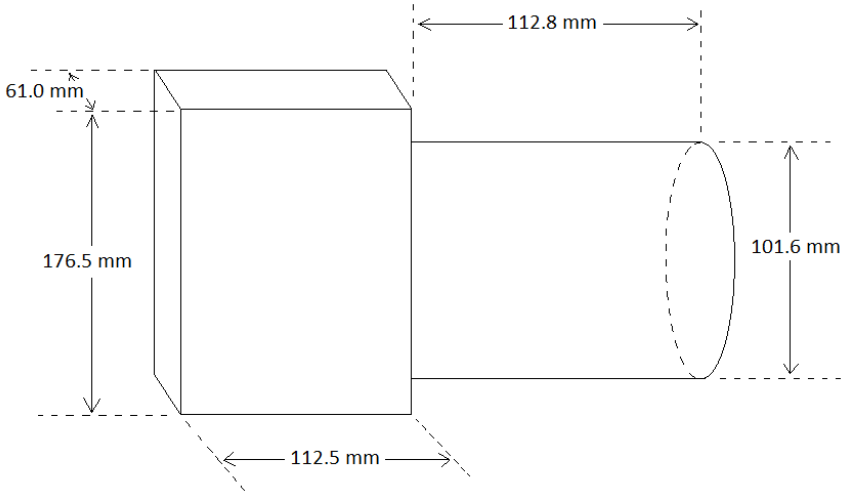

Fig. 3.4: Dimensions of sonar head for worst case analysis. Worst case flow is into page.

The worst case sonar drag is found to be 641.1 N (144.1 lb), which is actually greater than the pole drag, and more than twice the drag for a forward facing sonar. This means that at the design speed, total worst case drag on the mount is 1250 N (281 lb). Making use of assumption 2 in Table 3.1, this force is centered at a depth of 0.73 m, or 1.46 m from the pivot. Because this moment arm is so large, it leads to very large bending stresses in the pole. For this reason it is prudent to examine ways to decrease the total drag.

Decreasing drag on the sonar is possible, but due to its irregular shape it would be very difficult to reduce its drag for all potential orientations. It is also possible that placing structures near the sonar may negatively affect its performance. For these reasons the pole is the best candidate for drag reduction. The following section details the fairing designed for this purpose.

3.3 Fairing Design

There were two fairing designs that were considered to reduce the drag on the sonar mount's pole. The first consisted of three pieces of 6061-T6 aluminum tubing of varying sizes arranged one behind the other. At regular intervals, the tubes would be captured by ribs with an airfoil shape. A thin sheet of either plastic or metal would then be wrapped around the ribs and sealed to produce a smooth wing. Fig. 3.5 shows a rendering of the design with the skin removed. While this design is very robust and reduces drag considerably for flows with a low angle of attack, it is also very heavy, expensive, and greatly increases forces on the mount for high angles of attack. This could be especially problematic during turns, or when the boat is facing perpendicular to a current. For these reasons this first design was deemed unsuitable.

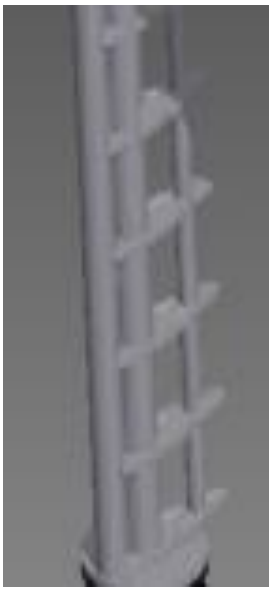

Fig. 3.5: Metal airfoil design (Image courtesy of Kevin Kline, 2015)

The second design, shown in Fig. 3.6, solves many of the problems with the first. The number of tubes is reduced to one, greatly reducing weight, and removing the need for ribs and clamps with complex geometry. The fairing portion is made of fiberglass with a foam core. It slides over the pole and is unfixed, so it can rotate freely depending on the direction of flow. This ensures that the angle of attack remains low at all times. The leading edge of the fairing is designed such that it is backed by the aluminum sonar pole, making it more durable against impacts.

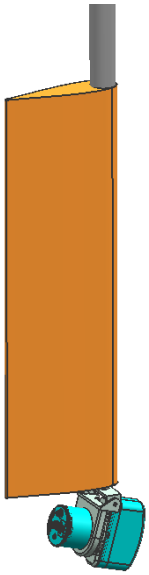

Fig. 3.6: Sonar pole with fiberglass fairing

One other benefit of the fiberglass and foam core fairing is that it is fairly simple to build. It requires only construction foam, glue, a 2.6 inch (66 mm) OD fiberglass tube, some method of

shaping foam, and fiberglass layup supplies. This simplicity allows it to be produced in-house, which helps reduce the overall build time and cost of the mount. A brief description of this process can be viewed in Appendix E.

With the new fairing design the drag was recalculated using results from an analysis performed in NASA's FoilSim III, an educational tool for modeling flow around airfoils [16]. It should be pointed out that FoilSim includes a disclaimer stating that its analysis is not rigorous enough to use for airplane wing design. However, the drag data it produces are interpolated from experimental data, and should be close enough for non-life-threatening situations. FoilSim predicts a drag of 98 N/m for the fiberglass fairing. The drag on the pole is estimated to be 89 N (19 lb), which is a reduction of 85% compared to the unfaired pole. With the faired pole and sonar moving through the water at 5.14 m/s, the total worst case drag is now 730 N (164.1 lb), centered at a depth of 0.933 m, a reduction of 42% compared to the worst case drag without a fairing. The moment at the sonar pole pivot is now of 1214.8 N-m.

3.4 Breakaway Mechanism

In the inland waterways the boat is expected to operate in, submerged rocks, logs, sand bars, and other obstacles are a common occurrence, and even with the best obstacle detection and control algorithms it can be assumed that the sonar will occasionally strike an object. The high-end imaging sonars required for mapping and obstacle avoidance are also very expensive, ranging from tens to hundreds of thousands of dollars. For these reasons, a breakaway mechanism is needed to protect the sonar from damage during an impact.

Three classes of solution to this problem were investigated: torque limiters; rare earth magnets; and mechanical fuses. One of the advantages of magnets and torque limiters is that they are nondestructive. If an overload occurs, the obstruction simply needs to be cleared, and then the sonar pole can be reset. However, torque limiters with the required torque capacity are very expensive, large, and heavy, and strong magnets are difficult to work with, and could be hazardous to hands and fingers. For these reasons the decision was made to use a mechanical fuse, but its material needed to be determined. A description of the mechanism is given below, after which the shear calculations is presented.

Fig. 3.7 shows the breakaway device. Body A in the figure is the linear actuator. It is attached to the lift bars (body B). The lift bars attach to the lift tab (body C), which is welded to the horizontal tube. The lift bars attach to the lift tab with two steel pins (body D) and a nylon shear bolt (body E). Viewing the mechanism from the left in the figure, along the axis of the horizontal tube, a clockwise torque on the tube will apply a shear load to the shear bolt. When the shear bolt's strength is exceeded, it breaks, and the horizontal tube rotates about its axis, while the lift bars are allowed to rotate about the upper steel pin. The mechanism then comes to rest in the

configuration shown in Fig. 3.8. To lift the sonar pole out of the water, the linear actuator is extended, which causes the lift bars to rotate about the upper steel pin until the lower steel pin contacts the face of the lift tab. The sonar pole then begins retracting. This functionality enables the sonar to be retracted without manual intervention after a breakaway, which allows the helmsman to remove the boat and crew from a dangerous situation without worrying about losing the sonar.

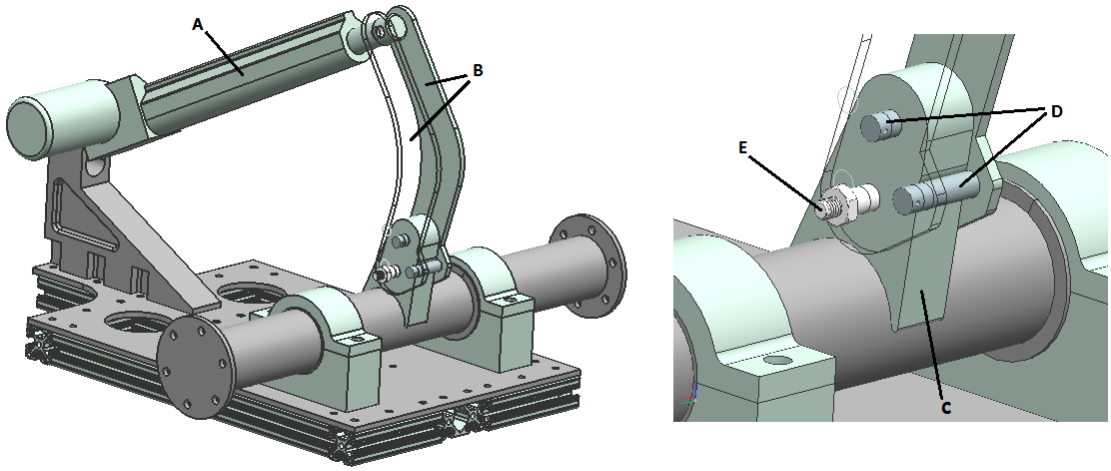

Fig. 3.7: First generation breakaway mechanism

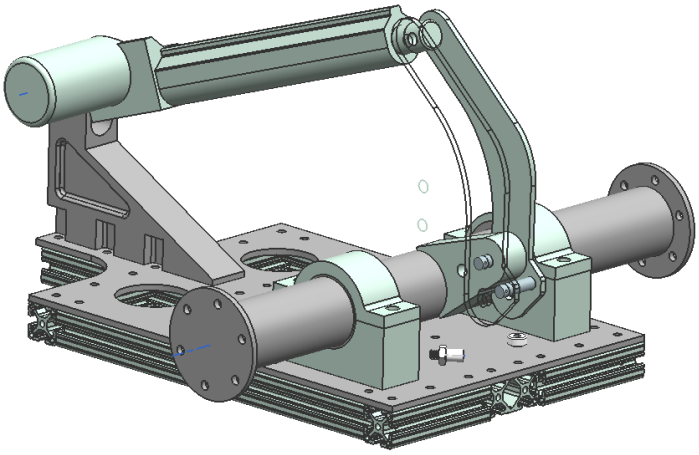

Fig. 3.8: Breakaway mechanism after breakaway

Determining the best choice for the shear pin material requires the calculation of the shear stress on the pin. Fig. 3.9 shows the free-body diagram for the lift bars when the sonar is deployed. See Appendix C page 78 for details about the force F_A. It is assumed that the two lift bars experience identical loads so that they can be modeled as a single lift bar. However, the shear pin is in double shear. All connections are assumed to be ideal pin connections and do not transmit moments. A shear pin diameter of 12.7 mm (0.5 in) is assumed, as this size should be a readily

available in a variety of materials. Lastly, the forces F_B and F_S are assumed to act perpendicular to an imaginary line connecting the center of their respective holes.

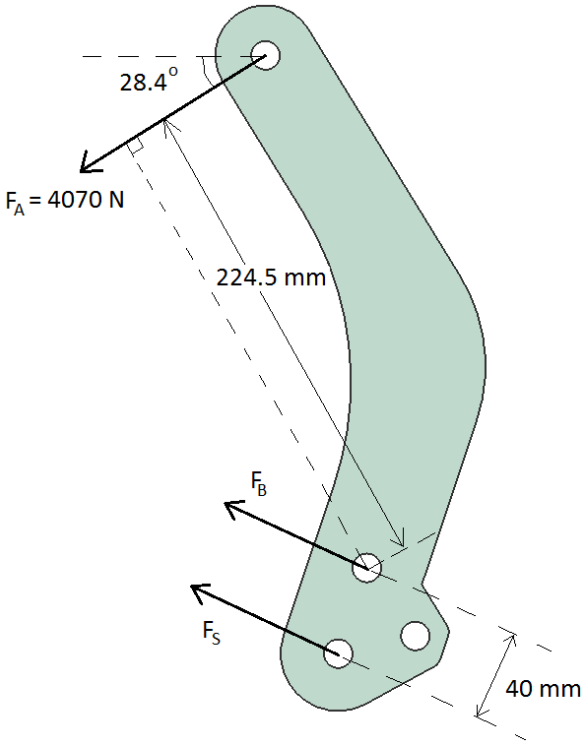

Fig. 3.9: Free-body diagram for lift bar

In this problem there are two unknowns F_B and F_S. To solve for the shear force F_s we can balance moments about the pin at F_B as follows, taking counterclockwise as positive.

$$4070\ N(0.2245\ m) - F_s(0.04\ m) = 0$$

$$F_s = 22843\ N$$

Assuming pure shear, computing the shear stress on the shear pin is then straightforward using the following relation

$$\tau = \frac{F}{2A} \tag{A.1}$$

Where F is the shear force, and A is the cross sectional area of the shear bolt. It is important to remember that there are two lift bars, requiring the bolt to shear in two places. This accounts for the factor 2 in the denominator. The shear stress is:

$$\tau = \frac{22843\ N}{2(\pi(0.00635\ m)^2)} = 90\ MPa$$

Some potential shear pin materials are listed in Table 3.2 below. Due to a lack of available shear strength data for some materials, we make the common assumption that a material's shear strength is roughly equivalent to 60% of its tensile strength. However, where data are available they are used.

Table 3.2: Potential shear pin materials. Values from [17] <McMaster-Carr, "More About Plastics," http://www.mcmaster.com/#8574kac/=v1bwlt, 15 Dec. 2014> unless otherwise noted (used under fair use, 2015)

Material	Tensile Strength Ult., MPa*	Shear Strength**
Brass [18]	345	207.0
20% glass filled polycarbonate	110.3	66.2
Polycarbonate rod	82.7	49.6
MDS filled nylon 6/6	80.7	48.4
PEEK	108.2	64.9
Nylon 6/6 PA [19]	79.3	68.9
Torlon®	120.7	72.4
ULTEM® [20]	104.8	103.4
PPS	93.2	55.9
Vespel® Polyamide	86.3	51.8
30% glass filled PEEK [21]	156.0	93.6

* if a range was given, then number cited is an average
** shear strengths approximated as 0.6 tensile strength for [17] and [18]. Remaining shear strengths are as listed in source.

Brass, ULTEM®, and PEEK are the only materials considered with a shear strength above the computed value. However, the shear strength of brass is much too high and would require modifications to the mount. This would make testing multiple materials difficult. It is also possible that a brass shear pin, due to its hardness relative to aluminum, would damage the lift bars over time. ULTEM® and PEEK both offer high shear strength, but PEEK is roughly six times more expensive.

The rest of the materials have a wide range of shear strengths, from 48.4 – 72.4 MPa. The materials also have a wide range of prices. With these two criteria in mind, three materials are chosen to test: 20% glass-filled polycarbonate, Nylon 6/6 PA, and ULTEM®. These three materials are inexpensive relative to the others, and possess shear strengths ranging from medium to high. The Nylon 6/6 was purchased in the form of a shoulder bolt with a nut, whereas the polycarbonate and ULTEM® come as rods and require mild finishing work.

The three shear pins purchased are shown in Fig. 3.10. The nylon shoulder bolt is on the left; in the center is the 20% glass-filled polycarbonate; and on the right is the ULTEM®. The nylon bolt is unmodified, but the polycarbonate and ULTEM® had to be cut to length and lightly sanded so

that they would fit in the shear pin hole. A cotter pin hole is drilled transversely near the end of each of the polycarbonate and ULTEM® rods to secure them.

Fig. 3.10: Three shear pins purchased. L to R: Nylon 6/6 shoulder bolt, 20% glass-filled polycarbonate, ULTEM®.

3.5 Vibration Analysis

One last area of concern with the sonar mount is vibration. Sonars are known to be extremely sensitive to sources of noise or vibration. Some potential sources are propeller noise, vibrating machinery, or flow induced vibration of the hull or sonar housing. In the case of a pole-mounted sonar, accuracy can be severely affected by pole vibration [22]. Having some understanding of the vibration characteristics of the sonar pole is therefore an important consideration.

Work completed toward the goal of modeling and experimentally measuring the sonar pole vibration is presented in Appendix D. The work is not presented in the body of this thesis for two reasons: for one, both the models and test setup failed to accurately model the operational scenarios for the mount; secondly, it is not currently known if sonar images acquired with the prototype sonar mount have been compromised by pole vibration. Therefore the work presented in Appendix D represents a first cut at modeling and testing the sonar mount. If it is determined that mount vibration is an issue, future vibration analyses will need to be more application specific.

3.6 Conclusions

In the preceding chapter, the design of the prototype sonar mount was discussed. The various design features of the mount were presented and each was justified based on the initial customer needs. The hydrodynamic drag was estimated after making some simplifying assumptions. This analysis justified the addition of a fairing, which reduces worst case drag on the mount by 42%. At 5.14 m/s (10 kt), the total worst case drag is 730 N, and produces a moment at the horizontal tube of 1214.8 N-m. A breakaway device was also designed which helps to reduce the severity of impacts to the sonar. It incorporates a nylon shear bolt that breaks when the sonar is heavily loaded. The design of the breakaway mechanism also allows for the sonar pole to be retracted after a breakaway. This is an important safety feature in combat scenarios, and also serves to protect the sonar if a quick escape is necessary.

Vibration of the mount is also suggested as a potential source of sonar inaccuracy. The study presented in Appendix D offers a starting point for future modeling efforts to better approximate the operational environment of the mount should it be necessary. With the design and analysis completed, field testing is needed to validate the mount design, with the ultimate goal of making further refinements.

Chapter 4

Field Trials

4.1 Overview

Field trials were conducted on the Pearl River in FY2012 and FY2013 with Navy Special Boat Team 22 at Stennis Space Center in Mississippi. After verifying the functionality of the prototype aboard the VT USV, the mount was attached to a Special Operations Craft-Riverine (SOC-R), shown in Fig. 4.1. SOC-R is 10.1 m (33 ft) long, has a draft of 0.61 m (2 ft), and is used in river networks and littoral areas for insertion and extraction of Navy SEALs [23]. It is designed to be air transportable, with a SOC-R and all of its crew and gear fitting into a C-130 aircraft.

The most important attributes of SOC-R are its speed and maneuverability. Riverine environments are inherently dangerous because boat crews are completely exposed to attacks from either bank. If an escape should be necessary there are only two ways to go: forward or backward. For this reason, SOC-R's speed is its most critical safety feature, as it helps to minimize the amount of time a boat crew is exposed to a threat. A top speed of over 40 kt is achieved with two 440 hp diesel engines, each driving a water jet [24].

While speed is an effective means of mitigating risk, without maneuverability, SOC-Rs speed would be largely ineffectual. SOC-R often travels in narrow passages, which requires it to be able to turn around in a very small space. This is especially important during an extraction, when the helmsman typically "noses-in" to shore, allows his men to board, and turns around and exits. This must all be done as quickly as possible to minimize exposure. To make this happen, SOC-R employs a bucket system, which allows the thrust from its jets to be directed in nearly any direction, including forward. This enables SOC-R to turn around in its own footprint, or to go from top speed to a complete stop in 1.5 boat lengths. By dropping only one bucket, it can be stopped from full speed and turned 180 degrees simultaneously. These capabilities were kept in mind during preparations for field trials.

Fig. 4.1: Navy Special Operations Craft-Riverine (SOC-R) [25] < Infinity Science Center, "Special Operations Craft-Riverine," http://www.visitinfinity.com/wp-content/themes/whiteinc/uploads/Riverine-Warfare-boat-courtesy-NASA-mailer.jpg, 17 Nov. 2014.> (used under fair use, 2015)

The objective of these trials was to test the systems developed jointly by VT and NPS. They also served as an opportunity to speak with end users to further refine the operational requirements of the sonar mount. In both trials the same mount was used, but the mounting location was changed to test its effect on data quality. In FY2012 the sonar was positioned on the starboard side of SOC-R; in FY2013 it was positioned at the stern.

4.2 Fall 2012

For the FY2012 field trial, two pieces of equipment needed to be designed to successfully interface with SOC-R. One was a clamp to hold two P-450-45 sonars, one above the other with a 45° heading offset. This was done at the request of NPS to increase the field of view of the sonar system from 45° to slightly less than 90°. This new configuration was analyzed in the same way the single sonar was. However, due to the expected orientation of the sonars, worst case flow now comes from the direction shown in Fig. 4.2. With two sonars of the dimensions shown experiencing the same flow, and again using assumptions 1, 2, and 4 in Table 3.1, worst case drag is 610 N (137.1 lb) based on a C_d for the prism of 1.7 from [15], a C_d for the cylinder of 0.8 from [14], and a fudge factor for clamps and cables of 1.2 applied to the prism drag. The drag for two sonars in this orientation is slightly less than the expected worst case drag for one sonar experiencing the flow depicted in Fig. 3.4.

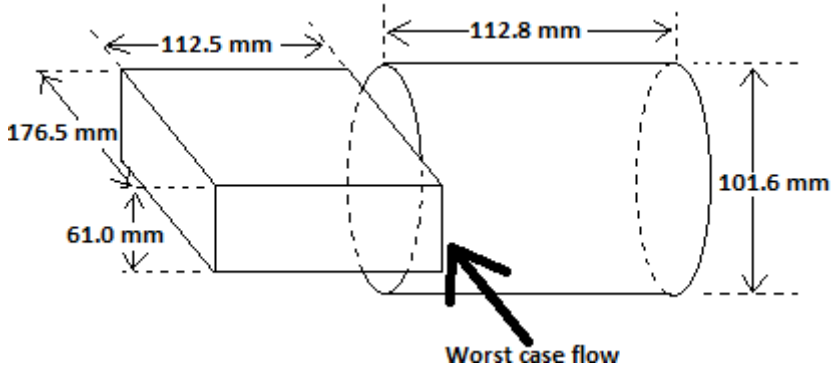

Fig. 4.2: Sonar dimensions used to approximate worst case flow for 2012 field trials.

In addition, a special cradle, shown in Fig. 4.3, was designed to support the sonar mount. The cradle is made of 1.5 inch 80/20® extruded aluminum and attaches to one of SOC-R's lift points. It incorporates U-bolts with plastic inserts and four leveling mounts with rubber feet to help isolate the sonar from vibration, and also to prevent damage to SOC-R.

Fig. 4.3: Sonar mount cradle for FY2012 field trials

Fig. 4.4 shows the sonar mount in the retracted position at the side of SOC-R. Clearly visible are the pan motor and gearbox on the left, the linear actuator and fairing in the center, and the two sonar heads at the top right.

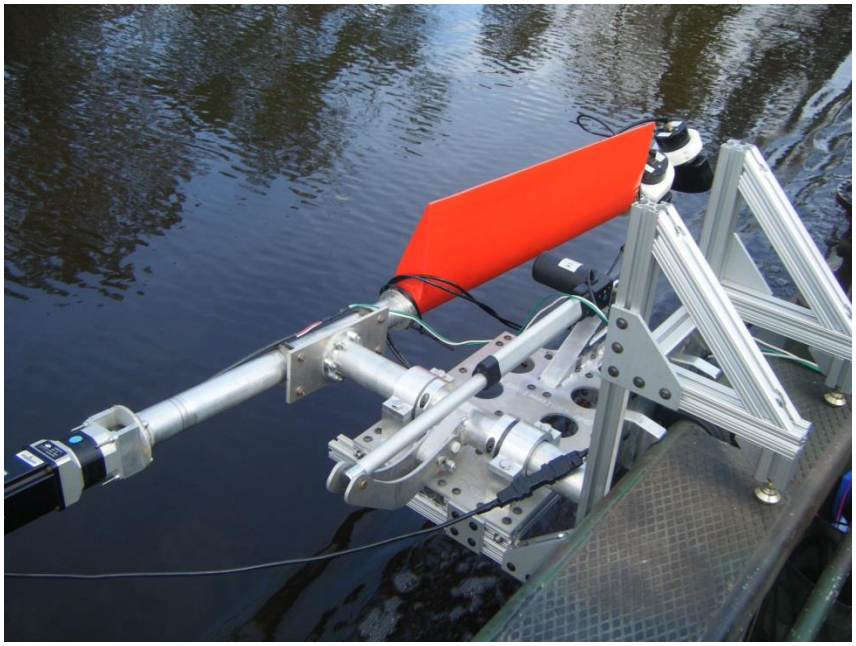

Fig. 4.4: Sonar mount in retracted position at side of SOC-R

The FY2012 trials were extremely beneficial in highlighting some of the strong points, as well as some of the limitations of the side mount. All mechanical components were confirmed as adequate. The shear pin mechanism in particular was very effective at limiting loads on the sonar. In the shallow, swampy areas of the Pearl River, despite cautious monitoring of boat speed and water depth, striking submerged objects with the sonar was unavoidable. When this occurred the nylon shear bolt broke, the sonar was raised, the bolt replaced, and the sonar redeployed, typically in less than 5 minutes. The fiberglass fairing proved effective, orienting itself to maintain a low angle of attack. The linear actuator also performed well. It had plenty of power to raise the sonar pole out of the water, and withstood significant splashing. The pan motor and gearbox were also very effective at panning the sonar back and forth, or positioning it as needed.

There were also several problems illuminated by the 2012 field trials. During the design stage, it was intended that the sonar cables would be fed through the center of the pan shaft and out a hole machined in the top. Upon inspection of the cables, we found that the connectors were too large to fit through the shaft. This meant the cables had to be secured to the support pole. This had a few negative side effects. The first was that the cables dragged in the water, which likely resulted in increased strain in the cables and connectors. However, this also led to increased forces on the sonar mount due both to the drag on the cables, and to the fact that the cables limited the range of motion of the fairing, making it less responsive to changes in current. The field test also revealed that there was too little clearance between the fairing and the metal parts of mount. This necessitated manually guiding the fairing during retraction to ensure it did not jam against the underside of the mount's base. Lastly, while the breakaway mechanism works very well for front impacts, it offers no protection for impacts from any other direction. This is a problem due to the fact that SOC-R often needs to back up or turn around in narrow passages.

From the point of view of the SOC-R operator and crew, one of the biggest problems was that the presence of the sonars, even when retracted, placed an upper limit on boat velocity. When the operator attempted to speed up, the bow pitched up and the stern lowered, causing the sonars to dip into the water. This problem was exacerbated by an assembly mistake, in which the pins used to connect the linear actuator to the breakaway mechanism were slightly too small. This caused larger than expected backlash in the linkages, so that the sonar pole was not raised high enough. Because of the danger of the sonars being torn from the boat if they hit the water at high speed, the operator had to keep the speed below 3.6 m/s (7 kt). For a boat whose primary defense against attack is speed, this is unacceptable. It was also noted that adjustments to the mount were difficult to perform and could not be made in transit without placing personnel and tools at risk of falling overboard. They instead required the boat to dock so that someone could get out and make the adjustment from the dock or the shore.

Finally, there were two problems associated specifically with the mount's location. The first is that having the sonar at the side makes the boat wider, limiting the maneuverability and reducing the number of safe passages. Secondly, it places a minimum depth constraint on the sonars in order to ensure that part of the FOV is not being blocked by the hull. This means that the sonar must, by necessity, be positioned at a depth greater than the draft of the boat (0.61 m or 2 ft in the case of SOC-R). This has the unfortunate consequence of making the sonar the most likely part of the boat to strike the river bottom in shallow water.

4.3 Fall 2013

In an effort to correct some of the issues with the side mount, the design was modified so that it could be mounted behind the boat at the stern. For this to work, a new cradle had to be built. This is depicted in Fig. 4.5 below. Like the side cradle, the stern cradle is made of extruded aluminum framing. It uses three U-bolts with plastic inserts, two at the aft lift points, and one at the bottom of the aft gun mount. Two pieces of steel bar with curved ends hook under the edge of the aft swimmer's platform. When the U-bolts are tightened, these hooks are preloaded, locking the cradle securely in place.

Fig. 4.5: Stern cradle for FY2013 field trials

The other required modification was the design of a new breakaway mechanism, the purpose of which is to change the axis about which the sonar pole breaks away. Fig. 4.6 shows the breakaway mechanism for the stern mount. It is made up of two welded aluminum assemblies. Each assembly consists of a plate with four tabs welded to it. When the plates are positioned together, the holes in corresponding tabs line up allowing for the insertion of a bolt. The top tabs use stainless steel shoulder bolts to create a hinge, and the bottom tabs accept nylon shoulder bolts to act as shear pins. The rear plate in the figure bolts to the flange on the end of the sonar mount's horizontal lift tube, while the front plate mounts to the pipe clamps used to hold the sonar pole. When a large load is applied to the sonar pole, the shear pins break, allowing the pole to rotate back.

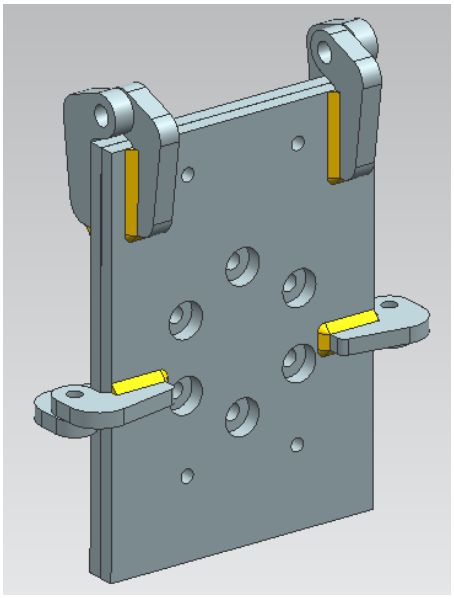

Fig. 4.6: Breakaway mechanism for stern mount

Fig. 4.7 shows the stern mount deployed on SOC-R. The sonar pole can clearly be seen, with the new breakaway mechanism behind it. In this configuration, the linear actuator is still used for retracting and deploying the sonar. In the retracted position, the sonar pole would be raised parallel to the water and the sonars would rest to the left in the figure below.

Fig. 4.7: Stern sonar mount in operation, FY2013

There were several positives noted with the stern mount. First, it is secure and out of the way, which means that it affects operations aboard SOC-R less. Also, because it does not make the

boat wider, it does not reduce the number of passable areas. Due to the fact that the pole can be mounted closer to the boat, and the sonar is raised up near the aft platform, it is possible to make minor adjustments to the mount or the sonar without having to dock. Lastly, because the sonar pole is now always perpendicular to the surge axis, SOC-R's pitching action upon acceleration no longer causes the sonar to dip into the water.

Despite these improvements, there were also a few flaws that became apparent during testing. Shortly after fixing the mount to the boat, we found that the linear actuator used for retraction did not work. The spare actuator failed as well. Both were connected to a benchtop power supply to troubleshoot the problem, but neither actuator worked. The actuator was still useful for holding the mount steady in the deployed position, but retraction became difficult. After disconnecting the actuator, the sonar had to be pulled up by hand and tied off. This exposed the need for the final design to be manually retractable. The second design flaw occurred at the welded flange on the horizontal tube. On the final day of testing, after several successful breakaways, the welds on this flange broke. This necessitated a redesign of the welded joint, which is discussed in Appendix C on page 85. Lastly, while the redesigned breakaway mechanism worked well, it still does not offer protection for non-forward impacts.

Despite the improvements over the side mount, there are two problems with mounting at the stern that make it infeasible. Similar to the side mount, the sonar must be positioned below the hull, increasing SOC-R's effective draft as well as the likelihood of the sonar sustaining damage. It was also found that having the hull and jets in front of the sonar compromised data quality. This problem can be mitigated by positioning the sonar deeper, but that only further increases draft. For these reasons the stern is not an ideal mounting location for any boat operating in shallow water.

4.4 Conclusions

This chapter has discussed in detail the field testing of the prototype sonar mount. The ultimate goal of these tests was to gain insight into the needs of the end user so that the design could be further refined. Field trials were extremely useful in this regard, and highlighted many of the mount's positive and negative attributes.

On the positive side, both breakaway mechanisms were very effective at limiting load on the sonar. The shear pins broke as expected, and were easily replaced. Most mechanical components performed well. The fiberglass fairing worked as designed, rotating to maintain a low angle of attack for reduced pole drag. All motors and actuators worked well in 2012, but the linear actuators malfunctioned for unknown reasons in the 2013 trials. This highlighted the need for a manually retractable sonar mount.

While the prototype performed well in the field, there were several flaws that became apparent. In the 2012 trials, it was noted that the side mounted sonar effectively made the boat wider, reducing areas of safe passage. The sonar's position when retracted caused it to dip into the water under acceleration, limiting the top speed. In addition, adjustments could not be made while on the water due to safety concerns. At the 2013 trials, many of the issues with the side mount were addressed. However, the welded flange was not strong enough to carry the bending loads placed on it, and the linear actuators proved unreliable. It was also noted that sonar performance was diminished at the stern, likely due to its proximity to the hull and propulsion systems.

There were two limitations that were made apparent at both field tests. The first deals with the breakaway mechanism. While the mechanism protected the sonar as designed, it is only effective for impacts from the front. This means that the sonar is left unprotected if the boat is traveling sideways or backwards, which is especially common in shallow passages where precise and varied maneuvers are required. This increases the risk of damage to the sonar, the mount, or the boat. The second limitation is a problem inherent with the mounting locations. Whether the sonar is mounted at the side or the stern, by necessity its depth must exceed the draft of the boat to ensure the full field of view is being utilized. As a consequence the sonar increases the draft of the boat. This not only limits where the boat can go, but also increases the chance that the sonar will strike objects.

Because of these issues, we conclude that the side and stern are poor mounting locations on boats that operate in shallow water. With the insights gained from these field trials, a new mount has been designed to alleviate many of the issues with the prototype.

Chapter 5

Bow Mount Design

5.1 Mount Overview

The updated mount will be positioned at the bow. Fig. 5.1 shows the mount as it might sit on SOC-R. The bow mount shares many components with previous versions, although actuation is now completely manual. Retraction is achieved with a lever attached to one end of the horizontal tube, shown in Fig. 5.2. If future designs require an actuated retraction, this design is not expected to inhibit this modification. The design consists of a platform which mounts to the deck. Extending from this platform is a large cylinder about which a disk is allowed to rotate. The disk is held to the base plate by a circular plate of larger diameter than the large cylinder which bolts to the top of the large cylinder. The disk provides the mounting surface for the sonar pole, and enables the entire apparatus to be rotated inboard (Fig. 5.3) for adjustment or when not in use. The sonar used is expected to be the ATLAS (autonomous topographic large-area survey) from the Applied Research Labs at the University of Texas, chosen for its exceptional performance and wide FOV. The ATLAS has a 200° field of view and a 400 m swath width [26]. Currently the ATLAS' shape is not known. Based on the press release in [26], it is known to have at least two different housings, one of which is spherical, the other of which is more cylindrical. For design purposes it is assumed that the cylindrical housing will be used with the sonar mount.

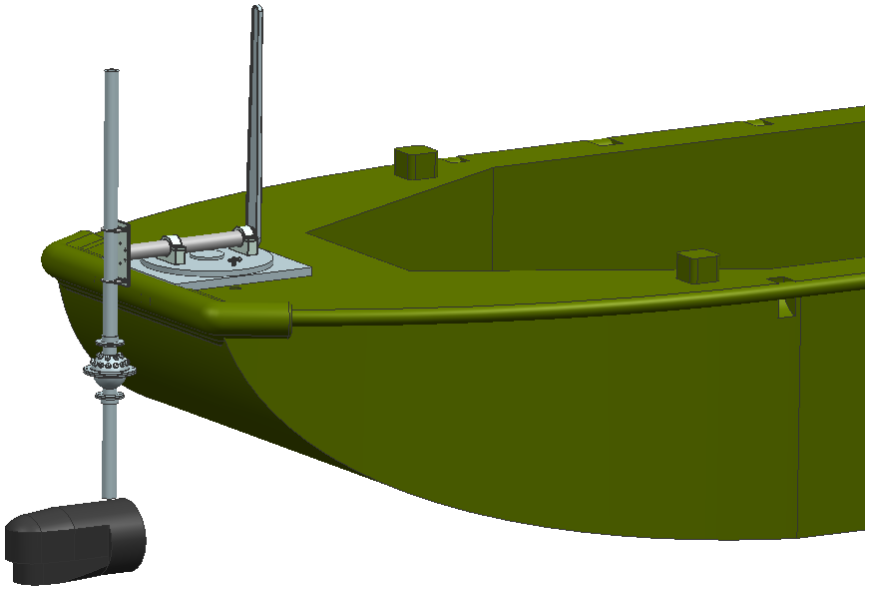

Fig. 5.1: Bow mount on SOC-R

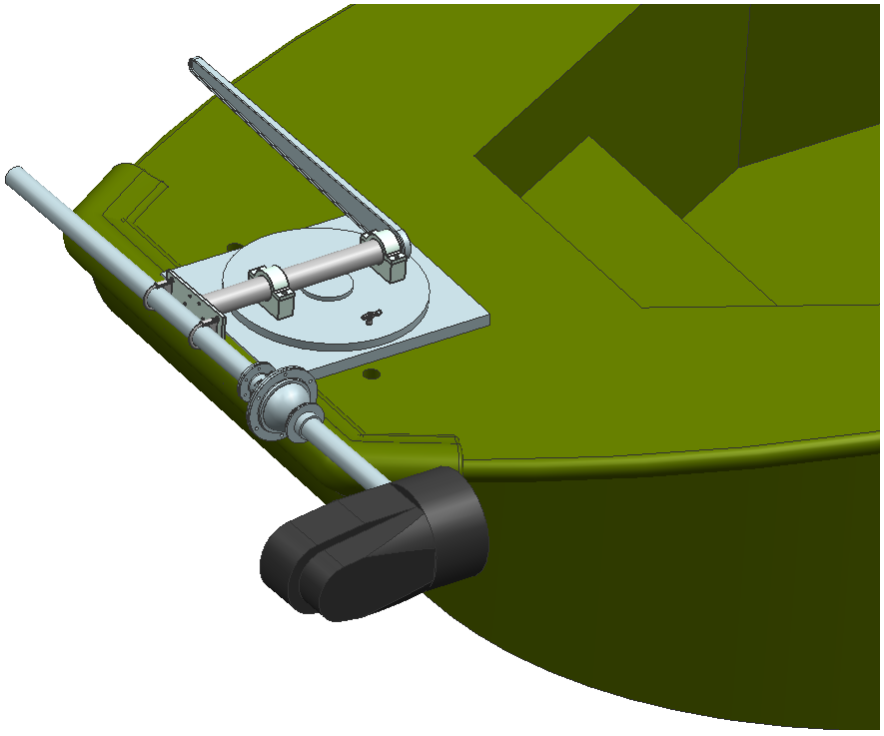

Fig. 5.2: Bow mount in retracted position

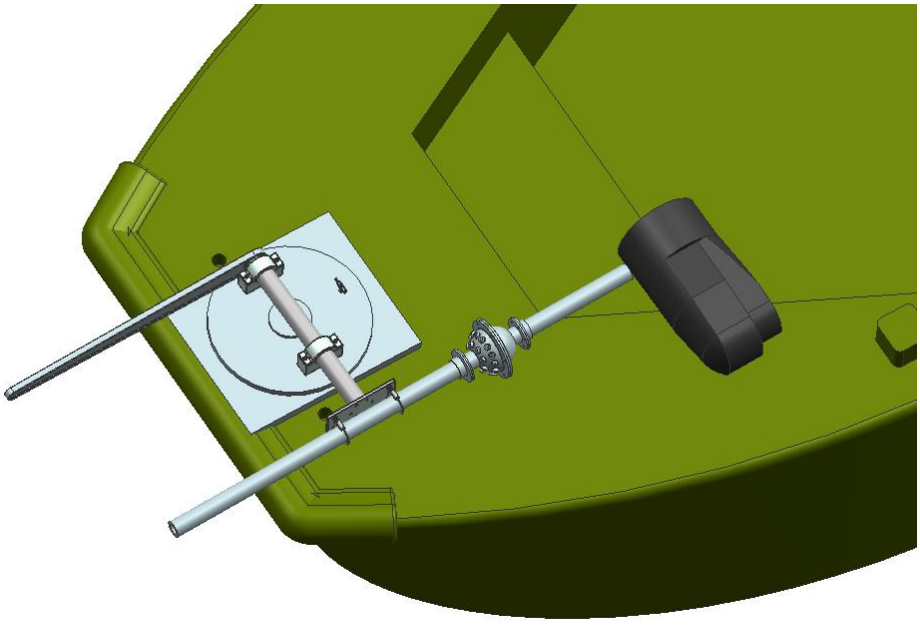

Fig. 5.3: Bow mount rotated inboard

The rest of the mount is very similar to previous versions with the exception of the breakaway mechanism. This mechanism is discussed in detail in the following section.

5.2 Ball and Socket Breakaway

Undoubtedly the most important design modification is to the breakaway device. Previous versions of the mount incorporate a shear pin that breaks if the sonar strikes an object or hits bottom. This feature is very effective at preventing damage to the sonar, but only for forward impacts; if the operator needs to back up or turn around, the sonar is left unprotected. An added disadvantage is the need to replace a component each time the pin breaks.

To remedy this problem a breakaway device is needed that can hold the sonar rigidly, but that responds to impacts from any direction. The proposed solution to this problem is a ball and socket breakaway (BSB) device, shown in Fig. 5.4. This device is designed to attach two sections of flanged structural tubing together. The tubes are held fixed relative to one another until a radial load applied to one of the tubes induces a moment at the BSB which causes the device to release. There are three basic components: a socket, a ball, and a retainer. The ball is six inches in diameter and fits into the socket. It is held in place with the retainer, which bolts to the socket. The holding power of the BSB comes from 22 off-the-shelf ball plungers threaded into bosses positioned around the socket. In the locked position, the nose of each ball plunger fits into a detent machined into the surface of the ball. When a radial load is applied to one of the tubes, the resulting moment is carried by the ball plungers until the holding power of the plungers is overcome, at which point the BSB slips and rotates freely.

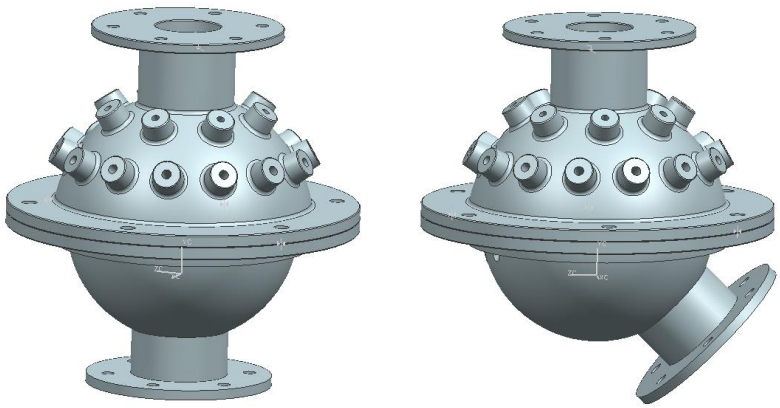

Fig. 5.4: Ball and socket breakaway device in the locked (left) and released (right) positions

To better illustrate how the ball detents work, Fig. 5.5 shows the three different slip stages for each ball detent. The first stage on the left represents a scenario where there is no side load. The ball is centered in the detent and experiences ring contact. The middle stage occurs when a side load is applied to the detent. The detent begins to move relative to the fixed ball plunger. This causes the ball-detent contact to transition from ring to point contact. As the ball slides up the side of the detent it depresses the spring behind it. The third stage on the right occurs when the ball finally exits the detent. At this point the holding power of the device is minimal and comes only from the friction between the ball and the upper surface of the detent.

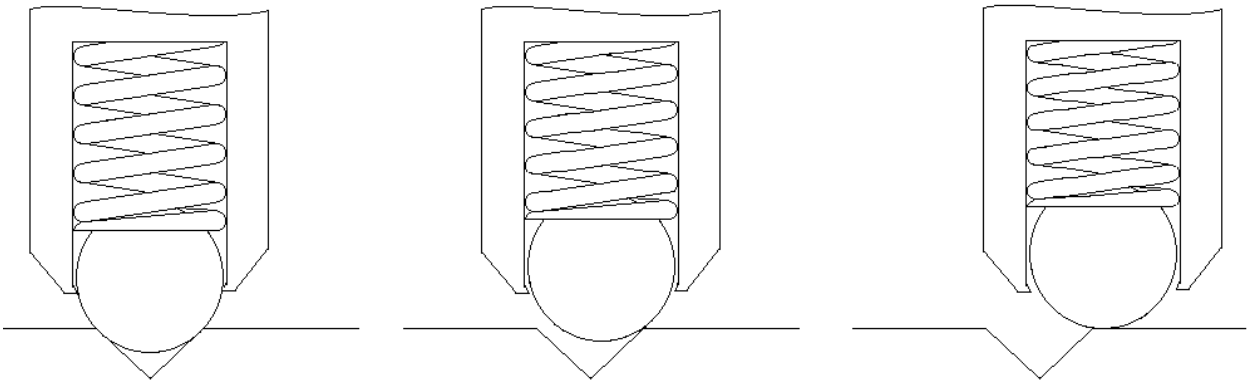

Fig. 5.5: Three different slip stages for the ball detents

One important design question that needed to be answered for the BSB was determining how many ball plungers are necessary. Each has a maximum nose force of 222.4 N (50 lbs). The nose force is an industry standard term for a load applied to the ball in the up direction of Fig. 5.5. The maximum nose force is based on the spring constant, and occurs when the ball is fully depressed into the body of the plunger. Determining how much side load the ball plungers can support, or their holding power, requires some computation, and depends largely on the detent geometry. It is assumed that each ball plunger will have the same holding power, but due to the spherical shape of the BSB, the moment arm for each plunger will change. The overall moment holding capacity of the BSB will be the summation of the moment holding capacities for each individual ball detent. A MATLAB code was written (see Appendix F) to compute the contribution of each detent. A discussion of these computations follows.

First consider how to estimate the holding power of a single ball detent. Fig. 5.6 shows a ball plunger and detent. The detent angle is represented by ϕ, which can also be thought of as the point angle of the tool used to cut the detent.

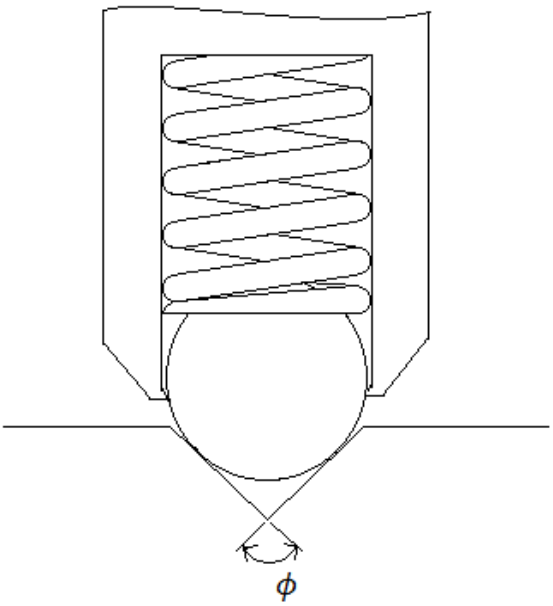

Fig. 5.6: Ball plunger and detent

A free-body diagram for the ball bearing is drawn to gain a relationship between the forces acting on it. This is depicted in Fig. 5.7. This free-body diagram applies to the moment just before the plunger and detent start to shift relative to one another. In the figure, F_E is the end force, which is the force applied to the ball bearing by the spring, F_S is the side force, which is the transverse load applied to the ball acting to cause the ball to slip from the detent, and F_R is the reaction force applied by the side of the detent. Two important assumptions were made in this analysis. The first is that the detent is large and deep enough that its inner surface always contacts the ball at a tangent. The second is that friction can be neglected.

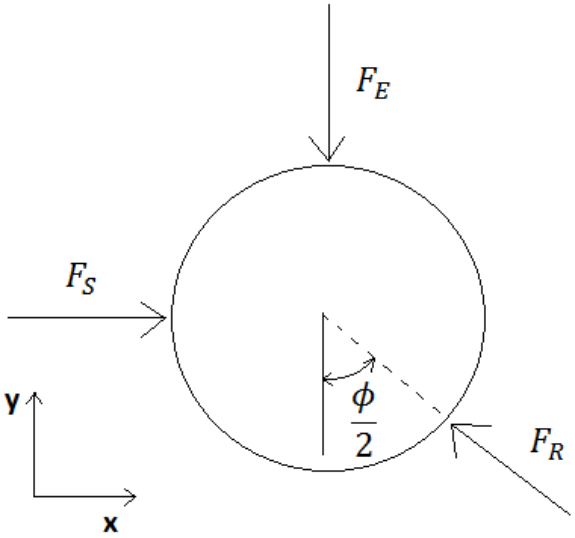

Fig. 5.7: Free-body diagram showing forces acting on a ball bearing in a detent

Balancing forces in the x and y directions, we can write the following relations

$$\Sigma F_x = 0 = -F_{Rx} + F_s$$

$$0 = -F_R \sin\left(\frac{\phi}{2}\right) + F_s \tag{5.1}$$

and

$$\Sigma F_y = 0 = F_{Ry} - F_E$$

$$0 = F_R \cos\left(\frac{\phi}{2}\right) - F_E \tag{5.2}$$

Solving for F_R in Eq. (5.1) and substituting the expression in Eq. (5.2) we get the following:

$$0 = \frac{F_S}{\sin\left(\frac{\phi}{2}\right)} \cos\left(\frac{\phi}{2}\right) - F_E$$

$$F_S = \frac{F_E}{\tan\left(\frac{\phi}{2}\right)} \tag{5.3}$$

Eq. (5.3) describes the relationship between the end force, which is a specification of off-the-shelf ball plungers, and the side force necessary for motion to occur. This relationship allows us to compute the holding power for any number of ball detents given the end force and the detent angle. Furthermore, given the configuration of a set of ball detents arranged on a sphere, the moment required to cause them to slip can be estimated.

The following example illustrates this process. Consider the socket shown in Fig. 5.8. The points A and B represent the locations of two ball plungers and are located by the vectors $\vec{A}$ and $\vec{B}$ relative to the origin at O. The M-M axis represents some axis of rotation that must pass through the origin.

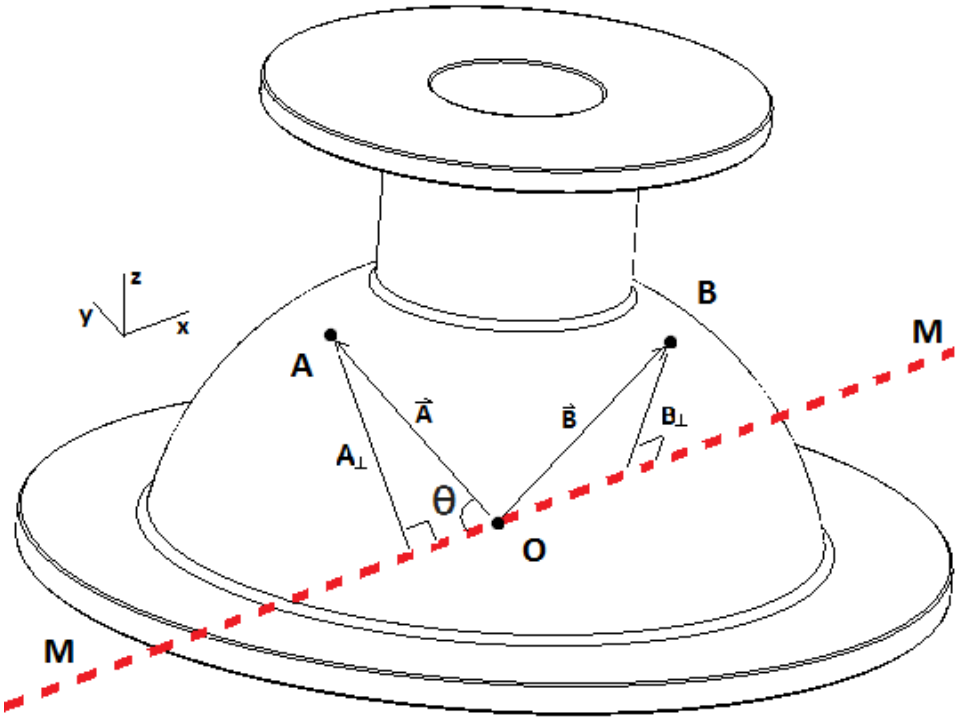

Fig. 5.8: Hypothetical ball plunger configuration on the socket of the BSB.

Begin by computing the moment holding power of the detent at A. First calculate the right angle distance between point A and the axis M-M. Solve for the angle between $\vec{A}$ and the axis M-M using the definition of the dot product as follows.

$$\theta = \cos^{-1}\left(\frac{\vec{M}\cdot\vec{A}}{\|M\|\|A\|}\right) \tag{5.4}$$

where $\vec{M}$ is a vector of arbitrary length that is collinear with the axis M-M. With θ, the right angle distance $A_\perp$ can be computed, and the moment holding contribution of the detent at A about the axis M-M is

$$T_A = A_\perp F_S \tag{5.5}$$

The torque contribution at B is computed in the same manner. When this is complete, the total moment holding capacity of the BSB about M-M with two detents is simply

$$T_{tot} = T_A + T_B \tag{5.6}$$

Or for n detents,

$$T_{tot} = T_A + T_B + \cdots + T_n \tag{5.7}$$

where T_n is the torque holding contribution of the nth ball detent.

An important note about the above example is that the moment holding capacity will change depending on where the axis M-M is in relation to points A and B. Therefore there will be a minimum and maximum moment holding capacity for any configuration of detents. Assuming evenly spaced detents, these minimum and maximum capacities will converge as the number of detents increases. All design calculations assume evenly spaced detents.

These computations were completed in MATLAB. In doing this, three assumptions were made about the detents. First, the ball detents are assumed to be arranged in a circular pattern, the plane of which is parallel to the x-y plane of Fig. 5.8. They are evenly spaced on this circle, with each being equidistant from the origin O in Fig. 5.8. Also, the holding power of each ball detent is assumed to be the same (the moment holding power will change depending on each detents moment arm). The MATLAB code is shown in Appendix F.

Using the design depicted in Fig. 5.4, which has 22 detents, and using a maximum nose force of 222 N (50 lb), the maximum breakaway torque for the BSB is 299 N-m (2650 lb-in). The code also computes a design speed for the sonar, which is the maximum speed it can travel through the water before the breakaway releases due to hydrodynamic drag. However, because the ATLAS sonar has not yet been provided, and because it has at least two different housings, assumptions about its dimensions needed to be made to estimate the drag it will induce. This was done using the following photograph (Fig. 5.9) of an ATLAS sonar mounted on the front of a REMUS 600.

Fig. 5.9: ATLAS sonar mounted on a REMUS 600 [26] < Loeffler, C., 15 Sept. 2011, "Sonar and AUV Technology," National Oceanic and Atmospheric Administration, Web. 5 Nov. 2014.> (public domain, 2015)

The sonar in the photograph has an OD of 30.5 cm (12 in) and 41.3 cm (16.25 in) length. For simplicity, the sonar is assumed to be cylindrically shaped as in Fig. 5.10.

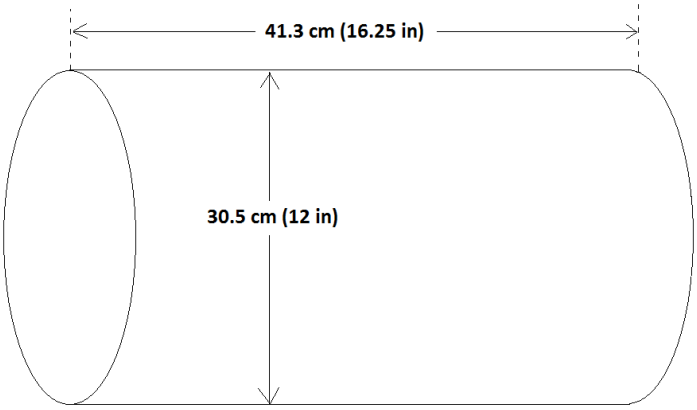

Fig. 5.10: Dimensions of body used to represent ATLAS sonar for drag estimation.

Assuming a sonar depth of 0.6 m (2 ft), which will position the sonar at the bottom of SOC-R's hull, this should allow the sonar to travel through the water at speeds of up to 3 m/s (6 kt) before the breakaway releases due to hydrodynamic drag.

It is important to note that a 3 m/s (6 kt) speed and a depth of 0.6 m (2 ft) are both 40% lower than the original design speed of 5.14 m/s (10 kt) and depth of 1 m (3.3 ft) for the mount. Due to the uncertainty about how fast an imaging sonar can travel through the water and still acquire useful imagery, the decrease in design speed is deemed acceptable. There is also uncertainty in how shallow is too shallow for the sonar. However, positioning the sonar within the draft of the vessel will offer much better impact protection. If during testing it is determined that the new mount design does not position the sonar deep enough, or that the breakaway device is the limiting factor in how fast an area can be scanned, then steps need to be taken to position the sonar deeper and allow for faster speeds. If this occurs, fairing the lower sonar pole is an option which has been proven to drastically reduce drag. Also, because the ATLAS sonar does not require panning capability due to its much larger FOV, the sonar is now a candidate for fairing as well.

5.3 Ball Plunger Testing

To check the results described above, a test was conducted with two off-the-shelf ball plungers. Data gathered from these tests would help not only to validate the BSB design, but also to inform design modifications. Both plungers have a 5/8"-11 thread and a 31.1 - 222.4 N (7 - 50 lb) nose force. Fig. 5.11 shows both plungers. The part on the left is a long nose ball plunger, and has a slightly longer body and a rounded, zinc-plated steel pin for the plunger. The part on the right is a round nose ball plunger which is shorter, and uses a polished steel ball bearing. Because the long nose plunger has much more travel than the round nose, its spring is much less stiff.

However, at full depression each plunger has a nominal 50 lb nose force. It is also useful to mention that the surface finish of the two plungers is very different. The round nose plunger has a highly polished steel ball bearing, while the pin of the long nose is dull, and shows what appear to be marks left over from a grinding operation.

Fig. 5.11: Photo of long nose (left) and round nose (right) ball plungers

Fig. 5.12 is a schematic of the ball plunger test setup. To apply the side load, a drill press is used because it includes a vise to hold the ball plunger, x and y adjustments to ensure the load is applied in line with the plunger, and a geared head to provide mechanical advantage. The head also helps to prevent binding by applying the load vertically. A PCB Piezoelectronics load cell (Model No. 1380-01A) with a series 8159 digital signal conditioner was used to measure the load applied to the test piece. Weights ranging from 1.16 N to 221.88 N (0.26 lb to 49.88 lb) were used to verify the accuracy of the load cell at the beginning and the end of testing. Readings taken at the end of testing were 0.2% lower on average.

The right side of Fig. 5.12 shows a top view of the vise. The ball plunger is threaded into a piece of steel plate which is clamped in the vise along with a backing plate of the same material and dimensions. These two plates are spaced such that the sample piece can slide freely between them when the plunger is not inserted. The sample piece, shown in Fig. 5.13, contains three types of detent: a 90° detent, a 120° detent, and a blind hole. The large hole at the top of Fig. 5.13 was not used, but its edges were filed to remove any burrs. All of the detents are machined to have an outer diameter of 0.330 in (8.38 mm) so that the end of the ball plunger fits inside them without touching the edge of the detent. This ensures maximum holding power. To ensure consistent testing conditions for each detent, the test piece is 76.2 by 76.2 mm (3 by 3 in), each detent is centered between two edges, and each is located 22.86 mm (0.9 in) away from the nearest edge. All flat surfaces are polished to a near mirror finish and oiled to reduce slipping resistance due to friction.

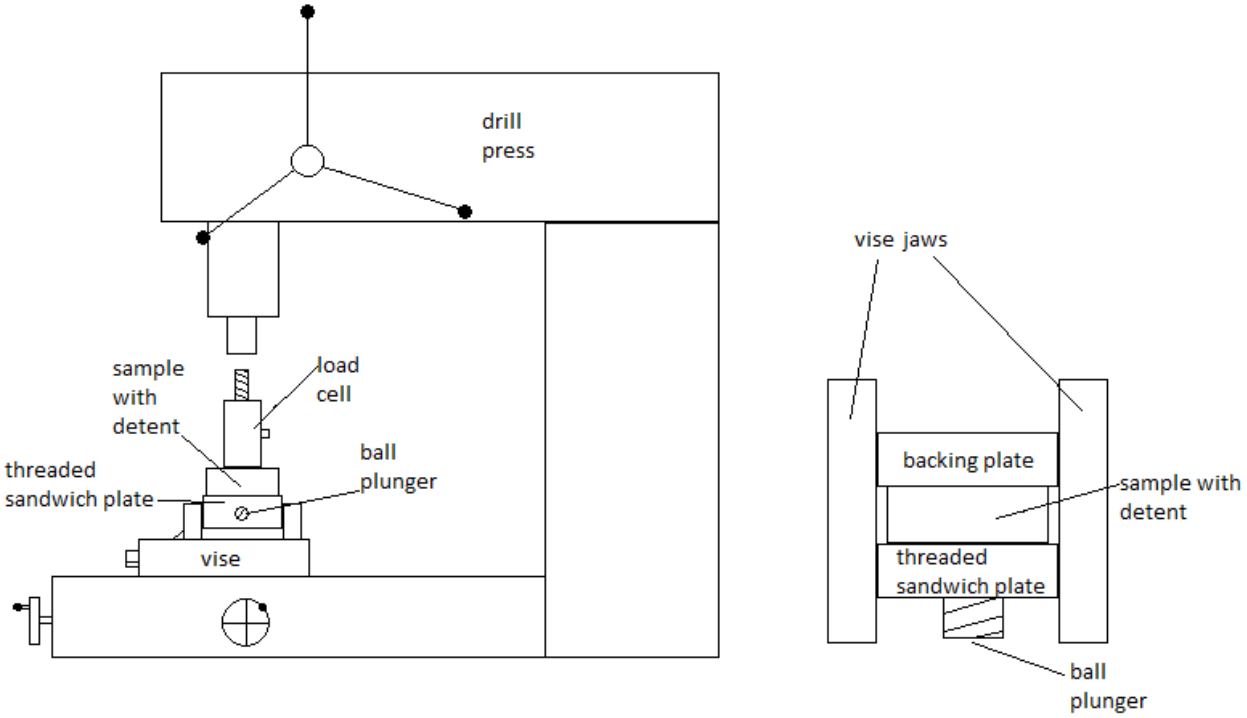

Fig. 5.12: Diagram showing ball plunger test setup

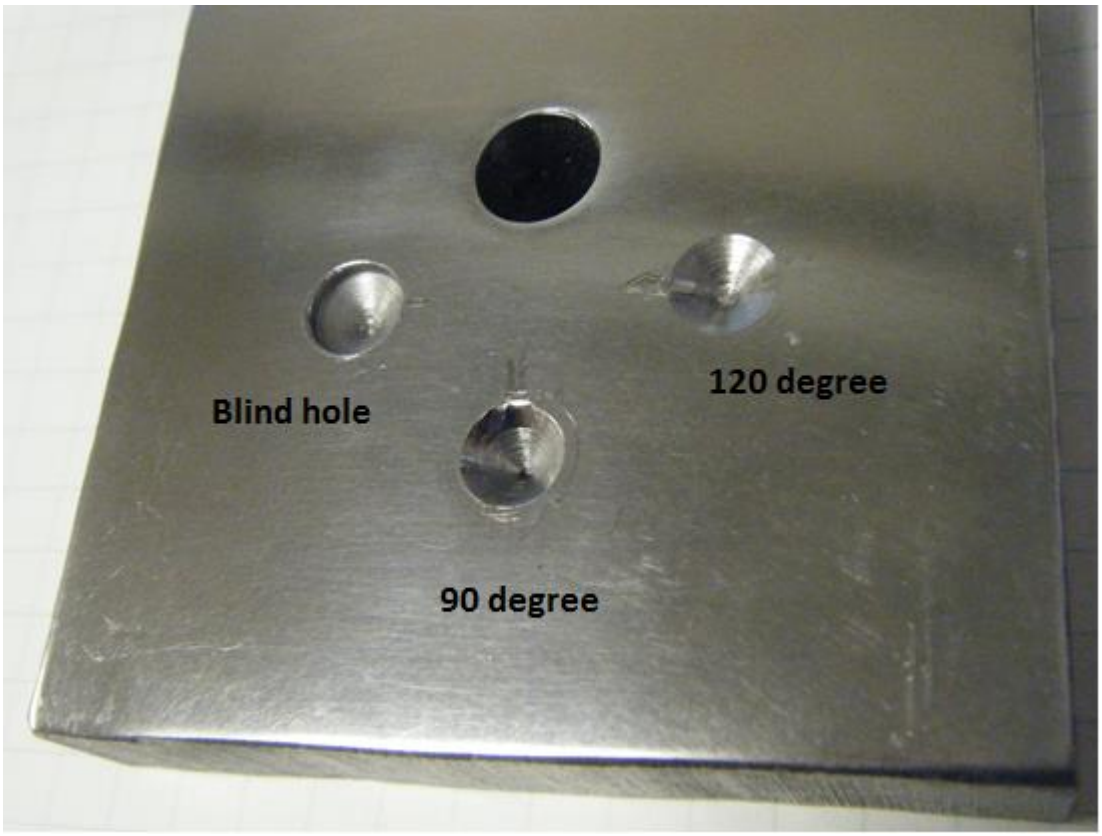

Fig. 5.13: Photo of test piece with detents

Each of the two ball plungers was tested using the above setup. The round nose plunger was tested with all three detent styles, and the long nose plunger was tested with the 90° and 120° detents. The geometry of the long nose plunger makes it unsuitable for use with a blind hole detent. Each plunger was threaded into the threaded sandwich plate and its nose positioned in the detent being tested. The plunger was tightened until it bottomed out against the sample, then backed out 1/8 turn. With a 5/8”-11 thread, this constitutes a clearance of about 0.279 mm (0.011 in), and helps to ensure that the majority of the load holding capacity of the plunger is used. With each run the ball plunger was reset in this way for consistency. Loads were applied slowly to allow the signal conditioner time to update the digital display.

Table 5.1 shows the results of the ball-detent tests. All forces in the table are listed in Newtons and represent the maximum force necessary for the plunger to exit the detent. The blind hole detent proved to be ineffective. It resulted in the lowest average holding power, and also experiences more plastic deformation during repeated plunger releases. For both the round nose and long nose plungers the 90° detent results in the largest holding power. Interestingly the long nose plunger achieved more than twice the holding power of the round nose. This likely has to do with the different surface finishes of the two plungers’ noses. The pin is much rougher than the ball bearing, and therefore resists side loads better. The rougher surface finish results in higher holding power, but also causes more damage to the detent over repeated releases. It is also worth noting that the long nose plunger with 120° detent achieved higher holding power than the round nose plunger in all cases. For this reason the long nose plunger is the best choice for the final design.

Table 5.1: Holding power for round nose and long nose ball plungers. All units are Newtons.

	Round nose			**Long nose**	
Run	**90°**	**120°**	**Hole**	**90°**	**120°**
1	191.4	144.9	137.7	442.4	284.8
2	187.8	147.9	154.8	474.6	280.5
3	207.7	169.3	140.0	486.4	234.4
4	182.4	157.2	141.4	460.2	250.1
5	167.2	146.1	138.3	477.7	265.3
Average	187.3	153.1	142.4	468.3	263.0
Std. Dev.	14.7	10.3	7.1	17.3	21.0
Relative Std. Dev.	0.078	0.067	0.050	0.037	0.080

Table 5.1 also lists the relative standard deviation for each test to give a measure of repeatability. It is important that the ball detents exhibit repeatable releases as this will have implications for mount performance and ease of installation/use. The round nose plunger showed good repeatability within 8% of the average holding power. The long nose plunger with 90° detent

was the most repeatable configuration, with relative standard deviation of less than 4%, while the long-nose and 120° detent showed repeatability similar to the round nose.

Lastly, one of the most important results gleaned from the ball plunger tests was simply experience with the hardware. The plungers were found to be very sensitive to small changes in test conditions. These might include loosening, amount of lubrication, and preload. The long nose plunger preload was easier to set because it has more than twice the travel of the round nose. Since both plungers have the same nose force range, this means the long nose is less sensitive to slight variations in clearance. Furthermore if clearance for each plunger is set at 0.279 mm (0.011 in), the long nose plunger will be using 95% of its rated capacity whereas the round nose will only be using 89% of its rated capacity. This may partly explain the fact that the long nose plunger outperformed the round nose for all detent types.

Table 5.2 illustrates the effects of loosening on holding power. In this case, instead of resetting the plunger clearance after each run, the test piece was simply repositioned and the test conducted again. Clearly the holding power decreases with each run. After run 4 the plunger clearance was reset, which resulted in holding power much closer to the first run. These results show the importance of maintaining plunger preload to achieve certain performance levels. For this reason plungers with nylon thread locking elements should be used in the final design.

Table 5.2: Effect of plunger loosening on holding power. All units Newtons.

Run	120°, Long nose
1	233.8
2	199.4
3	172.4
4	170.9
5	218.9
Average	199.1
Std. Dev.	27.9
Relative Std. Dev.	0.14

Holding power was also observed to significantly decrease when the plunger was not centered in the detent. This causes the plunger to slide out along the side of the detent, which is a much more gradual slope than when it slides straight out. In the first set of runs with the 90° detent, the test piece was found to have inadequate clearance with the vise jaws. This had the effect of positioning the plunger off center in the detent. Fig. 5.14 shows the burnish marks from the centered and off center runs. By following the off center mark from top to bottom on the figure, the path taken by the plunger is clear. The OD of the detent shows a distinct deformation at the point where the plunger exited the detent. Lighter burnish marks are also visible on the side of the detent. After correcting this problem average holding power for five runs increased 46%, even though the off center measurements included friction between the test piece and vise jaws.

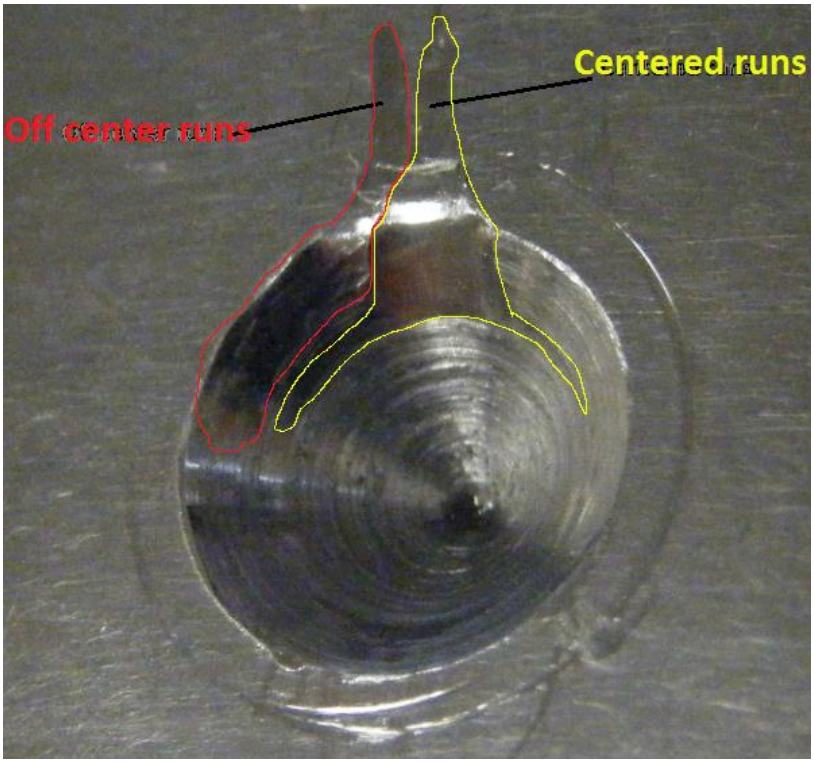

Fig. 5.14: Photo of 90° detent showing marks from centered and off center runs

One other important aspect to note about the ball plungers is that even when they are properly positioned in the detent, they still cause significant damage to the test piece. This is apparent in Fig. 5.14 and also in Fig. 5.13. For each detent type there are clear burnish marks present. To increase longevity of the BSB it would be wise to case harden the detents. This will likely decrease the holding power of the ball plungers slightly, as they will not be able to dig in to the material as much. Given that the BSB is a high cost part, this tradeoff is deemed acceptable to increase the life of the part. Clearly the long nose plungers provide the best holding power, but testing with case hardened detents is needed to determine which detent style should be used. This testing will also be necessary to update the overall holding power of the BSB. The ball plunger model was developed with the assumption that there is no friction between the plunger and the detent. With the no friction assumption the BSB is predicted to break at roughly 300 N-m (2650 in-lb) which corresponds to a drag-induced breakaway speed of roughly 3 m/s (6 kt). Using the holding power of the long nose plunger with 90° detent from testing in the MATLAB code, the predicted holding power increases to 629 N-m (5565 in-lb) which corresponds to 4.3 m/s (8.4 kt). With hardened detents, the BSB release should occur somewhere between these two extremes. If the 90° detent withstands multiple releases with minimal plastic deformation it may be considered, otherwise it would probably be better to use the 120°.

5.4 Conclusions

The preceding sections have detailed the design of the bow mount for a sonar, with particular emphasis on the BSB joint. Mounting at the bow has several distinct advantages over other locations, the most important which is that it allows the sonar an unobstructed forward view without placing it at an unsafe depth. While positioning the sonar at a more shallow depth should reduce the occurrence of impacts, it is understood that impacts will still occur. In the event that something strikes the sonar, the BSB should act to minimize damage. While more expensive than previous breakaway designs, the BSB is able to respond to impact forces from any direction, greatly enhancing sonar protection, and justifying its expense.

Preliminary designs have been completed for the BSB. Two types of ball plungers have been tested with three styles of detent, which showed the theoretical models based on a no-friction assumption to be inaccurate. These tests also revealed the need for thread locking elements to preserve the initial plunger preload over repeated releases, as well as the need to harden the detent material to increase durability. If plunger preload is maintained, plungers are expected to exhibit repeatable releases with a relative standard deviation of ~8%.

Questions remain about how to build the BSB. Several design-test cycles will be necessary to better understand the important design parameters. It makes sense to build a mock up BSB out of plastic using an additive manufacturing process. More testing also needs to be done with the ball plungers and case hardened detents to finalize the detent design.

Chapter 6

Conclusions and Recommendations

6.1 Research Goals and Objectives

In the first chapter of this thesis several research goals were listed. They are as follows:

The sonar mount must…

1. Hold the sonar securely, and in an appropriate position to gather useful data.
2. Have minimal influence on the capabilities of the boat and its crew.
3. Limit damage to the sonar in the event of a collision.
4. Be capable of mounting to a wide variety of vessels.
5. Be designed such that it can be used with autonomous vessels with minimal modifications.

Holding the sonar securely is a relatively simple task, and should not pose major problems when the form of the ATLAS sonar housing becomes known. Through experience gained testing in FY 2012 and 2013, it has been determined that the ideal location for the sonar is at the bow. Mounting at the bow has several advantages over mounting at the side or the stern. For one, a bow mount allows the sonar to be positioned at a shallower depth, ideally less than the draft of the boat. Positioning the sonar in this way helps protect it from impacts, but could also negatively affect image quality. However, it is also likely that a bow-mounted sonar will be less affected by the propulsion systems of the boat, and it will not be positioned in the boat's turbulent wake. These two factors are expected to improve image quality, and hopefully will offset some of the negative effects of positioning the sonar at a more shallow depth.

With regards to goal 2, the bow mount is arguably the most obtrusive of any of the designs considered. On SOC-R the bow experiences significant foot traffic, especially during loading and unloading. However, unlike the side mount, the bow mount does not widen the boat, limiting its ability to travel in narrow passages. In the near term, the purpose of having the sonar on the boat is to help make the boat and its crew more effective. Long term it is intended to keep the crew safe, and could eventually lead to a drastic reduction in risk to the crew as more and more autonomy is incorporated into the boat's systems. It is believed that these benefits of sonar technology are significant enough to allow for some infringement on the boat's capabilities. Furthermore, it is understood that it does not make sense to spend tens if not hundreds of thousands of dollars on a sonar that will then be mounted in a way that handicaps its potential.

One problem exposed by field testing was the inability of the breakaway mechanism to protect the sonar from rear or side impacts. The BSB device discussed in the previous two sections is expected to be much more effective at protecting the sonar from damage in a wider range of operational scenarios. The additional protection afforded by the BSB will allow research to be conducted in difficult environments like swamps with minimal risk to the sonar, and it will enable autonomous systems engineers to push the boundaries of the sonar's capability.

Goals four and five are closely related in that they are concerned with the ability to modify the mount to suit a particular application. One thing that has become apparent through this project is that there is no such thing as a "universal" sonar mount. Any mounting structure will need to be securely fixed to the boat it is used on; the wide variety of hull designs and materials means that how the mount is fixed will change depending on the boat. The current design is believed to satisfy research goal four, as it should be suitable for any vessel with a strong bow.

The current design satisfies goal five in that it does not contain any design features that would preclude the addition of an actuator. It is well understood that how the mount is actuated will change with the boat. When reliability and simplicity are primary concerns, then a manual retraction is best. For an autonomous vessel, this is obviously not an option, and other methods must be employed. These might include linear actuators, hydraulic actuators, winch and pulley systems, or a motor and gearbox. How retraction is achieved is a problem that has many potential solutions, and how it is accomplished will depend on the application and the boat.

6.2 Conclusions

The preceding chapters discussed the design, analysis, and implementation of a sonar mount. The design challenge was broken into six sub-problems which fully define the functions that any retrofitted sonar mount must perform. These are:

1. Mount location
2. Attachment method
3. Retraction method
4. Retraction actuation
5. Collision protection (sonar)
6. Depth adjustment method

These sub-problems must either be solved directly or circumvented, but they cannot be ignored. Field testing in 2012 and 2013 showed that the side and stern of a boat are not ideal locations to mount a sonar. They introduce propulsion noise, air bubbles, and turbulence effects into sonar images. They also require the sonar to be positioned below the draft which places it at risk for damage. Field tests also showed that the attachment method used, as well as how retraction is actuated will depend largely on the boat and the application. Field tests also proved depth

adjustment to be a useful feature to ensure adequate sonar depth for a variety of mounting locations.

One of the most important considerations, especially in a challenging environment where there is a high risk of sonar impacts, is sonar collision protection. Sonars are very sensitive and expensive. Field tests were extremely valuable in highlighting the importance of breakaway functionality to protect the sonar. Limitations of the prototype breakaway mechanism were also illuminated, and led to the design of the BSB, which is an omnidirectional breakaway device designed to improve sonar protection in a wider variety of scenarios. The expected moment holding power of the BSB is between 300 N-m (2650 in-lb) and 629 N-m (5565 in-lb), which corresponds to a drag-induced breakaway speed of between 3 m/s (6 kt) and 4.3 m/s (8.4 kt). These speeds assume an ATLAS sonar depth of 0.6 m (2 ft), which will position the sonar within the draft of SOC-R, reducing the likelihood of impacts. While these speeds and sonar depths are lower than the design speed of 5.14 m/s (10 kt) and depth of 1 m used for the prototype, the design is justified in its current level of detail by the fact that the effects of flow velocity and depth on sonar performance are not well understood. If greater speeds and depths are necessary, they can be achieved by fairing the pole, and since the ATLAS sonar's wide FOV negates the need to pan the sonar, it is also a viable candidate for fairing.

As mentioned in Chapter 2 (page 8), a hull-integrated sensor has significant advantages over other mount types. This solution has the potential to subvert several of the six sub-problems above that make designing a sonar mount challenging. It is a much simpler and lower maintenance solution. It frees the boat of bulky attachments which might limit its capabilities or hinder its crew. In the worst case the retraction mechanism could be made much smaller, and in the best case the need to retract could be completely eliminated.

While a hull-mounted system is the most elegant solution to this design problem, it is understood that it is far from the easiest or the cheapest. There are significant technical challenges to overcome for such a system to work. The hull must be designed from the start with the understanding that it will need to accommodate a sonar to mitigate both the effect the sonar has on boat performance, and the effect the hull has on sonar performance. The hull design must be capable of withstanding expected impact loads like any other hull, but the addition of an integrated sonar means that it must do so while insulating the sonar from these loads.

Designing a hull with an integrated sonar from the ground up is far beyond the scope of this research, and would easily cost millions of dollars to develop. The next best option is a retractable sonar mount with omnidirectional breakaway positioned at the front of the boat. The bow mount offers an unobstructed forward view, positions the sonar far from the boat's propulsion systems and its turbulent wake, and can be designed and prototyped for tens of thousands of dollars. Such a mount represents the best option for mounting an imaging sonar to an existing fleet of shallow-water vessels.

6.3 Future Work

Looking forward to the future of the sonar mount and BSB design, there are several points that need to be considered. The design described in Chapter 5 needs to be prototyped and field tested. Most importantly, the BSB needs to be prototyped and tested to make sure it functions at scale as intended. Important design parameters for the BSB, such as surface finish and hardness of the detents, are currently not well understood. For this reason it remains a priority, and will likely require two or three design cycles to reach a final design. The VT USV and first generation sonar mount would be ideal for testing the BSB since they are inexpensive to operate and have proven themselves in the field.

An interesting area of future research would be to investigate the integration of an imaging sonar with a boat hull. What effect would hull proximity have on image quality? Could any negative effects be mitigated through data processing, repositioning the sonar, or hull design changes? What effect would hull material have on sonar performance? Another important question is how can the sonar be isolated from impacts to the hull? Would protecting the sonar from shock require some actuation to retract the sonar out of harm's way, or could the hull be designed such that the sonar was protected from impacts while allowing it a full FOV? How these questions are answered will determine whether or not a hull-integrated sonar is technically possible, which will have clear implications for future USVs.

The goal of a fully autonomous USV is still a long way off, and for good reason. Giving large powerful machines the ability to make decisions, especially in a combat scenario, can have life and death consequences. For this reason the adoption of this technology will be a gradual process, with more and more autonomy being slowly incorporated into existing systems. The sonar mount described in this thesis is a relatively inexpensive method of mounting a sonar safely, which will aid the development of future autonomous water-based vehicles and the algorithms that control them. It is a small but significant step towards the ultimate goal of a fully autonomous USV.

Bibliography

[1] Thomsen, J. E., 2007, "The Navy Unmanned Surface Vehicle (USV) Master Plan," Department of the Navy, Web. 21 May 2015.

[2] "Historical Report: Atomic Bomb Tests Able and Baker (Operation Crossroads)"pg. 219, http://www.dtic.mil/dtic/tr/fulltext/u2/a995213.pdf.

[3] Sinclair, E. B., 2005, "The Long Tao Sweepers – MSB's in Vietnam 1965-1970," Mobile Riverine Force Association, http://www.mrfa.org/pdf/The%20Long%20Tao%20Sweepers%20-%20Spring%202005%20%281%29.pdf, 22 May 2015.

[4] Caruso, R., 2003, "Enterprise Carrier Strike Group Deploys Unmanned Surface Vehicle," Story Number: NNS031217-04.

[5] Teledyne BlueView, 2013, "P-Series User Handbook," http://www.blueview.com/assets/Uploads/downloads/202914-01-REV-G.pdf

[6] "P450 Series 2D Imaging Sonar Data Sheet," BlueView Technologies, Retrieved from http://pdf.nauticexpo.com/pdf/blueview-technologies/p450-series/39788-54947.html.

[7] "Ribcraft 4.8," Ribcraft USA, Retrieved from http://www.ribcraftusa.com/rib48.html.

[8] Powerhouse Systems, Retrieved from http://www.powerhousesystems.net/u.s.-navy-special-warfare-command.html.

[9] "Hand-Held Suction-Cup Lifter: Aluminum Handle, 3 Cups, 220 Pound Lift Capacity," McMaster-Carr, Retrieved from http://www.mcmaster.com/#5608a91/=z2vc4g.

[10] "Cylinder Magnets: DZ0X8-N52," K&J Magnetics, Inc., Retrieved from https://www.kjmagnetics.com/proddetail.asp?prod=DZ0X8-N52.

[11] "Shaft Mounting Collars 2-Piece Stackable," Stafford Manufacturing Corp., Retrieved from http://www.staffordmfg.com/Product-Categories/Shaft-Mounting-Collars-2-Piece-Stackable.

[12] "83mm / M8 U BOLT EXHAUST CLAMP WITH NUTS PIPE CLAMPS TUBE CLIPS CONNECTORS," eBay, User ID: armartradingltd, Retrieved from http://www.ebay.co.uk/itm/83mm-M8-U-BOLT-EXHAUST-CLAMP-WITH-NUTS-PIPE-CLAMPS-TUBE-CLIPS-CONNECTORS-/321332404796.

[13] "EAS®-smartic® Installation space-optimised torque limiting clutches," [Product guide] Mayr, Retrieved from http://www.industrialclutch.com/pdf/mayr-eas-smartic.pdf.

[14] Munson, B. R., Young, D. F., Okiishi, T. H., 2006, *Fundamentals of Fluid Mechanics*, 5th ed., John Wiley and Sons, Hoboken, NJ.

[15] Bruno, L., Fransos, D., Coste, N., and Bosco, A., 2010, "3D Flow Around a Rectangular Cylinder: A Computational Study," Journal of Wind Engineering and Industrial Aerodynamics, 98(6-7), pp. 263-276.

[16] Benson, T., 2010, FoilSim III Student Version 1.5a [Computer software], National Aeronautics and Space Administration, Retrieved from https://www.grc.nasa.gov/www/K-12/airplane/foil3.html.

[17] McMaster-Carr, "More About Plastics," http://www.mcmaster.com/#8574kac/=v1bwlt, 15 Dec. 2014.

[18] Elgin Fastener Group, "Brass Material Property Data Sheet," http://elginfasteners.com/resources/raw-material-technical-data-specifications/brass-material-property-data-sheet/, 15 Dec. 2014.

[19] Advanced Polymer Technologies, "Nylon 6/6 Resin," http://aptllc.net/assets/pdf/Nylon-66-Datasheet.pdf, 15 Dec. 2014.

[20] Ensinger, "ULTEM," http://www.sdplastics.com/ensinger/ultem.pdf, 15 Dec. 2014.

[21] MatWeb, "Victrex® PEEK 450GL30 30% Glass Fiber Reinforced," http://www.matweb.com/search/datasheet.aspx?matguid=c937e0c6fb3d4990a827cefe5f186d9b, 15 Dec. 2014.

[22] Zhang, C., 2005, "Pole-mounted Sonar Vibration Prediction Using CMAC Neural Networks." University of New Hampshire.

[23] Warboats of America, "SOC-R (Special Operations Craft – Riverine)," http://www.warboats.org/SOCR.htm, 17 Nov. 2014.

[24] American Special OPS, "Special Operations Craft – Riverine (SOC-R)," http://www.americanspecialops.com/boats/soc-r/, 25 Aug. 2015.

[25] Infinity Science Center, "Special Operations Craft-Riverine," http://www.visitinfinity.com/wp-content/themes/whiteinc/uploads/Riverine-Warfare-boat-courtesy-NASA-mailer.jpg, 17 Nov. 2014.

[26] Loeffler, C., 15 Sept. 2011, "Sonar and AUV Technology," National Oceanic and Atmospheric Administration, Web. 5 Nov. 2014.

[27] Oberg, E., Jones F. D., Horton H. L., and Ryffel H. H., 2012, Machinery's Handbook. 29th ed. Industrial Press, New York.

[28] Repair Engineering, "Bolt Torque Chart," http://www.repairengineering.com/bolt-torque-chart.html, 16 Dec. 2014.

[29] Budynas, R.G., and Nisbett, J. K., 2008, *Shigley's Mechanical Engineering Design*, McGraw-Hill, New York.

[30] Inman, D., 2008, *Engineering Vibration*, 3rd ed., Upper Saddle River, New Jersey: Pearson Prentice Hall.

[31] "Free Vibration of a Cantilever Beam with a Lumped Mass at Free End." Sakshat Virtual Lab. IIT Guwahati, n.d. http://iitg.vlab.co.in/?sub=62&brch=175&sim=1078&cnt=1, Web. 15 Dec 2013.

[32] Laura, P.A.A, 1974, "A Note On The Vibrations of a Clamped-Free Beam with a Mass at the Free End," Journal of Sound and Vibration, 37.2, pp. 161-168.

[33] Blevins, R. D., 1979, *Formulas for Natural Frequency and Mode Shape*, New York, NY: Van Nostrand Reinhold Company.

Appendix A: Design Challenges

Table A.1: Pros and cons of solutions to the various design challenges associated with a sonar mount

Mount Location	Pros	Cons
Side	Most boats have a clear space on side Can be adjusted bow to stern	Sides may not be strong enough
Transom	Strong Almost every boat has one	turbulence Space limitations depending on outboard
Rails	Sturdy Can use pipe clamps	Not all boats will have them Limited placement
Deck	Strong	Boat mods required, bolted or welded Taking up deck space More weight to reach up and over gunnel
Hull	Very easy to use Minimal mechanical maintenance Uses zero deck space	Sonar not accessible unless boat is on trailer Difficult to protect sonar from impacts Not feasible as an add-on to an existing vessel Hull proximity may interfere with sonar
Attachment method	**Pros**	**Cons**
Magnets on sides	Very Strong Easy to use	Very Strong (hard to remove) Requires a thin wall May mess with data from sonar and magnetic cumpasses May not clamp hard enough to hold mount rigid in a collision
2x large C clamp (custom)	Easy to use Easy to adjust Can accommodate different size walls	Could crack the hull if fiberglass May loosen with vibration
Pipe clamp	Simple Cheap Strong Easy to adjust	Only works on pipes
Suction cups	Quick to set up	Requires pump Requires a smooth, clean surface May lack strength to hold mount rigid during collision
Bolts	Strong Cheap Standardized	Requires modifying the boat Can't adjust position easily
Scissor-lift clamp	Easy to use Easy to adjust Can accommodate different size walls	Could crack the hull if fiberglass Tougher to distribute force
Retraction method	**Pros**	**Cons**
Telescoping (multi-stage)	Packages into a smaller area Adjust depth on the go Pulls sonar straight up so less water resistance	Multipule parts that could bind Any dents would prevent the device from working Weaker than a single pole

Linear slide	Adjust depth on the go Pulls sonar straight up so less water resistance	Long Slow to retract and extend
Rotation about pitch axis	Same direction as breakaway point Easier to bring up by hand if necessary Can use a torque limiter instead of shear pins	
Rotation about roll axis		Angle of shear point changes when retracting/extending Requires more room to deploy
Giant ball screw	Pulls sonar straight up so less water resistance	Slow Expensive
4-bar linkage	Moves weight back over the boat Pulls sonar straight up so less water resistance	Expensive to build Holds sonar farther from boat, so moments will increase
Power	**Pros**	**Cons**
Motor and gearbox	Can be geared to work quickly Plenty of torque	Needs to be waterproof Complex, expensive
Linear actuator	Waterproof actuators readily available Cheap Wide range of load ratings and throw lengths	Slow
Pneumatics/hydraulics	Waterproof	Compressor/Tanks need to be added Difficult setup
Cable system	Mechanical advantage	Potentially difficult setup
MANpower	Simple, effective Grunts during retraction will deter alligators	Can't lift easily if $\perp$ to boat Likely requires some mechanical advantage
Ball screw	Reliable, strong	Slow
Collision protection	**Pros**	**Cons**
Magnets	reusable, strong, nondestructive	difficult to disengage, crushing hazard for fingers and hands
Acrylic block	Cheap Simple	Needs to be replaced after collision
Torque limiter	Nondestructive Adjustable to set torque	Expensive Tougher to install (must isolate from lateral load) Large, heavy
Shear dowel	Cheap Simple	Needs to be replaced after collision Could fall out
Shear bolts	Cheap Simple, nut ensures bolt stays in place	Could rust Needs to be replaced after collision

Depth adjustments	Pros	Cons
Telescoping	Adjust depth on the go Quicker to adjust Don't need to worry about dropping sonar off boat	Easy to bind Weaker than a single pole
Linear slide	Adjust depth on the go Quicker to adjust Don't need to worry about dropping sonar	Limits the shape of the post
Interchangable sections of varying length	Never have much extra weight/post out of the water More universal on retraction devices	Can't adjust when in motion Could drop assembly during length change
Two pipe clamps	Fewer moving parts More universal on retraction devices	Can't adjust when in motion

Table A.2: Prioritization matrix for customer needs

Scoring		Hydrodynamic	Breakaway	Durability	Depth	Mounts to different boats	Rigid	Ease of retraction	Easy to maintain	Easy to install	Corrosion	Safe	Aesthetic appeal	Lightweight	Compatible with P-450-45 sonar	Steerable sonar	Inexpensive
2	much more important																
1	more important																
0	equally important																
-1	less important																
-2	much less important																
Hydrodynamic			1	1	0	-1	1	2	1	0	1	2	0	0	-1	1	1
Breakaway		-1		0	-1	-1	-1	1	-1	-1	-1	1	-1	-1	-1	0	-1
Durability		-1	0		0	-1	0	1	-1	-1	-1	1	-2	-1	-1	-1	-1
Depth		0	1	0		-1	0	1	-1	0	0	2	-1	0	-1	0	-1
Mounts to different boats		1	1	1	1		1	2	1	1	0	2	-1	0	0	1	0
Rigid		-1	1	0	0	-1		1	-1	-1	-1	2	-2	-1	-1	-1	-1
Ease of retraction		-2	-1	-1	-1	-2	-1		-1	-1	-1	2	-2	-1	-1	-1	-1
Easy to maintain		-1	1	1	1	-1	1	1		-1	0	2	-1	0	-1	-1	-1
Easy to install		0	1	1	0	-1	1	1	1		1	2	-1	0	-1	0	-1
Corrosion		-1	1	1	0	0	1	1	0	-1		1	-1	-1	-1	0	-1
Safe		-2	-1	-1	-2	-2	-2	-2	-2	-2	-1		-2	-1	-2	-1	-2
Aesthetic appeal		0	1	2	1	1	2	2	1	1	1	2		0	-1	1	0
Lightweight		0	1	1	0	0	1	1	0	0	1	1	0		-1	0	-1
Compatible with P-450-45 sonar		1	1	1	1	0	1	1	1	1	1	2	1	1		0	0
Steerable sonar		-1	0	1	0	-1	1	1	1	0	0	1	-1	0	0		-1
Inexpensive		-1	1	1	1	0	1	1	1	1	1	2	0	1	0	1	
Total		-8	8	8	0	-11	6	14	-1	-5	0	23	-14	-5	-13	-2	-11
Scaled Total		20	36	36	28	17	34	42	27	23	28	51	14	23	15	26	17
Weight (%)		4.58	8.24	8.24	6.41	3.89	7.78	9.61	6.18	5.26	6.41	11.67	3.20	5.26	3.43	5.95	3.89

Appendix B: Bill of Materials

Ordered
Not Ordered/May Not Need

Materials for boat mount

Recd? (x)	Item	Use	Vendor	Part no.	Unit Price	Qty.	Total Price	Notes
x	single 5-hole 90 deg. Plate		www.mcmaster.com	47065T178	$7.76	4	$31.04	
x	zinc plated T-nuts and bolts		www.mcmaster.com	47065T97	$2.71	14	$37.94	
x	6" heavy duty 90 deg. braces		www.mcmaster.com	47065T12	$17.86	2	$35.72	
x	1.5" pipe clamps	clamps for mounting support poles	www.mcmaster.com	2236T36	$31.95	12	$383.40	
x	1.25" pipe clamps	clamps for mounting support poles	www.mcmaster.com	2236T34	$26.93	8	$215.44	
x	6-ft section 1.5" 80/20	Mounting bracket	www.mcmaster.com	47065T148	$36.82	2	$73.64	
x	1.25"OD x 10' long galvanized EMT conduit tube	supports for antenna tower	www.mcmaster.com	7126K4	$17.22	1	$17.22	*Received 1.5" conduit NOT 1.25" (can make this work)
x	single two-hole 90 deg. braces	braces for attaching boat mount to sonar mount	www.mcmaster.com	5537T51	$7.98	10	$79.80	
x	double 4-hole 90 deg. mounting braces	braces for attaching boat mount to sonar mount	www.mcmaster.com	47065T222	$6.06	4	$24.24	
x	4-hole right angle brackets	brackets for connecting base plate 80/20	www.mcmaster.com	47065T51	$4.38	4	$17.52	
x	5/16"-18 x 2.5" socket head cap screw		www.mcmaster.com	92185A593	$8.17	1	$8.17	
x	1/4"-20 x 2.25" stainless hex-head screw	bolts for securing pipe clamp	www.mcmaster.com	93190A551	$8.88	1	$8.88	
x	1/4" stainless washers	washers for pipe clamp bolts	www.mcmaster.com	91525A119	$8.19	1	$8.19	
x	1/4"-20 x 24" threaded rod	threaded rod for pipe clamps	www.mcmaster.com	93250A440	$4.23	1	$4.23	
x	1/4"-20 stainless nuts	nuts for threaded rod	www.mcmaster.com	94819A043	$7.64	1	$7.64	
x	1-5/16" shaft collars	shaft collars to be machined and used as pipe clamps	www.mcmaster.com	6436K145	$9.61	4	$38.44	
						SubTot.	$991.51	

Materials for Sonar Mount

Recd? (x)	Item	Use	Vendor	Part no.	Unit Price	Qty.	Total Price	Notes
x	Linear Actuator	Lift	www.dcactuators.co	6112CH	$170.00	1	$170.00	
x	Iglide T500 2.75in bushing	Bushings	www.igus.com	TFI-4447-32	$70.66	2	$141.32	
x	2.75in Shaft Collar	Lift Pipe	www.mcmaster.com	6436K168	$42.33	2	$84.66	
x	2.5" u bolt	Clamping bolts	www.mcmaster.com	3042T79	$1.56	2	$3.12	
x	1in sealed ball bearings	Rotation Bearings	www.mcmaster.com	2782T77	$23.67	2	$47.34	
x	1in aluminum shaft collar	Rotation shaft collar	www.mcmaster.com	6436K73	$4.85	2	$9.70	
x	2.6" OD x 2.555ID x41" fiberglas tube	Foil tube	www.madcowrocketry.com		$45.95	1	$45.95	
x	6ft 1.5inx1.5in 80/20 Fractional 15 Serie	base plate edging	www.mcmaster.com	47065T148	$36.82	1	$36.82	
x	2ft 1.5inx3in 80/20 Fractional 15 Series	base plate center	www.mcmaster.com	47065T158	$24.55	1	$24.55	
x	32x Tnut		www.mcmaster.com	47065T97	$2.71	10	$27.10	
x	4-hole right angle brackets		www.mcmaster.com	47065T51	$4.38	10	$43.80	
x	1" Stretch-Fit Rotary-Shaft Ring Seals		www.mcmaster.com	9562K46	$4.38	1	$4.38	
	10'x40" Fiberglass Fabric Sheeting	fiberglass	www.mcmaster.com	8816K521	$66.00	1	$66.00	
x	0.5" Shldr x 1-3/4" length 3/8"-16 thread	shear pin	www.mcmaster.com	93897A709	$6.00	1	$6.00	
x	3/8"-16 thread nylon hex nuts	shear pin nuts	www.mcmaster.com	94812A031	$7.98	1	$7.98	
x	1/2"-20 x 3.5" length , 316 stainless bolt	bushing block bolts	www.mcmaster.com	92186A392	$5.49	4	$21.96	
x	1/2"-20, 316 stainless hex lock nuts	bushing block nuts	www.fastenal.com	77884	$2.28	10	$22.80	
x	3/8"-24 x 1.5" length , 316 stainless bolt	clamping plate to flange	www.mcmaster.com	93190A367	$12.23	3	$36.69	
x	3/8"-24, 316 stainless hex lock nuts	clamping plate to flange nut	www.fastenal.com	37584	$0.22	15	$3.33	
x	3/8"-24 x 3/4" length, 316 stainless bolts	tilt adjustment bolts	www.mcmaster.com	93190A360	$6.13	1	$6.13	
x	1/2" Shldr 1.75" length 3/8"-16, 316 stai	lift bar to lift bar block bolt	www.fastenal.com	11127209	$19.93	2	$39.86	
x	3/8" washers, 316 stainless	washers	www.mcmaster.com	90107A031	$8.36	1	$8.36	
x	1/2" washers, 316 stainless	washers	www.mcmaster.com	91950A033	$12.08	1	$12.08	
x	7/16" x 1.75", galvanized clevis pins	actuator pins	www.fastenal.com	0156240	$2.98	2	$5.96	
x	1/8" x 3/4", cotter pin	actuator pin retainers	www.fastenal.com	65074	$4.06	1	$4.06	
x	#10-32 x 3.5" zinc finish steel socket cap	gearbox to flange	www.fastenal.com	93177	$4.07	8	$32.56	
x	#10-32 lock nuts	gearbox to flange nuts	www.fastenal.com	37015	$0.07	8	$0.56	
x	3/8"-16 lock nuts	lift bar to lift block bolt nuts	www.fastenal.com	37025	$0.47	5	$2.35	
x	2.5" shaft collar	shaft collars to hold fairing	www.mcmaster.com	6436k164	36.63	2	$73.26	
	3/8-16 UNC - 3/4	cap screws, sonar mounting bracket to sonar clamp	Heavener			2		
x	IP65 rated pan motor	Motor	http://www.animatic	SM34165MT-IP	$2,239.00	1	$2,239.00	
x	Matching gearhead	Gearbox	http://www.animatic	GH34SP070-0.5	$662.00	1	$662.00	
x	Power Cable	cables for motor	http://www.animatic	CBLIP-PWR4-FI	$101.00	1	$101.00	
x	Comunications Cable	cables for motor	http://www.animatic	CBLIP-COM-FL-	$53.00	1	$53.00	
	12-24V DC-DC Converter	takes 12V from battery to 24V for motor	current logic					
x	Black marine paint	waterproof paint for fairing	http://www.ipaint.us	8620SeriesQuart	29.95	1	$29.95	
x	Sonar Clamp	Clamp for sonar head	http://www.blueviev	201392-01	360.4	1	$360.40	
						SubTot.	$4,434.03	

Heavener Stuff

Recd? (x)	Item	Use	Vendor	Part no.	Unit Price	Qty.	Total Price	Notes
x	5/16"-18 x 2.5"	screws for connecting 80/20 frame	heavener		$1.25	8	$10.00	
	3/8"-24 x 1"	tilt adjustment bolts	heavener			2		
x	5/16" - 18 tap	for tapping 80/20	heavener			2		
						SubTot.	$10.00	

Extra Items

Recd? (x)	Item	Use	Vendor	Part no.	Unit Price	Qty.	Total Price	Notes
x	1 -5/16" shaft collars	shaft collars to be machined and used as pipe clamps	www.mcmaster.com	6436K145	9.61	4	$38.44	
x	1/2"-20 x 3.5" length , 316 stainless bolts		www.mcmaster.com	92186A392	$5.49	4	$21.96	
x	zinc plated T-nuts and bolts		www.mcmaster.com	47065T97	$2.71	5	$13.55	
x	2.5" u bolt	Clamping bolts	www.mcmaster.com	3042T79	$1.56	2	$3.12	
x	1" Stretch-Fit Rotary-Shaft Ring Seals		www.mcmaster.com	9562K46	$4.38	2	$8.76	
x	1in sealed ball bearings	Pan shaft bearings	www.mcmaster.com	2782T77	$23.67	2	$47.34	
x	1in aluminum shaft collar	Pan shaft collar	www.mcmaster.com	6436K73	$4.85	2	$9.70	
x	1/2" Shldr 1.75" length 3/8"-16, 316 sta	lift bar to lift bar block bolt	www.fastenal.com	11127209	$19.93	3	$59.79	
x	7/16" x 1.75", galvanized clevis pins	actuator pins	www.fastenal.com	0156240	$2.98	2	$5.96	
x	3/8"-16 lock nuts	lift bar to lift block bolt nuts	www.fastenal.com	37025	$0.47	5	$2.35	
						SubTot.	$210.97	

Total $5,646.51

Appendix C: Detailed Calculations

Calculation of drag on a pole moving through water at 5.14 m/s (10 kt)

Compute Reynolds number

$$Re = \frac{\rho u D}{\mu} \tag{C.1}$$

Where ρ is density of water, u is the velocity, D is the diameter of the pole, and μ is the dynamic viscosity. Plugging in values gives:

$$Re = \frac{\left(998.2\,\frac{kg}{m^3}\right)\left(5.14\,\frac{m}{s}\right)(0.0635\,m)}{1.002 \times 10^{-3}\,\frac{Ns}{m^2}} = 3.25 \times 10^5 \tag{C.2}$$

From Figure 9.21 of Fundamentals of Fluid Mechanics, 5th Ed., the coefficient of drag for a smooth cylinder with the preceding Reynolds number is 0.8 [14]. Using this, we compute the drag force on the pole as follows.

$$F_{dB} = C_{dB}\frac{1}{2}\rho u^2 D l \tag{C.3}$$

Where C_{dB} is the coefficient of drag, and l is the submerged length of the pole. Plugging in values gives:

$$F_{dB} = 0.8\left(\frac{1}{2}\right)\left(998.2\,\frac{kg}{m^3}\right)\left(5.14\,\frac{m}{s}\right)^2(0.0635\,m)(0.908\,m) = 609.2\,N \tag{C.4}$$

Calculation of drag on a faired pole moving through water at 5.14 m/s (10 kt)

NASA's FoilSim software results in a drag of 98 N/m. With 0.908 m of the faired pole submerged, this constitutes a drag force of 89 N (19 lb) [16].

Calculation of drag on sonar analyzed as a rectangular prism moving through water at 5.14 m/s

The BlueView P450 sonar used for this research has an unusual shape that makes it difficult to analyze without the use of CFD. Fig. C.1 shows a detail drawing of the P450. In order to reduce

the design time, the P450 is approximated as a rectangular prism with the same frontal area, and equal in overall length to the P450.

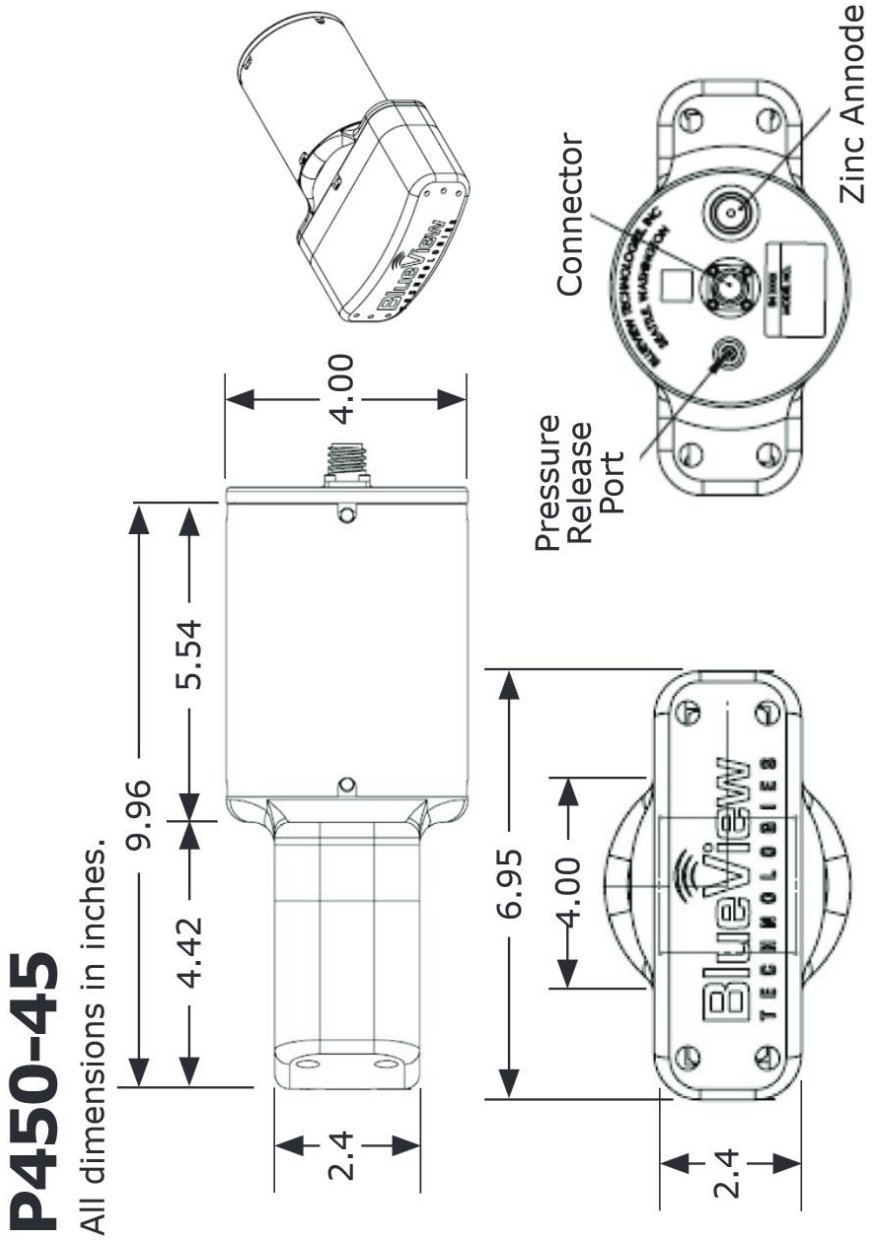

Fig. C.1: Dimensions of BlueView P450 sonar [6] <"P450 Series 2D Imaging Sonar Data Sheet," BlueView Technologies, Retrieved from http://pdf.nauticexpo.com/pdf/blueview-technologies/p450-series/39788-54947.html.> (used under fair use, 2015)

Recent research by Bruno, et al, confirms the findings of previous researchers showing that, for high Reynolds number flows ($Re > 10^5$), the coefficient of drag acting on a rectangular prism is heavily dependent on the prism's chord to depth ratio. From the prism of Fig. C.2 below, the chord to depth ratio is defined as

$$\frac{B}{D} \tag{C.5}$$

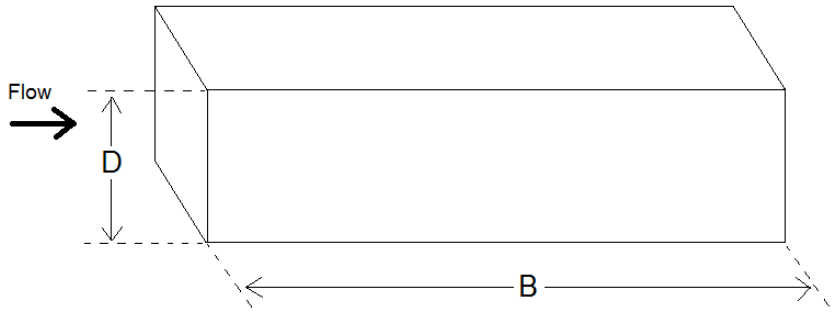

Fig. C.2: Generic rectangular prism in a high Reynolds number flow

Because the sonar is equivalent to or larger than the pole in all dimensions, we can conclude that it will have a Reynolds number greater than the pole. This clearly establishes that the Reynolds number of the sonar at a velocity of 5.14 m/s will be greater than 10^5.

Remembering that the simplified sonar has $B = 253\,mm$ and $D = 176.5\,mm$, the chord to depth ratio is $B/D = 1.43$. Because most scientific papers do not examine such specific chord to depth ratios, we round up to 1.5. Bruno et al. list four data points for the drag coefficient at $B/D = 1.5$, the average of which is 1.74 [15]. Using this in the following equation, where A is the frontal area of the sonar, and f is a correction factor to account for the brackets, we get

$$F_{ds} = C_{ds}\frac{1}{2}\rho u^2 A f \tag{C.6}$$

$$F_{ds} = \frac{1}{2}(1.74)\left(998.2\frac{kg}{m^3}\right)\left(5.14\frac{m}{2^2}\right)^2(0.061\,m)(0.1765\,m)1.2$$

$$F_{ds} = 296.4\,N\ (66.6\,lb)$$

Worst case sonar drag

We also must consider the fact that the sonar will be panning back and forth as the USV moves through the water. From the shape of the BlueView P450, it is clear that the worst case will occur when the sonar is pointed at 90˚ from the USV heading.

For the worst case sonar drag, the sonar will not be modeled as a rectangular prism as it is likely that this would yield numbers that would be much too high. Instead, it will be modeled as a rectangular prism with a cylinder. The assumption is made that the prism and cylinder can be analyzed independently of one another, which should yield drag forces which are larger than the actual forces. The model used for analysis is shown in Fig. C.3. As described, it consists of a

rectangular prism with a cylinder attached to one face. In the figure, the worst case flow is directed into the page.

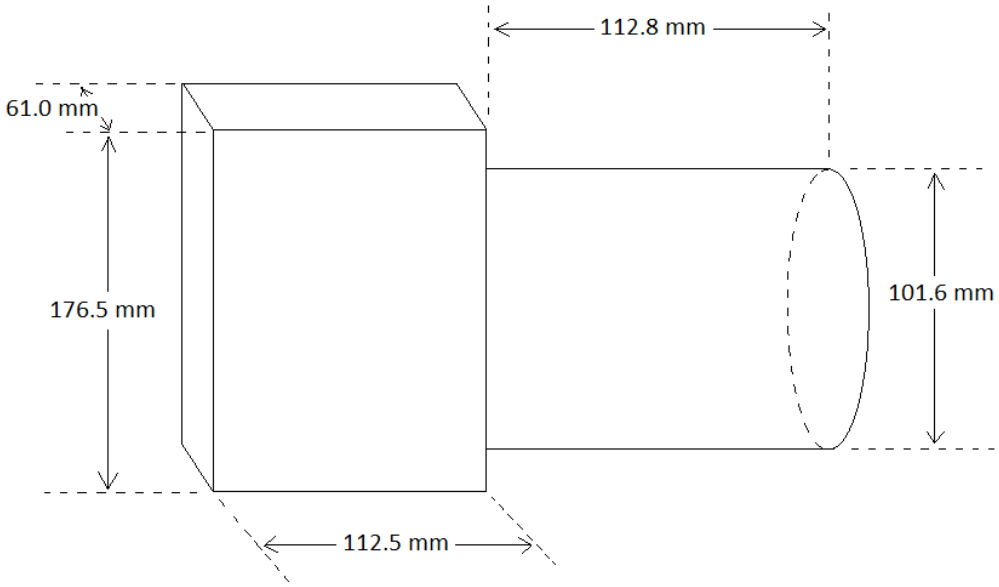

Fig. C.3: Body used for worst case sonar drag analysis

We define the worst case sonar drag as equal to the sum of the prism drag and the cylinder drag as follows.

$$F_{dsw} = F_{dp} + F_{dc} \tag{C.7}$$

Making use of Eqs. C.3 and C.6 and rearranging yields

$$F_{dsw} = \frac{1}{2}\rho u^2 [C_{dp} A_p f + C_{dc} D_c l_c] \tag{C.8}$$

Where C_{dp} and A_p are the coefficient of drag and frontal area of the prism, respectively, f is the scaling factor for the brackets, and C_{dc}, D_c, and l_c are the drag coefficient, diameter, and length of the cylinder.

We again use Bruno et al to estimate the drag coefficient of the prism. The chord to depth ratio of the prism is $B/D = 0.346$. Due to a scarcity of data in the vicinity of this chord to depth ratio, the coefficient of drag is determined using linear interpolation between the nearest two points which are

$$(0.2, 2.01) \ \ and \ \ (0.4, 2.22)$$

Where the first number of each pair is the chord to depth ratio, and the second number is the drag coefficient. From these numbers the drag coefficient at $B/D = 0.346$ is estimated to be 2.16.

Plugging values into Eqn. B.8 yields

$$F_{ds} = \frac{1}{2}\left(998.2\frac{kg}{m^3}\right)\left(5.14\frac{m}{s}\right)^2 [2.16(0.1765\ m)(0.1125\ m) + 0.3(0.1016\ m)(0.11278\ m)(1.2)]$$

$$F_{ds} = 641.09\ N$$

Therefore the maximum drag expected with a faired pole and a side-facing sonar at 5.14 m/s (10 kt) is: 730 N. This drag force is centered at a depth of 0.933 m, and exerts a moment of 1214.83 N-m at the sonar pole's pivot.

Compute stresses on sonar pole

The sonar pole has a 2.5 in (63.5 mm) OD and 1.5 in (38.1 mm) ID.

It is clear that the largest stresses on the pole will occur while it is deployed, so stresses on the pole in the retracted position will not be considered. Torsion should not be a major factor, so it will be neglected. We will also neglect to consider the smaller inner pole, since it should not contribute much to the stiffness of the assembly.

In the deployed position, the sonar pole experiences plane stress, with bending stress and shear stress due to drag. The location of maximum stress should be at the pivot on either the fore or aft side of the pole.

The cross sectional area of the pole is $0.00202683\ \text{m}^2$. The area moment of inertia is computed using

$$I = \frac{\pi}{64}(D^4 - d^4) \tag{C.9}$$

where D is the OD and d is the ID. I is found to be $6.92 \times 10^{-7}\ m^4$.

The shear stress is computed as

$$\tau = \frac{F}{A} = \frac{730\ N}{0.00202683\ m^2} = 0.3602\ MPa$$

And the bending stress is

$$\sigma = \frac{Mc}{I} = \frac{(1214.83\ Nm)(0.03175\ m)}{6.92 \times 10^{-7}\ m^4} = 55.7\ MPa$$

Clearly the bending stress dominates, so the shear stress can be neglected. The yield strength for 6061 Al is 276 MPa (p. 541 of [27]). The factor of safety against yield of the sonar pole by bending is 5.

Determine lifting capacity of linear actuator to lift sonar pole.

This problem is a simple moment balance. There are about 10 different parts making up the sonar pole. These components are grouped and analyzed as follows: the sonar with clamps; fairing; outer and inner Al tubes; gearbox; and motor. The weight of seals, clamps, and bearings is neglected. A free-body diagram for the system is shown in Fig. C.4 below.

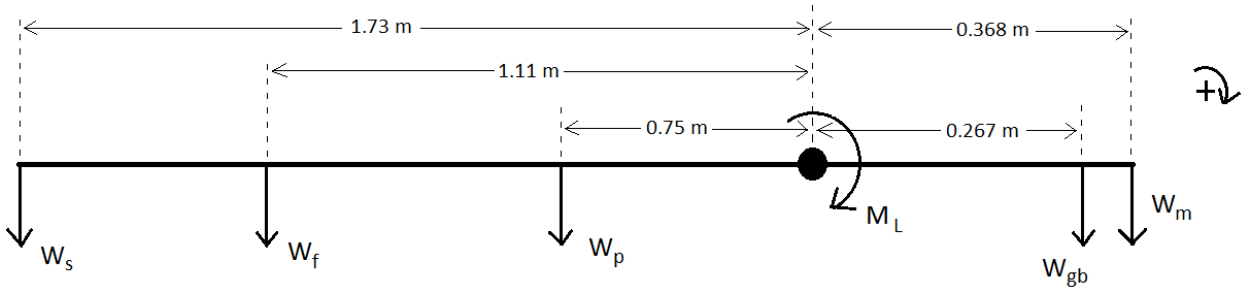

Fig. C.4: Free-body diagram for sonar pole when horizontal

Balancing moments about the lifting axis yields:

$$-M_s - M_f - M_p + M_L + M_{gb} + M_m = 0$$

$$[-(2.27\ kg + 0.8\ kg)(1.73\ m) - (1.18\ kg)(1.11\ m) - (9.63\ kg)(0.75\ m) + (2.72\ kg)(0.267\ m) + (2.31\ kg)(0.368\ m)]\ (9.81\frac{m}{s^2}) + M_L = 0$$

$$-52.1\ Nm - 12.85\ Nm - 70.85\ Nm + 7.12\ Nm + 8.34\ Nm + M_L = 0$$

$$M_L = 120.3\ Nm \quad when\ horizontal$$

When fully retracted, the lift bars give a moment arm of 73 mm, so the max lift force is

$$F_{Lmax} = \frac{M_L}{0.073\ m} = \frac{126.2\ Nm}{0.073\ m} = 1648.5\ N\ (370.6\ lb)$$

From this we conclude that a 1000 lb actuator will be adequate, and will leave sufficient room for future equipment additions if they are necessary.

Stress Calculations for bushing block bolted connections

There are two bushing blocks which are shown in Fig. C.5, along with the other parts of the base assembly. Not shown is the 80/20® which is fixed to the bottom of the large flat base plate for strength. Each block is fixed to the flat plate with two 1/2”-20 bolts.

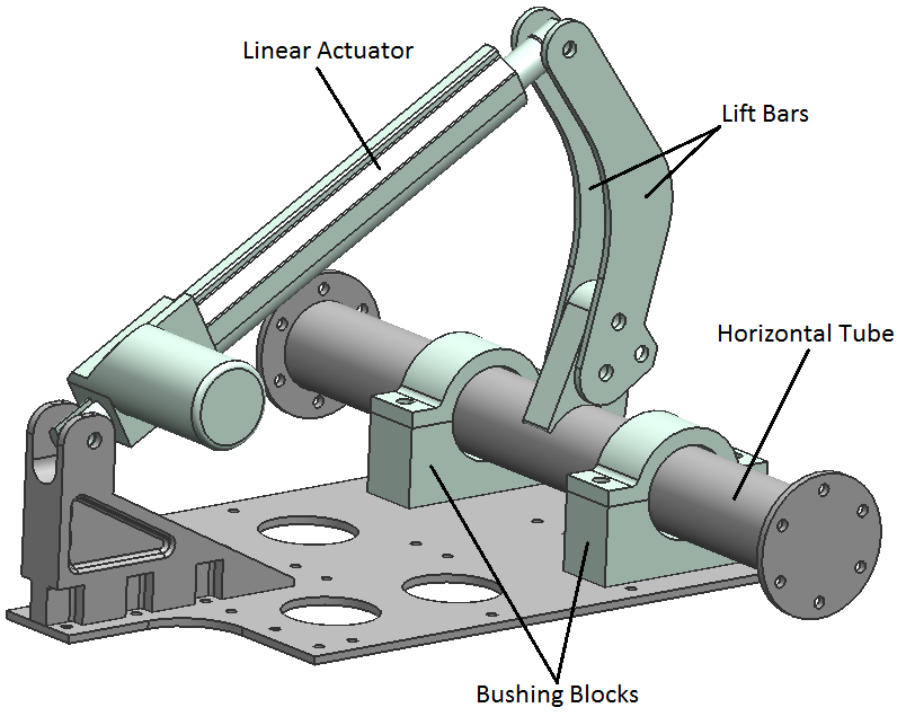

Fig. C.5: Sonar mount base assembly

The first step in this problem is to determine the loads present. A simplified version of the base assembly with unnecessary components removed is shown in Fig. C.6. The forces and moments present are the drag force and its associated moment, F_d and T_d, and the reaction forces F_{B1}, F_{B2}, and F_a, which are the reactions at bushing block 1 and 2, and the reaction from the actuator resisting the torque due to drag, respectively.

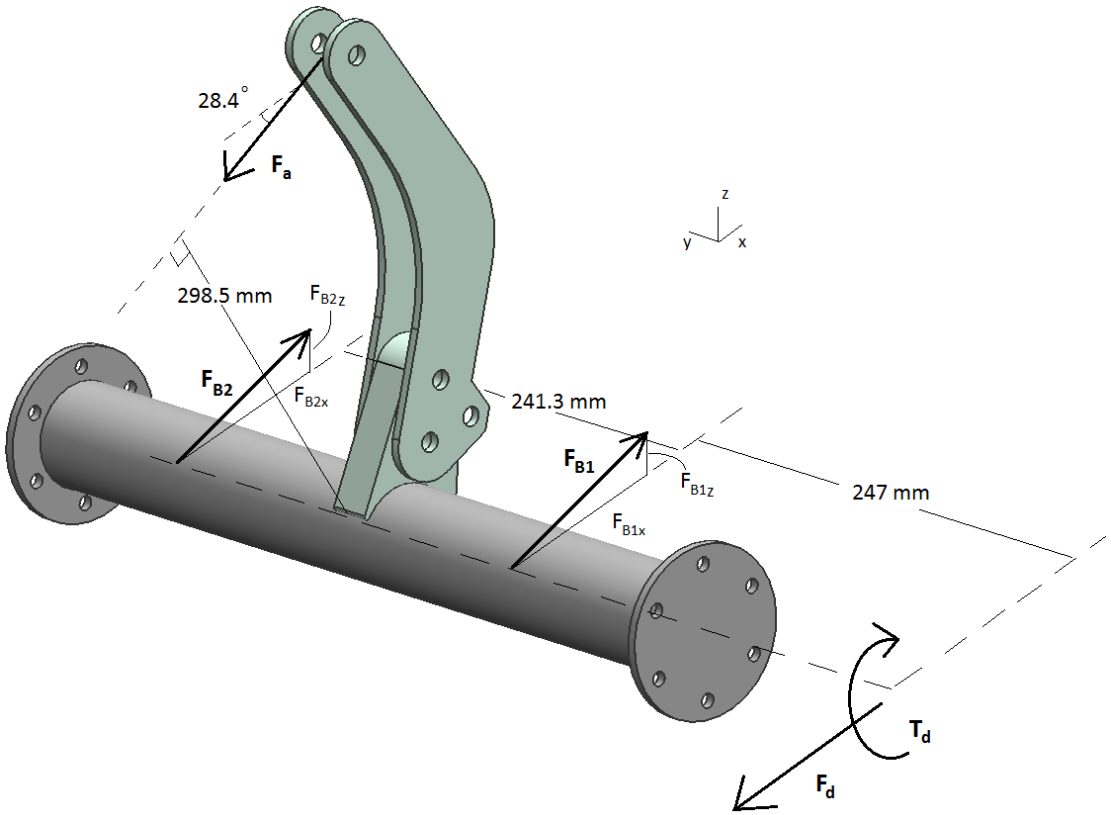

Fig. C.6: FBD of horizontal tube and lift bars

It is important to note that the x-z plane containing the force F_a is equidistant from the x-z planes containing F_{B2} and F_{B1}. Also, we neglect the weight of the sonar pole since its foam fairing will offset much of its weight when submerged.

From previous computations, we know that the worst-case drag force acting on the sonar pole is:

$$F_d = 641.1\ N + 89\ N = 730.1\ N$$

so the worst-case torque acting at the horizontal tube due to drag is:

$$T_d = (730.1\ N)(1.664\ m) = 1214.9\ Nm$$

Balancing torques about the horizontal tube's axis gives

$$T_d = F_a M \tag{C.10}$$

where M is the moment arm for the actuator force F_a. Plugging in values gives

$$1214.9\ Nm = F_a(0.2985\ m)$$

$$F_a = 4070.0\ N$$

This represents the load present on the actuator when the sonar is deployed and moving at 5.14 m/s (10 kt). The linear actuator has a load rating of 5000 N (1124 lb), so this is acceptable.

Next we must solve for the forces F_{B1} and F_{B2}. These two values represent four unknowns, so we need four equations to solve. Balancing forces along the x-axis gives the following relation

$$\Sigma F_x = 0 = -F_d + F_{B1x} - F_a \cos(28.4) + F_{B2x} \tag{C.11}$$

Balancing forces along the z-axis gives

$$\Sigma F_z = 0 = F_{B1z} - F_a \sin(28.4) + F_{B2z} \tag{C.12}$$

The last two equations needed come from moment balances about the z and x axes. We choose to write the moment balances at the point of application of F_{B1}. This yields

$$\Sigma M_{zB1} = 0 = -F_d(0.247\ m) + F_a \cos(28.4) - F_{B2x}(0.2413\ m) \tag{C.13}$$

$$\Sigma M_{xB1} = 0 = -F_a \sin(28.4)\left(\frac{0.2413\ m}{2}\right) + F_{B2z}(0.2413\ m) \tag{C.14}$$

Solving the system of equations (C.11 - C.14) gives

$$F_{B1x} = 3266.2\ N$$

$$F_{B1z} = 967.9\ N$$

$$F_{B2x} = 1041.4\ N$$

$$F_{B2z} = 967.9\ N$$

It follows that $F_{B1} = 3406.4\ N$ and $F_{B2} = 1421.3\ N$.

Once we have these numbers, there are two failure modes to consider: failure of the bolts in pure shear; and failure of the base plate by crushing (bearing stress). We are neglecting rupture of the base plate by pure tension since the plate is large and therefore the bearing stress on the plate should be limiting. We also neglect edge shearing of the plate since the 13.5 mm (0.531 in) holes are 57.15 mm (2.25 in) from the edge of the plate.

In computing the bolt shear, we make two important assumptions. The first is that the bolt preload has been lost, so that the bolts carry the entire shear load. This is an unlikely scenario, but represents a worst case. The second assumption is that the bolt threads do not enter the shear plane. This ensures that the bolt's shank carries the load as opposed to the threaded portion. One

last important note is that since F_{B1} is much larger than F_{B2} it will be used for all stress calculations. With these assumptions the bolt shear is computed as

$$\tau_b = \frac{F_{B1x}}{A} \tag{C.15}$$

where A is the cross-sectional area of all bolts in the group. In this case there are two. The bolt shear is then

$$\tau_b = \frac{3266.2\ N}{2\pi(0.00635\ m)^2} = 12.89\ MPa$$

The tensile strength of 316 Stainless steel is 483 MPa ultimate, and 207 MPa yield (p. 430 of [27]). We estimate the shear strength of stainless steel to be $S_s = 0.6S_y = 124.2\ MPa$. It is clear that the computed bolt shear is well within the limitations of the material.

The next scenario to consider is crushing of the aluminum base plate. This is computed using the following bearing stress equation

$$\sigma_m = \frac{-F_{B1x}}{td} \tag{C.16}$$

Where t is the plate thickness, and d is the bolt diameter. Remembering there are two bolts carrying the load, substituting values gives

$$\sigma_m = \frac{-3266.2\ N}{2(0.00635\ m)(0.0127\ m)} = 20.25\ MPa$$

The ultimate and yield strengths for 6061 Al are 310 MPa and 276 MPa, respectively (p. 541 of [27]). Estimating the shear strength of aluminum to be 165.6 MPa, we conclude that we have a factor of safety over four for failure of the plate by crushing.

While both the bearing stress and bolt shear stress suggest that we are well within the strength limitations of stainless steel and aluminum, it should be kept in mind that stress concentrations could occur, which would increase these numbers. However, with a proper preload, this should not be an issue. For this reason it is suggested that a torque wrench and locknuts be used during assembly to ensure an adequate preload is maintained. (Note: torque required to reach 70% of proof load of a Grade 2, ½”-20 bolt is 74.6 N-m (55 ft-lb) [28]. A 316 SS bolt should have a strength similar to a Grade 2 bolt.)

Compute max shear stress in flange welds on horizontal tube as designed

One of the sonar mount's most important welded assemblies is the lifting assembly. This assembly is shown in Fig. C.6 in the stress calculations for the bushing block bolted connections above. In this assembly there is a flange fillet welded to each end of the lift tube. The flange's purpose is to transmit the torque from the sonar pole to the lift tube. The moments on the sonar pole are large, so these welds must be strong. Fig. C.7 shows a detail drawing of one of the flanges with its weld callout. In the figure the lift tube is labeled as body 1 and the flange is body 3. While there is no throat size specified in the weld callout, it was expected that the largest weld possible would be applied. Based on the part dimensions, the expected size of the weld was around 6.35 mm (0.25 in).

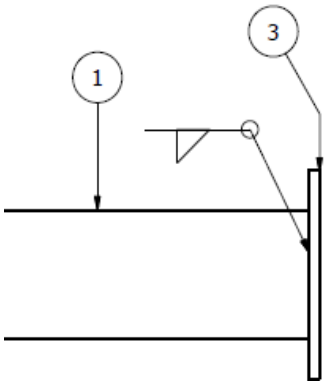

Fig. C.7: Detail drawing showing flange weld as designed

Fig. C.8 shows a cross section view of the expected weld bead. It is assumed that both legs of the weld are the same length. The cross section of the throat area is also shown, with its midpoint denoted by point P.

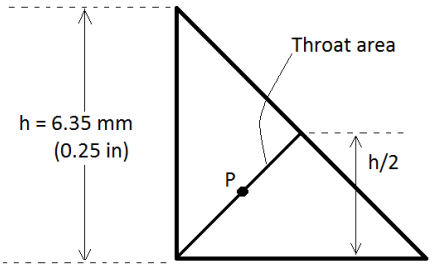

Fig. C.8: Cross section of fillet weld at flange

A free-body diagram for the flange weld is shown in Fig. C.9. It shows the flange with its circular bolt pattern, the weld, which traverses all the way around the 69.85 mm (2.75 in) horizontal tube (not shown), and the shear force and torque from drag.

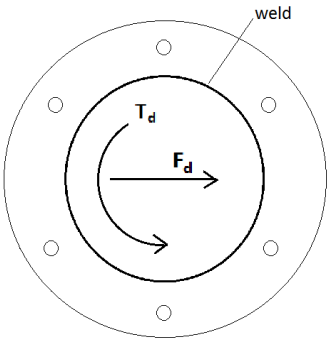

Fig. C.9: Flange weld FBD

It is clear that the weld is in torsion, so there are two stresses to compute. The first is primary shear, which comes from the shear force, F_d, and then secondary shear, which comes from the torque, T_d. The equation for primary shear takes the form

$$\tau' = \frac{F}{A} \tag{C.17}$$

Where F is the shear force and A is the throat area of the weld. The shear force is known, and computing the throat area is straightforward as follows.

$$A = \pi dh sin(45°) \tag{C.18}$$

where d is the weld diameter and h is the weld's leg length. The primary shear is

$$\tau' = \frac{730\ N}{\pi(0.06985\ m + \frac{0.00635\ m}{2})(0.00635\ m)\sin(45°)} = 0.709\ MPa$$

The secondary shear equation for a weld in torsion is

$$\tau'' = \frac{Mr}{J} \tag{C.19}$$

where M is the moment acting on the weld, r is the distance from the centroid of the weld group to the point in the weld of interest, and J is the second polar moment of area of the weld group about its centroid. M and r are both known, but J must be computed.

Computation of J is completed using Table 9-1 of Shigley's Mechanical Engineering Design, Eighth edition [29]. We first compute the unit second polar moment of area, which is the second polar moment of area of a weld of unit width. For a circular weld, this quantity takes the form

$$J_u = 2\pi \frac{d^3}{2} \tag{C.20}$$

J_u is thus 305847.25 mm^3, and J is computed using

$$J = 0.707 h J_u \tag{C.21}$$

$$J = 0.707(6.35\ mm)(305847.25\ mm^3) = 1373085.93\ mm^4$$

$$= 1.373 \times 10^{-6}\ m^4$$

We can now compute the secondary shear. Clearly the location of highest secondary shear stress will be at the point in the weld farthest from its centroid, where $r = 34.925\ mm + 6.35\ mm = 41.275\ mm$. Plugging in to Eq. (C.19) gives

$$\tau'' = \frac{(1214.83\ Nm)(0.041275\ m)}{1.373 \times 10^{-6}\ m^4} = 36.52\ MPa$$

From the FBD in Fig. C.9, we see that the location of maximum stress will be at the bottom of the weld. The value of this maximum stress is simply

$$\tau_{max} = \tau' + \tau'' \tag{C.22}$$

$$\tau_{max} = 37.23\ MPa$$

Recalling that the shear strength of 6061 Al is 165.6 MPa, the weld design is adequate. However, in actual fact, the weld was not provided as designed. The calculation below provides further detail.

Compute max shear stress in flange welds on horizontal tube as provided

Due to a design flaw in the flange welds, the machine shop was unable to weld all around the flange. The problem was that the bolt holes in the flange were too close to the weld, such that welding all around likely would have damaged the holes. Because of this flaw, the weld computations above needed to be redone to accurately model the part that will be deployed.

Fig. C.10 shows a CAD representation of the welds that were actually provided by the machine shop. There are six separate weld beads, each with a throat of roughly 6.35 mm (0.25 in). The average length of each weld is 20.3 mm (0.8 in).

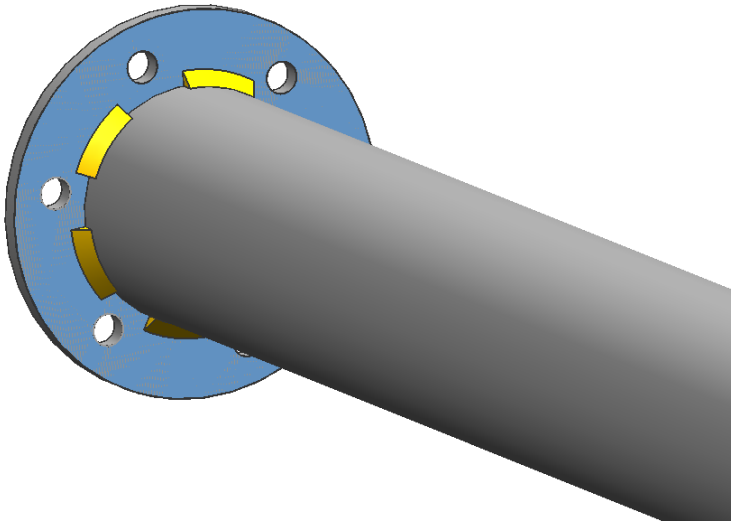

Fig. C.10: Flange welds provided by machine shop

For the weld provided, both the throat area and the second polar moment of area change by a factor equal to the total length of the provided welds divided by the length of the designed welds. This factor takes the form

$$c = \frac{l_{wp}}{l_{wd}} \tag{C.23}$$

$$c = \frac{6(20.3\ mm)}{\pi(73.02\ mm)} = 0.531$$

Equations (C.17) and (C.19) then become

$$\tau' = \frac{F}{cA} \tag{C.24}$$

$$\tau" = \frac{Mr}{cJ} \tag{C.25}$$

Thus $\tau' = 1.33\ MPa$, $\tau'' = 68.78\ MPa$, and $\tau_{max} = 70.1\ MPa$. Despite the flaw, the welds should still be strong enough to carry the load, but fatigue loads may be a concern.

Compute max shear stress for welds on redesigned flange

As was discussed in Chapter 4, the flange welds did not perform very well. When subjected to high bending loads they proved to lack the necessary strength and broke. As such this welded

connection has been redesigned so that it can better handle bending loads. The calculations for the new welds follow. Calculations for torsional loads are not be redone since they have already been done for the old, weaker assembly, and were found to be sufficiently strong.

Fig. C.11 shows the updated drawing for the flange welds on the horizontal tube. The dimensions shown are in mm. The part is now made of a solid machined piece of aluminum with a thick hub protruding out from the flange. This hub fits over the end of the horizontal tube, where it is designed to be welded in place. The part is welded in two places. There is a 6.35 mm (0.25 in) fillet weld on the right in the figure and a 6.35 mm (0.25 in) V-groove weld on the flange face. The flange diameter has increased to accommodate the changes and thus the bolt pattern has also changed. This necessitates changes to the plate that the flange bolts to, which captures the sonar pole.

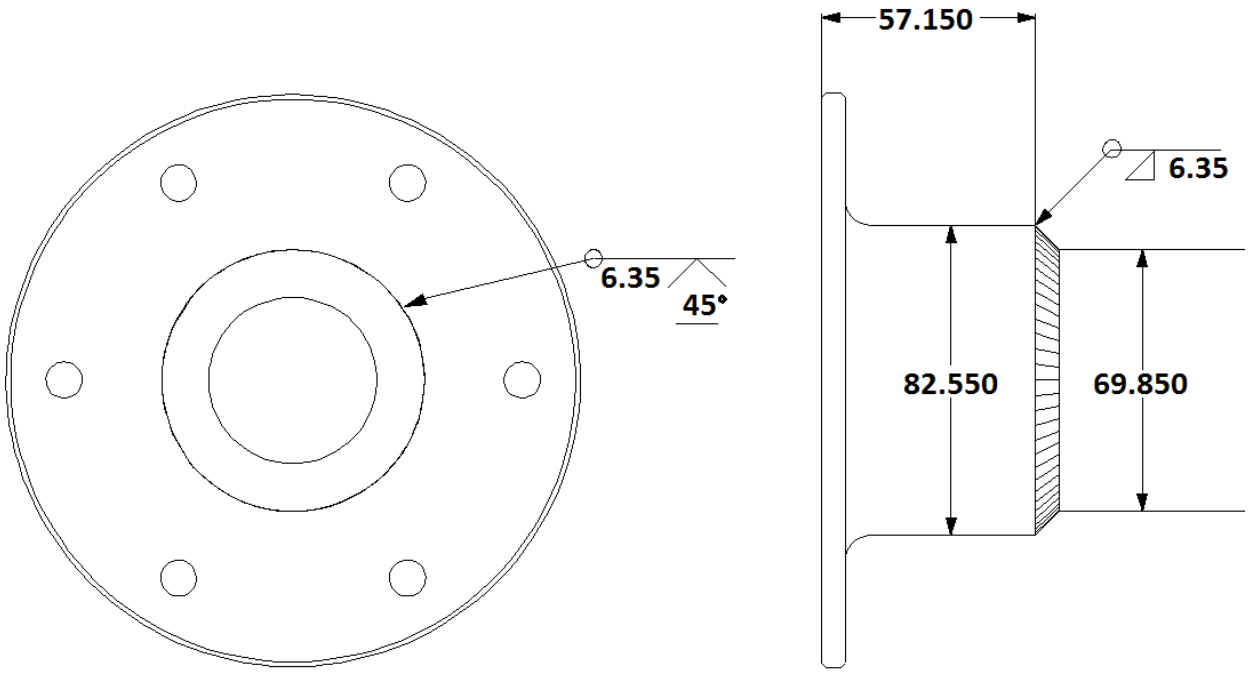

Fig. C.11: Updated flange welds on horizontal tube

Analyzing these welds is fairly straightforward. Fig. C.12 shows a free-body diagram for the welded assembly. Drag on the pole induces a large bending moment and a shear force acting at the centroid, G, of the weld group.

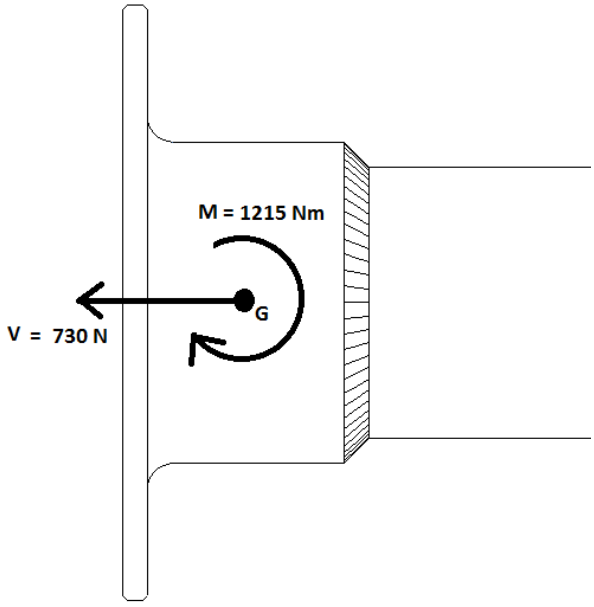

Fig. C.12: FBD for flange welds on horizontal tube

The total throat area for the weld group is

$$\begin{aligned} A_{tot} &= \pi\big(0.06985 + 0.00635(0.5)(0.5)\big)(0.707)(0.00635) + \pi(0.06985)(0.00635) \\ &= 0.00100755\ m^2 + 0.00139342\ m^2 \\ &= 0.002401\ m^2 \end{aligned}$$

And the primary shear is then

$$\tau' = \frac{730N}{0.002401\ m^2} = 0.304\ MPa$$

Computing the secondary shear stress requires the second moment of area of the weld group. Making use of Table 9-2 from [29] we have

$$I_{v-joint} = \pi 0.707(0.00635\ m)(0.06985\ m)^3 = 4.807E-6\ m^4$$

$$I_{fillet} = \pi 0.707(0.00635\ m)\big(0.06985\ m + 0.00635\ m(0.5)(0.5)\big)^3 = 5.142E-6\ m^4$$

And using the parallel axis theorem to translate the moments of area to the centroid G gives

$$\begin{aligned} I_G &= 4.807E-6\ m^4 + 5.142E-6\ m^4 \\ &\qquad + (0.028575\ m)^2(0.00100755\ m^2 + 0.00139342\ m^2) \\ I_G &= 1.1909E-5\ m^4 \end{aligned}$$

Now we can compute the secondary shear, but before we do this we need to make an educated guess as to where the maximum stress in the weld group will be. Typically the location of maximum stress is simply the point in the weld group that is farthest from the centroid. This

situation is slightly more complicated since we have two different types of weld. The throat area of the fillet weld takes the shape of a truncated cone, the sides of which intersect the axis of the horizontal tube at a 45 degree angle. The throat area of the v-groove weld takes the shape of a cylinder, the axis of which is collinear with the axis of the horizontal tube. Thus the primary and secondary shear acting on the fillet weld make up a Pythagorean combination, whereas the two shear components simply add for the v-groove weld. Therefore the location of maximum stress will be at the edge of the v-groove weld.

The secondary shear stress takes the form

$$\tau'' = \frac{Mr}{I_G} \tag{C.26}$$

where M is the moment, and r is the distance from the centroid of the weld group to the critical point in the weld.

Using trigonometry to find r we have

$$\tau'' = \frac{(1215\ Nm)(0.0451256\ m)}{1.1909E-5\ m^4} = 4.603\ MPa$$

And the maximum shear stress is

$$\tau_{max} = \tau' + \tau'' = 0.304\ MPa + 4.603\ MPa = 4.907\ MPa$$

The new welded joint should be much better at carrying the expected bending loads.

Appendix D: Vibration Analysis

It should be stated that whether sonar images acquired while using the prototype sonar mount have been affected by pole vibration is currently undetermined. For this reason, as well as the restrictive assumptions made in modeling, and the simplifications made to the test apparatus, the analyses in Appendix D are intended to be a first cut at modeling and experimentally measuring pole vibration. They provide a starting point for further research in pole vibration should it become necessary. To limit the scope of the vibration study, several potential sources of nonlinearity and damping were removed from the models and the test setup. This helps to simplify the analyses and makes testing more feasible. These are as follows:

1. Tests were conducted in air, not water
2. The fairing was not included
3. The sonar mount base assembly was excluded so that the test configuration included only the sonar pole and related components.
4. The pole was mounted by clamping its upper flange to the floor whereas it is normally connected to the base assembly with u-bolts positioned somewhere along its length.

The above simplifications will affect the results of the vibration study in several ways. Testing in air neglects the damping and inertial effects due to water immersion. Observed mode frequencies in air should be higher compared to the frequencies one would expect in water. The removal of the fairing reduces the overall mass of the apparatus by about 4%, and makes the sonar pole more symmetric. The fairing is also expected to be a source of nonlinearity due to its contact with the sonar pole. In excluding the mount's base assembly its pins and bushings are neglected. This neglects another source of nonlinearity, and also neglects the vibration characteristics of the base itself. Simplification 4 is probably the most impactful of all of the simplifications. Because the sonar mount is designed to be depth adjustable, its vibration characteristics will change based on where it is clamped. Changes in where the pole is clamped are expected to have a significant effect on its mode shapes and frequencies. Therefore future vibration analyses should be application specific.

A rendering of the parts of the mount used for analysis and testing is shown in Fig. D.1. The left image shows the pole assembly with sonar, the middle image shows the sonar, its clamp, and brackets, and the right image shows the top of the pole. The fairing was removed as it was expected to exhibit highly nonlinear behavior.

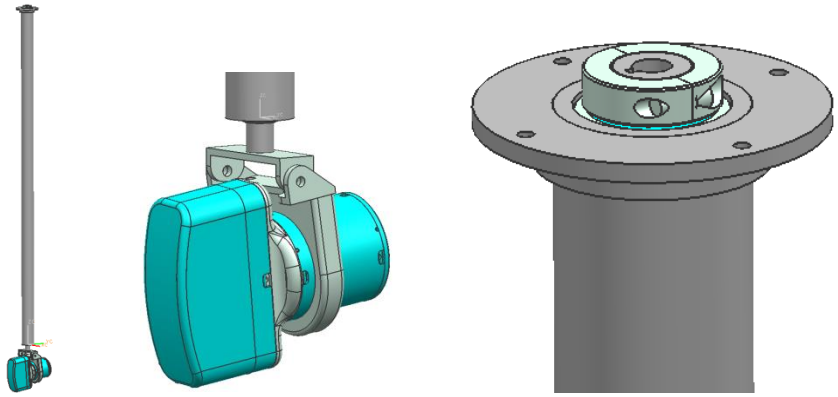

Fig. D.1: L to R: sonar mount pole assembly; sonar head, clamp and brackets; top portion of pole

D.1 Modeling

Three models were developed to gain a fundamental understanding of mount vibration: single degree of freedom; distributed parameter; and finite element.

Single Degree of Freedom Model

In order to describe the system with an SDOF approach, the dynamics were simplified to a basic cantilevered tip mass with a beam of constant cross section, as seen in Fig. D.2. For this figure, x is the reference direction, with the clamped end corresponding to $x = 0$, and the tip mass corresponding to $x = 177.8$ cm (70 in). The mass of the sonar, M, includes the mass of the clamps and brackets used to secure it. Also, $w(x,t)$ is the deflection at a particular distance x, and a particular time, t. The right side of Fig. D.2 shows the cross section. The following assumptions were made:

1. Constant beam cross section
2. No damping
3. Inner and outer pole deflect together
4. Neglect 5.1 cm (2 in) of inner pole protruding from outer pole
5. Isotropic material properties
6. Symmetry

Assumption 1 is used to calculate the beam's cross sectional area and moment of inertia. Assumption 2 implies that the inner and outer pole do not move relative to each other. A further simplification neglects the additional 5.1 cm (2 in) of inner pole that protrudes from the outer pole which allows it to be secured by a pipe clamp at each end. The beam material is 6061 Al and is considered isotropic. For this analysis the pole and mass are assumed symmetric, and as such the analysis describes vibration in two planes. Boundary conditions are modeled as clamped at $x = 0$, and as a tip mass at the end, $x = l$.

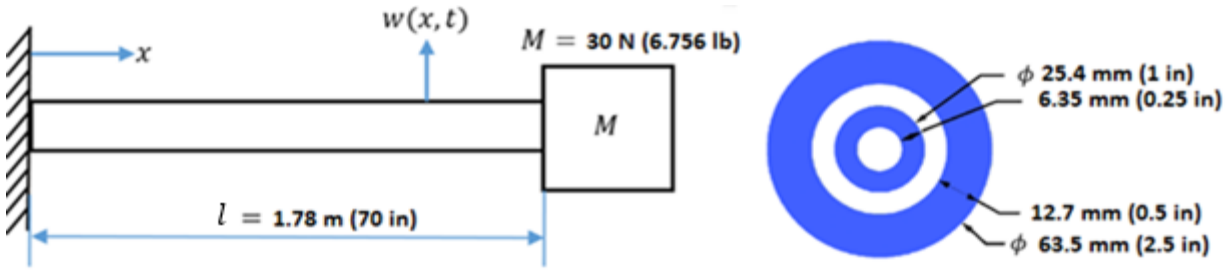

Fig. D.2: SDOF and DPM model simplification with cross section

With the simplifying assumptions, the transverse vibration stiffness model is given by [30],

$$k = \frac{3EI}{l^3} \tag{D.1}$$

where $\boldsymbol{k}$ is the pole stiffness, $\boldsymbol{E}$ is Young's modulus, $\boldsymbol{I}$ is the second moment of area, and $\boldsymbol{l}$ is the length of the pole. Using a standard second order model, the natural frequency is expressed as

$$f_n = \frac{1}{2\pi}\sqrt{\frac{3EI}{l^3 M}} \tag{D.2}$$

where M is the mass of the sonar at the tip of the pole. Using this relationship, along with the beam properties and previously stated assumptions, the natural frequency for transverse vibration is found to be

$$f_n = 12.2 \text{ Hz}$$

Work presented in [31] suggests that the mass of the pole can be expressed as an equivalent mass placed at the tip of the pole with the sonar. Taking into account previous assumptions and the relationship of Eq. (D.2), the natural frequency can be expressed as

$$f_n = \frac{1}{2\pi}\sqrt{\frac{3EI}{l^3\left(M + \frac{33}{140}\rho A l\right)}} \tag{D.3}$$

where ρ is the density of 6061 aluminum and A is the cross sectional area. Incorporating known physical quantities, the natural frequency of the system is found to be

$$f_n = 9.8 \text{ Hz}$$

Distributed Parameter Model

As with the SDOF model, transverse vibration for the distributed parameter model (DPM) is considered in only one direction as the beam is assumed symmetric. This analysis uses the same configuration given by Fig. D.2 with the same guiding assumptions presented in the SDOF analysis. According to [32] and [33], the equation of motion for a transverse vibrating beam is

$$c^2 \frac{\delta^4 w(x,t)}{\delta x^4} + \frac{\delta^2 w(x,t)}{\delta t^2} = 0 \tag{D.4}$$

where $w(x,t)$ is the deflection of the beam at a particular time, t, at a particular location, x, and

$$c = \sqrt{\frac{EI}{\rho A}} \tag{D.5}$$

For Eq. (D.5), ρ, A, E, and I are consistent with the quantities used in the FEA.

The clamped boundary condition is described as

$$w(0,t) = 0, \tag{D.6}$$

$$\frac{\delta w(0,t)}{\delta x} = 0, \tag{D.7}$$

which implies there is no displacement at the clamp, and that the slope of the beam is zero. Next, the boundary condition of a tip mass is considered. There is assumed to be no bending moment at the tip of the beam which leads to the following boundary condition,

$$\mathcal{M}(l,t) = EI \frac{\delta^2 w(l,t)}{\delta x^2} = 0 \tag{D.8}$$

where $\mathcal{M}(x,t)$ is the bending moment at a particular location, x, at a particular time, t. By equating the acceleration of the tip mass to the shear force at the tip, then using general knowledge of deformable bodies, the second boundary condition for the tip mass is given as

$$\frac{EI}{M} \frac{\delta^3 w(l,t)}{\delta x^3} = \frac{\delta^2 w(l,t)}{\delta t^2} \tag{D.9}$$

Using the principle of separation of variables,

$$w(x,t) = X(x)T(t) \tag{D.10}$$

the equation of motion given in Eq. (D.4) can be rewritten as

$$c^2 \frac{X''''(x)}{X(x)} = -\frac{\ddot{T}(t)}{T(t)} = \omega^2 \tag{D.11}$$

which leads to the temporal and spatial equations given respectively as,

$$\ddot{T}(t) + \omega^2 T(t) = 0 \tag{D.12}$$

$$X''''(x) - \beta^4 X(x) = 0 \tag{D.13}$$

where

$$\beta^4 = \left(\frac{\omega}{c}\right)^2 \tag{D.14}$$

The general solution of the temporal and spatial equations are respectively given as

$$T(t) = A\sin(\omega t) + B\cos(\omega t) \tag{D.15}$$

$$X(x) = a_1 \sin(\beta x) + a_2 \cos(\beta x) + a_3 \sinh(\beta x) + a_4 \cosh(\beta x) \tag{D.16}$$

Substituting Eq. (D.15) and (D.16)) into (D.10) and applying the boundary conditions gives the following matrix equation

$$\begin{bmatrix} 1 & 0 & 1 & 0 \\ 0 & 1 & 0 & 1 \\ -\sin(\beta l) & -\cos(\beta l) & \sinh(\beta l) & \cosh(\beta l) \\ \sigma\sin(\beta l) - \cos(\beta l) & \sigma\cos(\beta l) + \sin(\beta l) & \sigma\sinh(\beta l) + \cosh(\beta l) & \sigma\cosh(\beta l) + \sinh(\beta l) \end{bmatrix} \begin{bmatrix} a_1 \\ a_2 \\ a_3 \\ a_4 \end{bmatrix} = \begin{bmatrix} 0 \\ 0 \\ 0 \\ 0 \end{bmatrix} \tag{D.17}$$

where

$$\sigma = \frac{\beta M}{\rho A} \tag{D.18}$$

In this case, the first two rows are derived from the clamped condition whereas the last two rows come from the tip mass conditions. In order for there to be nontrivial solutions to a_1, a_2, a_3, and a_4, the determinant of the multiplying matrix must be equal to zero, which is to say that the

matrix must be singular. Taking the determinant and equating to zero gives the characteristic equation of

$$\beta_n^3(\cos^2(\beta_n\, l) + \cosh^2(\beta_n\, l) + \sin^2(\beta_n\, l) - \sinh^2(\beta_n\, l) + \frac{2\beta M}{\rho A}\cos(\beta_n\, l)\sinh(\beta_n\, l)$$

$$-\frac{2\beta M}{\rho A}\cosh(\beta_n\, l)\sin(\beta_n\, l) + 2\cos(\beta_n\, l)\cosh(\beta_n\, l) = 0 \qquad \text{(D.19)}$$

Substituting in physical values and solving numerically, the first four values for β_n are found and are given in Table D.1. In this case, the scenario of $\beta_n = 0$ is not considered since there is no rigid body mode.

Table D.1: First four mode parameters for clamped beam with tip mass

n	β_n	$\omega_n\left(\frac{\text{rad}}{\text{s}}\right)$	$f_n(\text{Hz})$
1	0.8218	61.32	9.754
2	2.3267	491.5	78.23
3	4.0549	1429	237.6
4	5.8005	3055	486.2

Using the matrix equation relationships given in Eq. (D.17), the spatial solution can be manipulated to give the following mode shape relationship,

$$X_n(x) = \sin(\beta_n x) - \tau_n\cos(\beta_n) - \sinh(\beta x) + \tau_n\cosh(\beta x) \qquad \text{(D.20)}$$

where

$$\tau_n = \frac{\sin(\beta_n l) + \sinh(\beta_n l)}{\cos(\beta_n l) + \cosh(\beta_n l)} \qquad \text{(D.21)}$$

Using the numerical results of Table D.1, the first four mode shapes are depicted in Fig. D.3. As expected, the first mode shape corresponds strongly with the SDOF frequency. The DPM, however, has the added value of predicting higher frequencies of interest.

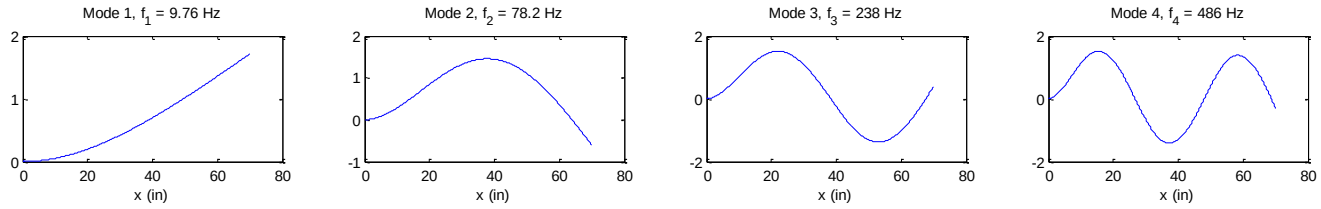

Fig. D.3: First four mode shapes of distributed parameter model.

Finite Element Analysis

Since the DPM makes reasonably restrictive assumptions, such as assuming no inner pole deflection relative to the outer pole, the decision was made to make use of the finite element method. Several assumptions are made to simplify the model. Like the distributed parameter and SDOF models, the FE approach assumes no damping. Furthermore, one end of the pole is assumed to follow a clamped boundary condition while the other end is assumed to have a point mass, also consistent with previous models. Lastly, while the model does not make restrictive assumptions on the geometry and length of the poles, the contact between the bearings and poles is not modeled, as it is beyond the scope of this study. The poles are instead modeled as fixed relative to one another at the bearings.

First, a defeatured pole is modeled in Unigraphics NX7. Material properties and boundary conditions are set, and the model is meshed with 10-noded tetrahedra. The simulation uses the NX Nastran SEMODES103 solver. Table D.2 shows the first 5 modal frequencies in two planes as the number of elements in the model is increased. The number of elements was increased from 4770 to 147,309 in order to investigate the symmetry of the model. It is important to note that the FE model is symmetric and as such the ten rows below only represent five distinct modes, with each of the five modes represented once about the x-axis, with a duplicate about the y-axis. It is clear from the table that for small element quantities, the x and y modes differ slightly. As the number of elements increases, the model becomes increasingly symmetric, and this discrepancy vanishes. Standard deviations are also listed for each mode and show that modal frequencies are not greatly affected by the number of elements in the model, with the standard deviation residing at less than 1% for each frequency.

Table D.2: Study of convergence. Table shows modal frequencies in Hz for increasing numbers of elements.

Mode	Axis	Number of elements					Standard Deviation
		4770	8021	15669	19512	147309	
1	X	10.42	10.43	10.4	10.42	10.41	0.0114
	Y	10.46	10.44	10.4	10.42	10.42	0.0228
2	X	40.8	41.26	40.72	41.4	41.33	0.3174
	Y	40.83	41.41	40.81	41.41	41.33	0.3104
3	X	79.38	79.55	79.31	79.33	79.27	0.1092
	Y	79.63	79.58	79.31	79.33	79.28	0.1653
4	X	112.2	113.4	111.9	113.7	113.5	0.8264
	Y	112.3	113.9	112	113.8	113.5	0.8860
5	X	216.3	218.5	215.3	218.5	218	1.4464
	Y	216.4	219	215.8	218.5	218	1.3777

Fig. D.4 shows the first five amplitude normalized mode shapes of the pole with tip mass. In the first mode, both the inner and outer pole move together, but no other mode exhibits this behavior. Modes 2 and 4 are not predicted by the DPM. This is likely because they are dominated by inner pole vibration, which the DPM has no way of predicting since it assumes the inner and outer pole are lumped into a single pole of equivalent stiffness and moment of inertia.

Because the pole dynamics are driven mainly by the dynamics of the outer pole, it makes intuitive sense that the DPM only predicts modes that show significant outer pole deflection.

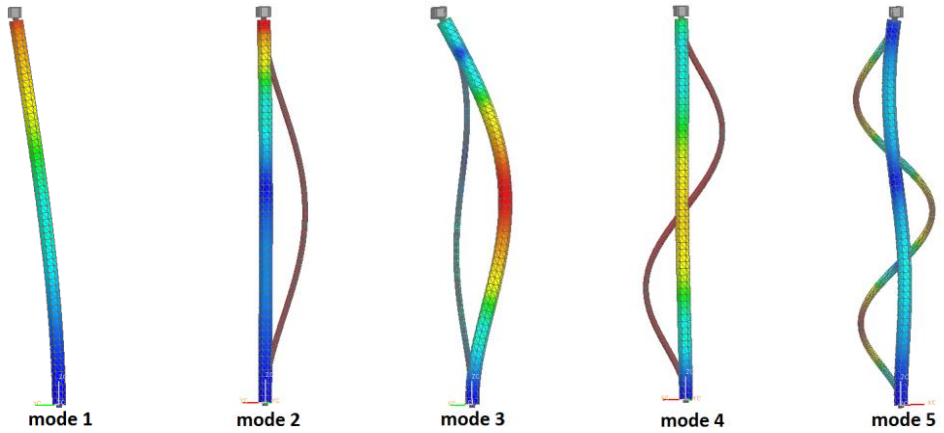

Fig. D.4: First five mode shapes from FEA, amplitude normalized

D.2 Experimentation

Following development of the SDOF, distributed parameter, and FE models, the sonar pole was instrumented and tested in the Vibrations, Adaptive Structures, and Testing (VAST) Lab at Virginia Tech. Fig. D.5 shows the test setup. To test the pole in a clamped condition, steel plates were used to clamp the flanged end of the pole to a T-slotted concrete floor. A modal hammer was used to excite the beam 38.1 cm (15 in) from the base. This point is marked by a black dot and is labeled in Fig. D.5. This location was chosen because models showed that it would allow excitation of modes with natural frequencies less than the band of interest, around 200 Hz. A single accelerometer was used to collect data at 11 points along one axis of the beam, which corresponds to a measurement point every 17.8 cm (7 in). These points are marked by the light blue dots in Fig. D.5, and the points at $x = 0$ cm and $x = 177.8$ cm (70 in) are labeled. Three additional measurements were taken out of plane, 90 degrees from the 11 initial measurements, to test the symmetry assumption. Lastly, the pole was unbolted from the floor, moved to a new location, and three more measurements were taken to test the repeatability of the data. Measurements were found to be highly repeatable, but lacked symmetry. This was especially true for point 9, 142.2 cm (56 in) from the base, which showed both poor repeatability and poor symmetry. A more in depth discussion of the symmetry and repeatability tests can be viewed in Appendix D. For all measurements, a Kistler Type 9724A2000 modal hammer was used with a PCB Piezotronics accelerometer, Model No. U352C67. The sensors were interfaced through a SigLab measurement suite.

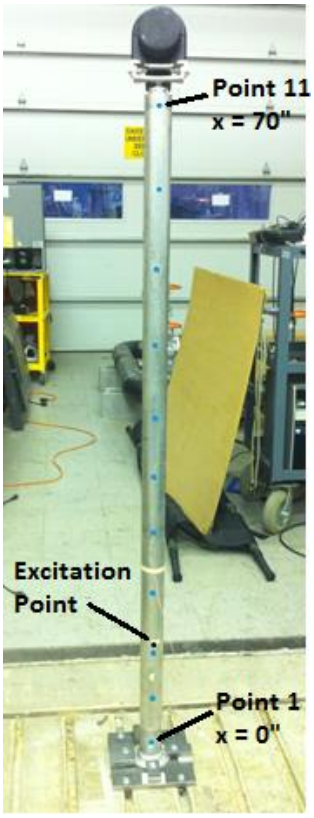

Fig. D.5: Test setup with excitation point (black dot) and measurement points (blue dots) shown

Measured Mode Frequencies and Damping Ratios

Using the data collected at the original 11 points of interest, the transfer functions are examined to determine the characteristic mode frequencies associated with the system. Fig. D.6 shows the FRF for the data collected at the tip of the beam, 70” from the clamped base. The remainder of the response functions are shown in Fig. D.10 through Fig. D.12 in Appendix D. The resulting discussion considers the entirety of the eleven different responses, but the response at the tip is used for demonstrative purposes. Additionally, the data collected is considered valid as the coherence levels presented in Fig. D.12 of the Appendix are kept above 0.7, except in cases in which the magnitude response is arbitrarily small, such as those points immediately after resonant behavior.

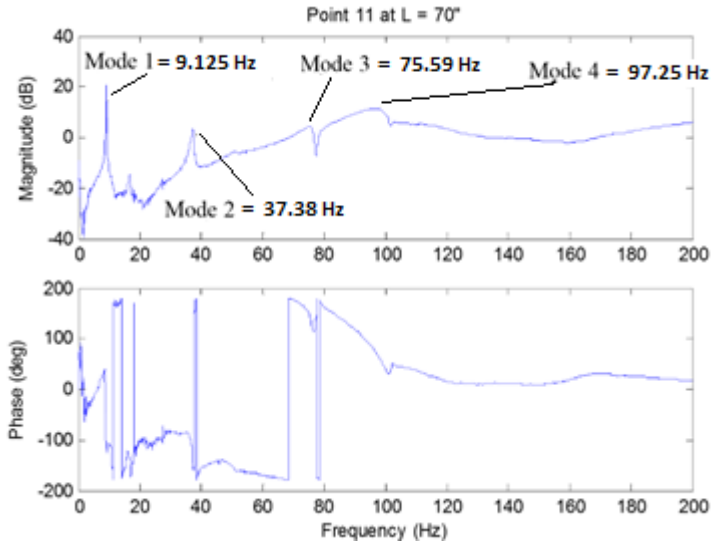

Fig. D.6: Frequency response function of pole tip to excitation at quarter point

From Fig. D.6, as well as the FRFs included in Fig. D.10 through Fig. D.12 of Appendix D, it is clear that four dominant frequencies occur at approximately 9.125, 37.38, 75.59, and 97.25 Hz. These frequencies are expected from the results of the FEA model. The first and third frequencies are also predicted by the DPM, but it lacks the ability to predict modes dominated by inner-pole vibration. Table D.3 compares the measured frequencies to those from the three modeling approaches, in Hertz. In general, the error between predicted and experimental is within 10-15%. An interesting note is that the DPM better predicts the frequencies for the first and third modes, although it fails to predict the second and fourth modes.

Table D.3: Comparison of experimental frequency measurements to model predictions

Mode	SDOF	DPM	FEA	Experiment
1	9.78	9.76	10.42	9.125
2	--	--	41.33	37.38
3	--	78.23	79.28	75.59
4	--	--	113.5	97.25

At this point, it is worth noting that another characteristic frequency shows up in several measurement locations which occurs at approximately 16.63 Hz. This frequency is believed to be one of many minor interactions associated with the bearings and clamps used to secure the system. Originally it was suggested that this may be an effect of aliasing. However, this is not believed to be the case as none of the modes studied corresponds to the 16.63 Hz frequency in situations in which they would be folded about the Nyquist frequency.

In examining Fig. D.6 it is clear that the first four modes are lightly damped, as would be expected from the system. Using the 3-dB down point method presented in [30], the damping ratios for modes 1-4 are respectively found to be 0.003, 0.01, 0.02, and 0.07, which corroborates

the observation of light damping. Given this finding, the decision to not include damping in the models is considered valid.

Symmetry Assumption

For modeling, the assumption of a symmetric system is made, however, in reality, the bearings and mass are not guaranteed to be symmetric. To test the validity of this assumption, we compare the FRF taken at three points along the axis of interest and compare the response to FRF's taken at corresponding points rotated 90 degrees about the longitudinal axis of the beam. Fig. D.7 shows the comparison of the FRFs. The blue lines represent data taken along the axis of interest, and the red lines represent the out of plane measurements.

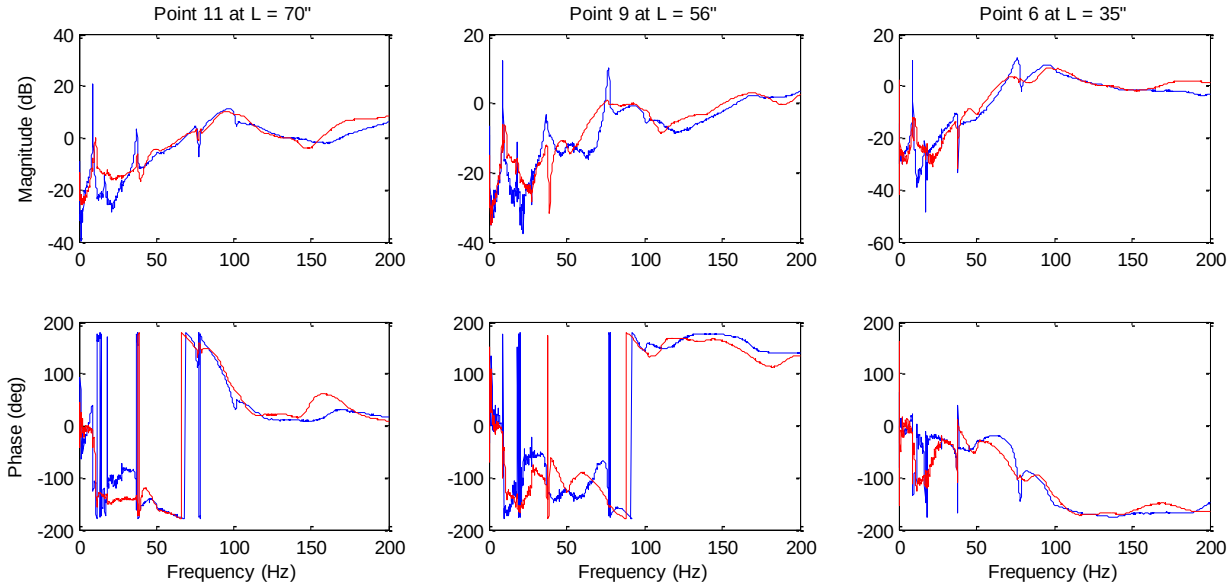

Fig. D.7: Comparison of in plane and out of plane measurements

From the comparison, it is clear that the same modal frequencies show up at approximately 9.2 Hz, 37.4 Hz, 75.6 Hz, and 97.3 Hz. However, the symmetry assumption is not valid as the out of plane measurements tend to exhibit a higher damping ratio. This change in behavior is attributed to complexities in the bearings which are not easily quantified. The asymmetric shape of the sonar also limits the ability to reproduce behavior in two planes. It's also likely that clamping the pole to a t-slotted floor introduced asymmetries. Further discussion will only concern data taken in one plane.

Repeatability of Measurements

Prior to examining experimental results, we examine the repeatability of the measurements taken along the axis of interest. Fig. D.8 shows a comparison of measurements taken from the original set of 11 data points (blue line), and data that was taken at the same points after re-clamping the pole to a different location on the floor (red line).

The measurements are found to be highly repeatable as evidenced by the high degree of overlap between the two data sets. Point 9 has a higher degree of deviation than either point 6 or point 11. Point 9 also has the highest degree of deviation with regard to the symmetry assumption. Both of these cases of deviation at point 9 are thought to be a result of unmodeled contact at the bearings.

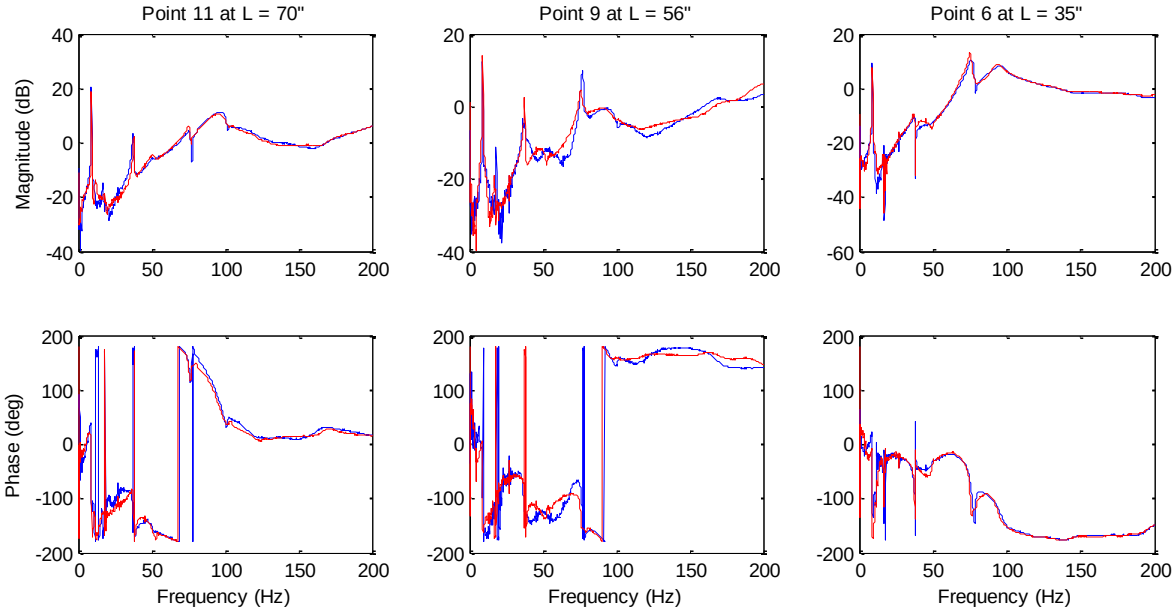

Fig. D.8: Repeatability of measurement results

Measured Mode Shapes

From the measured damping ratios, it is ultimately possible to determine the mode shapes from the FRFs. For this analysis, Point 3, which is 14" from the base, is taken to be the driving point. From the approach laid out in [30], we know that the i^{th} mode shape, u_i, holds the following relationship,

$$\left|u_i u_i^{\mathrm{T}}\right|_{sr} = \left|2\zeta_i \omega_i^2\right| |H_{sr}(\omega_i)| \tag{D.22}$$

where $|H_{sr}(\omega_i)|$ is the magnitude of a particular transfer function between input point, r, and output point, s, at the i^{th} natural frequency, ω_i. Using the generated FRFs, eleven simultaneous equations are solved to generate the mode shape magnitude, $|u_i|$. Finally, by using the phase information presented in Fig. D.11 of the Appendix, the individual signs of the elements in u_i are determined. With this approach, the data collected is used to generate the normalized mode shapes given in Fig. D.9. The left side of each plot corresponds with the fixed boundary condition at the base of the pole, while the right side corresponds to the free end with the sonar.

As expected from the FEA model, the first and second mode shapes are characterized by the outer pole deflecting in a manner consistent with the first mode from the DPM. Additionally, the third and fourth modes behave as expected, exhibiting a bowing of the center. This behavior is typical of the second mode predicted by the DPM. While following the predicted trend, it is

worth noting that these mode shapes contain a substantial amount of noise that prevents the curve from being as smooth as expected. This is attributed to the low number of sample points and a lack of precision in the location of hammer strikes and accelerometer placements. An off-center hammer strike could easily result in symmetric modes being excited, effectively reducing the energy of the strike for the mode of interest. Weak interactions in the bearings and clamps that are not modeled and are likely excited across a broad frequency range could also be a source. As it stands, however, the current measured mode shapes validate the FEA approach at its current level of detail for an un-damped, un-faired sonar pole vibrating in air.

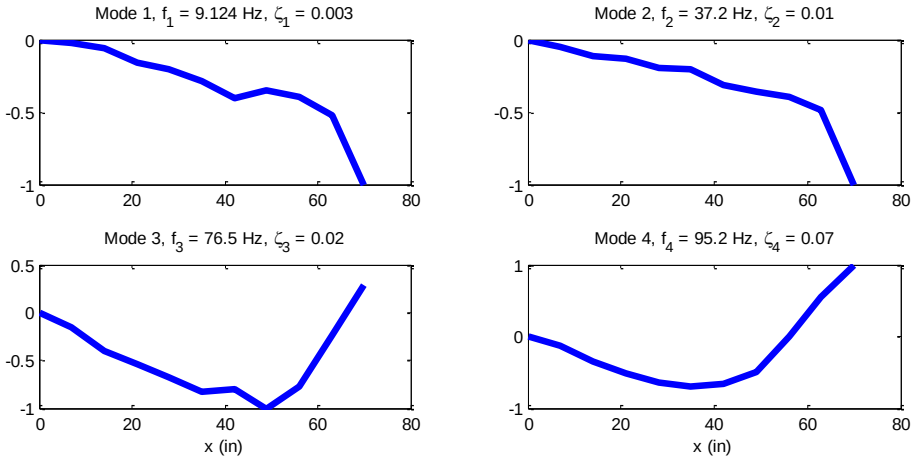

Fig. D.9: Experimentally measured mode shapes

Conclusion

SDOF, DPM, and FEA methods are used to investigate the vibration characteristics of the sonar pole. While each model has varying levels of complexity, the pole is modeled as a cantilevered beam with a clamped boundary condition at one end and a tip mass at the other. The DPM validated the frequencies given by the SDOF approach, with the added benefit of predicting additional mode frequencies and shapes. The FEA was then able to predict additional mode shapes that the DPM was not due to various assumptions made in modeling. In total, the FEA presents 5 distinct mode shapes. These mode shapes were validated through experimentation using methods presented in [30].

Additionally, experimental data was used to identify natural frequencies as well as modal damping ratios. As expected, the damping was very light, generally residing at less than 3% with the largest occurring at 7%. From experimentation, an unpredicted mode frequency was observed at approximately 16 Hz. This response is believed to be the result of weak interactions in the bearings and pipe clamps that are not modeled. In testing the symmetry assumption made in the models, it was found that the pole behavior did not fit this assumption. Out-of-plane measurements exhibited higher damping than in-plane measurements. This finding is attributed to the asymmetric shape of the sonar, as well as complexities in modeling that lie beyond the scope of this study. The measurements in this study were shown to be repeatable, but some

measurement points showed better repeatability than others. This is thought to be a result of unmodeled contact at the bearings.

The results of the vibration study offer a starting point for future modeling efforts to better approximate the operational environment of the mount. Specifically these should include inertial and damping effects due to fluid submersion, the inclusion of the fairing, and more accurately modeling the real-life mounting configuration. Due to the adjustability of the mount, future vibration studies will likely need to be specific to the application.

Fig. D.10 through Fig. D.12 give the experimental data for the 11 main data points considered in the vibration experimentation section.

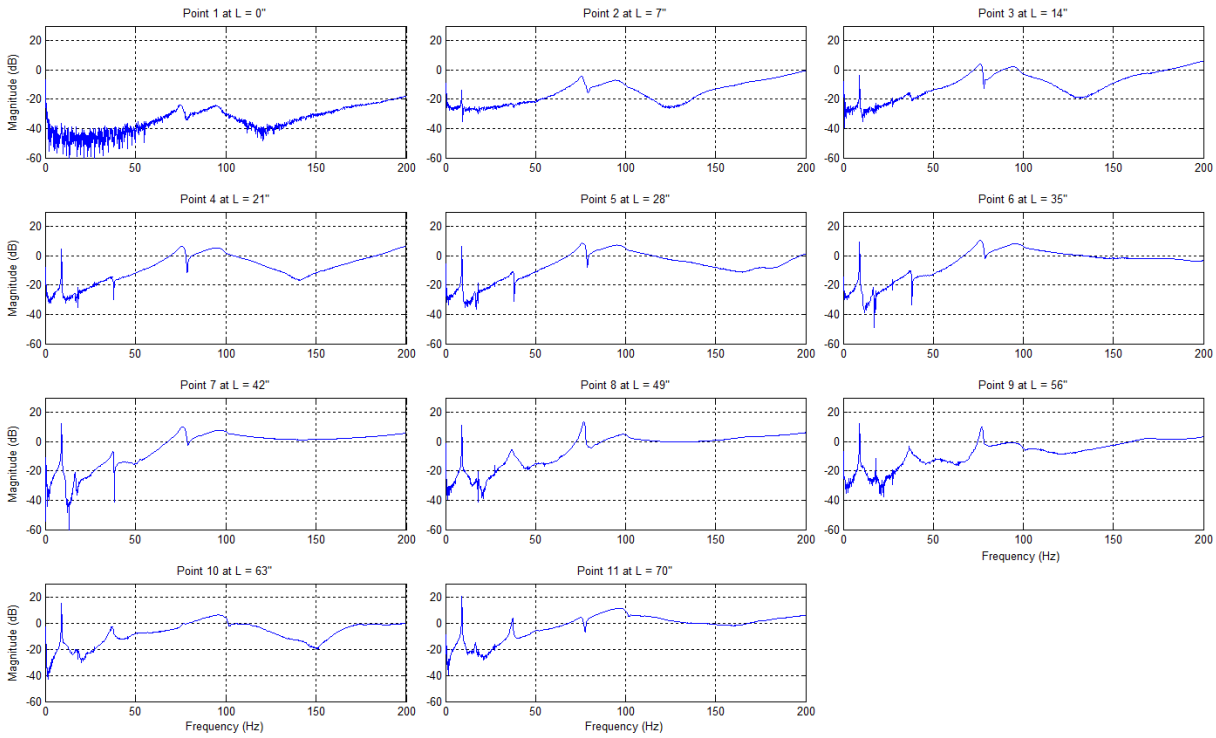

Fig. D.10: Magnitude of Frequency Response Functions for 11 main data points

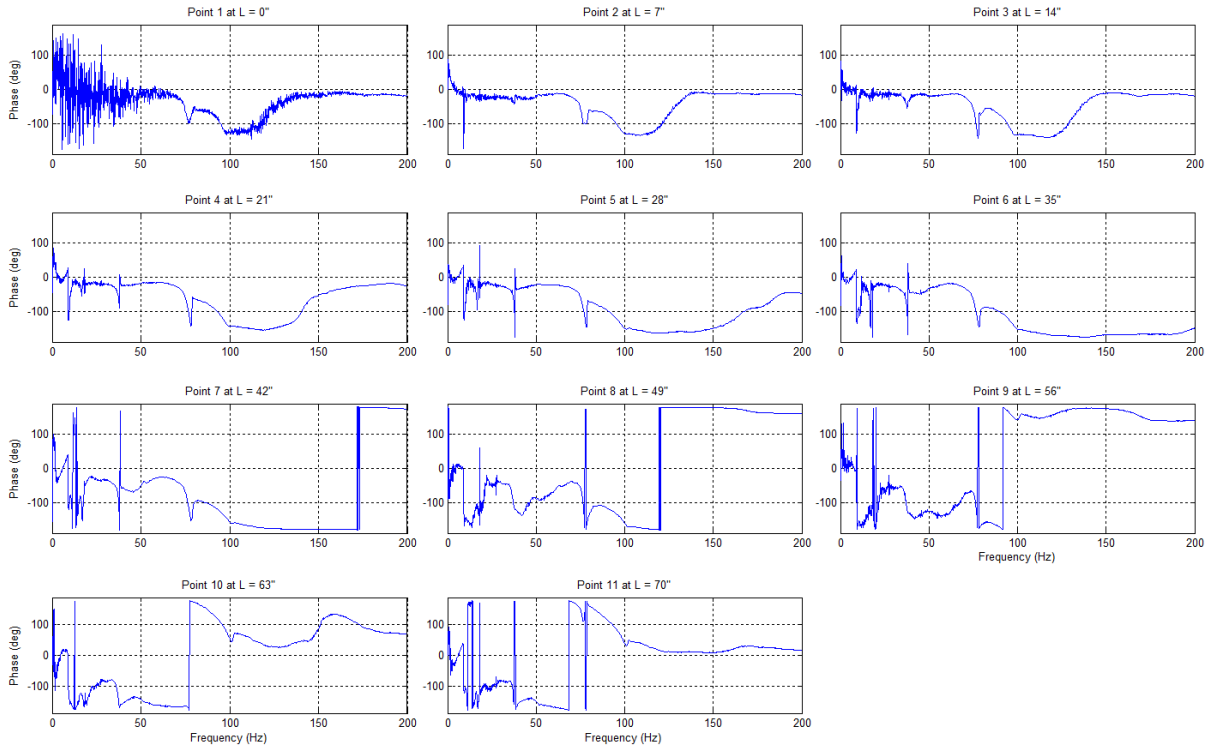

Fig. D.11: Phase of Frequency Response Functions for 11 main data points

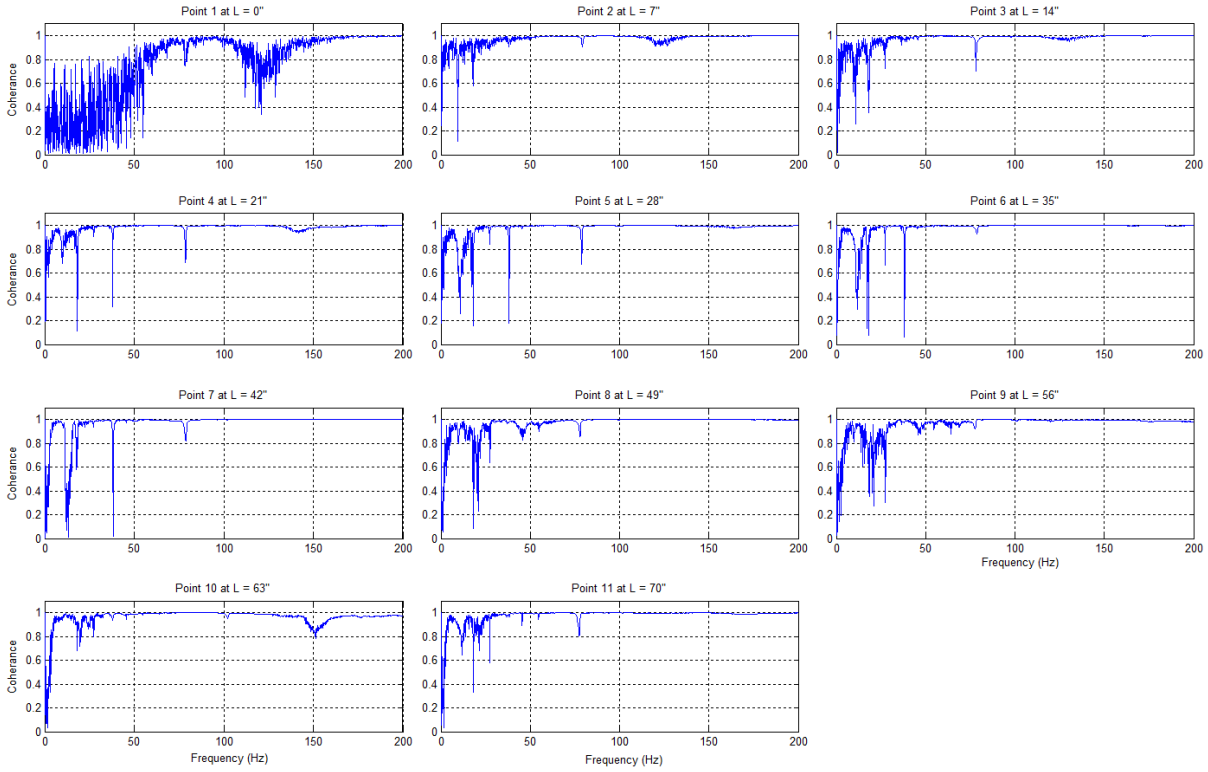

Fig. D.12: Coherence of Frequency Response Functions for 11 main data points

Appendix E: Fairing Manufacture

The process begins with one piece of 4 x 8 ft construction foam cut in half to make two 4 x 4 ft pieces. The pieces are then glued together to make a 4 in thick block. The fairing shape then needs to be cut out of the block. We used a CNC hot wire foam cutter, although the process could be done by hand if necessary. Note that the leading edge of the hydrofoil is replaced by a semicircular cutout. It was anticipated that the fairing would take some abuse in the field, with the leading edge being the most likely point of impact. The purpose of the cutout is to accommodate a fiberglass tube, which will then slide onto the aluminum pole. This limits the deformation of the fiberglass at the leading edge if it experiences an impact, thus improving the fairing's durability. Once the fairing is cut and the fiberglass tube glued to the front, the entire fairing is wrapped in four layers of fiberglass and vacuum bagged to cure. After curing, automotive body filler is used to fill any low spots. When the body filler hardens, the fairing is sanded and painted. Special care was taken to ensure the fairing was as smooth as possible prior to painting to minimize drag. The fairing is then painted with several coats of bottom paint, which is specially formulated to cover boat hulls. The color orange was chosen for increased visibility.

Appendix F: MATLAB Code for BSB Design

```
% Rand Pearson
% Masters Thesis
% Ball and Socket Joint Design
% This program computes the breakaway torque of a ball and socket joint
% breakaway device. The breakaway torque is computed as the summation of
% the torque holding capacity of each ball detent. This code also computes
% the speed the sonar can move through the water before the breakaway
% device releases due to hydrodynamic drag. For the drag analysis assumptions
% are made about the sonar's size, shape, and depth below the water's
% surface. These assumption are stated in the comments below.

clear all
close all
clc

%specify problem-specific variables
Fmin = 47; %min end force, lbs
Fmax = 47; %max end force, lbs
Favg = (Fmin+Fmax)/2; %average end force, lbs
numdet_1 = 14; %number of detents in bottom row
numdet_2 = 8; %number of detents in top row
numdet = numdet_1 + numdet_2; %total number of detents
D = 6; %joint diameter in inches

detang_1 = 2*pi()/numdet_1; %angle between detents in radians
detang_2 = 2*pi()/numdet_2;
r_1 = 25*2*pi/360; %angle between detent axis and horizontal
r_2 = 55*2*pi/360;
cs_ang = pi/2; %countersink angle of detent

%define rotation matrices
Rz_1 = RotationMatrix3d( detang_1/2 );
R_1 = RotationMatrix3d(detang_1);
Rz_2 = RotationMatrix3d( detang_2/2 );
R_2 = RotationMatrix3d(detang_2);

AOR = [1, 0, 0]; %axis of rotation

%Compute slip force for one of the given ball detents
 Fs = Favg / tan(pi/2-(pi - cs_ang)/2);
 % Fs = 105;
% create vector to hold torque values
T = [0, 0]; %index 1 will correspond with bottom row detents

%position of first detent
P_1 = [D/2*cos(r_1); 0; D/2*sin(r_1)];

thetatest1 = zeros(1,numdet_1);

% Compute torque holding capacity from 1st row of detents
for i=0:numdet_1-1
```

```
    %compute angle between detent and AOR
    theta = acos(AOR*P_1/(norm(AOR)*norm(P_1)));
    thetatest1(i+1)= theta;

    %compute torque
    T(1) = T(1) + D/2*sin(theta)*Fs;

    %go to next detent.
    P_1 = R_1*P_1;

end

thetatest2 = zeros(1,numdet_2);

%position of first detent
P_2 = [D/2*cos(r_2); 0; D/2*sin(r_2)];

% Compute torque holding capacity from 2nd row of detents
for i=0:numdet_2-1
    %compute angle between detent and AOR
    theta = acos(AOR*P_2/(norm(AOR)*norm(P_2)));
    thetatest2(i+1)= theta;

    %compute torque
    T(2) = T(2) + D/2*sin(theta)*Fs;

    %go to next detent.
    P_2 = R_2*P_2;

end

Ttot = T(1) + T(2); %total torque from both rows of detents


%compute drag at 10kt
v = 5.14444; %speed, m/s
wd = 1000; %density of water, kg/m^3
deep_s = 24*0.0254; %assumed sonar depth, meter
di_s = 12*0.0254; %sonar diameter, meters, assume sonar is cylindrical
length_s = 16.25*0.0254; %sonar length, meter
cd_s = 0.83; %coef of drag for sonar, fig 9.29 from Fund. of Fluid Mech
A_s = pi/4*di_s^2; %frontal area of sonar
D_s = cd_s*0.5*wd*v^2*A_s*1.2; %drag on forward-facing sonar, Newton, added
1.2 fudge factor to account for cables and brackets

di_p = 2.5*0.0254; %pipe diameter, meters
length_p = 16*0.0254; %submerged pipe length, meter
cd_p = 0.8; %coef of drag for pipe, from Fund. of Fluid Mech
D_p = 0.5*cd_p*wd*v^2*di_p*length_p;%drag on pole, Newton

%torque at joint, assume speed of 10kt, assume joint is not submerged,
%adding 8 in to moment arm should ensure this
T_10 = D_s*32 + D_p*16;
T_10 = T_10*0.224808943; %convert from N-in to lb-in
```

```
%compute design speed
torque_ratio = Ttot/T_10;
design_speed = sqrt(torque_ratio)*10; %knots
```